AN ABSTRACT OF THE DISSERTATION OF

Yu Zhang for the degree of Doctor of Philosophy in
Electrical and Computer Engineering presented on September 19, 2006.
Title: Multi-Antenna OFDM Systems in the Presence of Phase Noise and Doubly-Selective Fading

Abstract approved: _____

Huaping Liu

Orthogonal frequency division multiplexing (OFDM), which has been very attractive for future high rate wireless communications, is very robust to channel multipath fading effect while providing high transmission data rate with high spectral efficiency. Multiple antennas can be combined with OFDM to increase diversity gain and to improve spectral efficiency through spatial multiplexing and space-time coding (STC). This dissertation focuses on performance analysis and detection schemes of multi-antenna OFDM systems in the presence of phase noise and doubly-selective fading where channel is both time-selective and frequency-selective.

In space-time coded OFDM (ST-OFDM), channel time variations cause not only intercarrier interference (ICI) among different subcarriers in one OFDM symbol, but also intertransmit-antenna interference (ITAI). We quantify the impact of time-selective fading on the performance of quasi-orthogonal ST-OFDM systems by deriving, via an analytical approach, the expressions of carrier-to-interference ratio (CIR) and signal-to-interference-plus-noise ratio (SINR). We also evaluate the performance of five different detection schemes and show that all these schemes suffer from an irreducible error floor.

Multiple-input multiple-output (MIMO) antennas combined with OFDM are very attractive for high-data-rate communications. However, MIMO-OFDM systems are very vulnerable to time-selective fading. We apply frequency-domain correlative coding in MIMO-OFDM systems over doubly-selective fading channels and derive the analytical expression of CIR to demonstrate the effectiveness of correlative coding in mitigating ICI.

When applied in fast fading channels, common ST-OFDM receivers usually suffer from an irreducible error floor. We apply frequency-domain correlative coding combined with a modified decision-feedback (DF) detection scheme with low complexity to effectively suppress the error floor of quasi-orthogonal ST-OFDM over fast fading channels.

Similar to single-antenna OFDM, MIMO-OFDM suffers from significant performance degradation due to phase noise and time-selective fading. After characterizing the common phase error (CPE) caused by phase noise and ICI caused by phase noise as well as time-selective fading, we derive a minimum mean-squared error (MMSE)-based scheme to mitigate the effect of both phase noise and Doppler frequency shift. We also evaluate and compare the performance of various detection schemes combined with the proposed CPE mitigation scheme.

Throughout the dissertation, theoretical performance analysis is always presented along with corroborating simulations.

Multi-Antenna OFDM Systems in the Presence of Phase Noise and Doubly-Selective Fading

by

Yu Zhang

A DISSERTATION

submitted to

Oregon State University

in partial fulfillment of
the requirements for the
degree of

Doctor of Philosophy

Presented September 19, 2006
Commencement June 2007

Doctor of Philosophy dissertation of Yu Zhang presented on September 19, 2006

APPROVED:

Major Professor, representing Electrical and Computer Engineering

---

Director of the School of Electrical Engineering and Computer Science

---

Dean of the Graduate School

I understand that my dissertation will become part of the permanent collection of Oregon State University libraries. My signature below authorizes release of my dissertation to any reader upon request.

Yu Zhang, Author

ACKNOWLEDGMENTS

I would like to express my sincere gratitude and appreciation to my advisor, Dr. Huaping Liu, for providing me with the opportunity to work in the research area of wireless communications and digital signal processing, for his expert guidance and mentorship, and for his encouragement and support at all levels. I am also very grateful to his understanding, patience, and most importantly, his friendship during my graduate studies at Oregon State University. I have learned a lot from him, without his help I could not have finished my dissertation successfully.

I would also like to thank those members of my doctoral committee, Dr. Małgorzata Peszyńska, Dr. Gabor C. Temes, Dr. Albrecht Jander, and Dr. Zhongfeng Wang, for their input, valuable discussions and accessibility. Special thanks are also given to Dr. David S. Birkes from the Department of Statistics for his help with the proof in my papers.

I am very grateful for the friendship of all of the members of our research group, especially Shiwei Zhao, Liang Xian, and Jie Gao, with whom I worked closely and puzzled over many of the same problems.

Finally, I would like to thank my parents and my wife Qian for their lifelong love and support. It is far from sufficient to express my gratitude with only a few words. Without them, this work could not have been completed.

TABLE OF CONTENTS

TABLE OF CONTENTS (Continued)

Page

TABLE OF CONTENTS (Continued)

LIST OF FIGURES

LIST OF FIGURES (Continued)

Figure Page

Multi-Antenna OFDM Systems in the Presence of Phase Noise and Doubly-Selective Fading

1. INTRODUCTION

1.1. Background and Motivation

The demand for capacity in cellular and wireless local area networks (WLAN) has grown in a literally explosive manner during the last decade. In particular, the need for wireless Internet access and multimedia applications require an increase in information throughput with orders of magnitude higher than data rates made available by today's technology. One major technological breakthrough that will make this increase in data rate possible is the use of multiple antennas at transmitters and receivers in the system. The antenna elements in a multiple-input multiple-output (MIMO) system [1, 2] could be exploited to achieve larger coverage area and/or higher data throughput than traditional single-antenna systems. In a rich-scattering environment, MIMO systems could provide high spectral efficiency through spatial multiplexing. The transmit and receive antenna elements in a MIMO system could also be used to provide spatial diversity and to mitigate the effect of multipath fading. To achieve full transmit diversity, it is necessary to code across both space and time domains through space-time coding (STC) [3–5].

There are two main types of space-time codes: space-time trellis code (STTC) and space-time block code (STBC). Orthogonal STBC was originally proposed in [3] for systems with two transmit antennas. The orthogonal design was then generalized to systems with an arbitrary number of transmit antennas [5]. Since complex orthogonal

STBCs with full spatial diversity and full transmission rate do not exist for more than two transmit antennas [5], quasi-orthogonal design with rate one but partial diversity was investigated in [6, 7]. Recently, quasi-orthogonal STBC with constellation rotation was proposed in [8, 9] to provide full diversity.

Mobile wireless channels exhibit time-varying multipath fading, and the rapidity of which can be quantified by the Doppler shift. STBCs are typically designed assuming a quasi-static channel. Time-selective fading will cause intertransmit-antenna interference (ITAI) in orthogonal codes. For quasi-orthogonal codes, channel time variations cause ITAI among all symbols instead of pairs of symbols and the pairwise maximum-likelihood (ML) decoding scheme [8] becomes suboptimal. To mitigate ITAI caused by channel time variations, many schemes have been studied: a simplified linear quasi-ML decoder for orthogonal STBC with two transmit antennas was proposed to cancel ITAI when the channel varies from one signaling interval to another [10]; a low-complexity receiver was proposed to lower the bit-error-rate (BER) floor of orthogonal STBC with four transmit antennas using the conventional ML decoding method [11]; and a two-step zero-forcing (ZF) scheme was applied to cancel ITAI and to eliminate the error floor of quasi-orthogonal STBC [12].

For high-speed signaling that requires a wide signal bandwidth, wireless channels could introduce frequency-selective fading, and the effect of multipath delay must be considered in system design. Orthogonal frequency division multiplexing (OFDM) [13] techniques have been investigated extensively to combat the effect of multipath delay. Over the last decade, OFDM has been widely adopted and implemented in wire and wireless communications, such as digital terrestrial TV broadcasting (DTTB), digital subscriber line (DSL), European high performance local area networks (HIPERLAN), WLAN and wireless metropolitan area networks (WMAN). OFDM is a block modulation approach which transmits a block of symbols in parallel over a number of sub-

carriers. The simultaneous transmission of those subcarriers effectively increases the symbol duration, resulting in negligible intersymbol interference (ISI) that multipath delay might cause. OFDM may be combined with multiple antennas at the transmitter and receiver to increase diversity gain and to improve system spectral efficiency in frequency-selective environments [14].

OFDM is effective in avoiding ISI that multipath delay might cause. However, it is sensitive to time-selective fading which destroys the orthogonality among different subcarriers in one OFDM symbol, causing intercarrier interference (ICI) [15, 16]. Another disadvantage of OFDM is its sensitivity to phase noise, which is a random process caused by the fluctuation of the transmitter and receiver oscillators [36]. It is widely accepted that phase noise in OFDM has two major effects [18,37]: common phase error (CPE), a constant rotation to the signal constellation, and ICI due to the loss of orthogonality among subcarriers caused by the fast changes of the oscillator phase. The CPE term is the same for all subcarriers within one OFDM symbol interval and changes slowly from one symbol to another. If phase noise level is low, CPE approximately equals the mean of the phase deviation of an oscillator within one OFDM symbol. The ICI term is a random process. Schemes which compensate phase noise in OFDM systems have been proposed in [20, 24]. In [22], the signal-to-interference-plus-noise ratio (SINR) expression for single-antenna OFDM systems with various phase-noise levels and different number of subcarriers was derived.

MIMO antennas can be combined with OFDM to improve spectral efficiency through spatial multiplexing [14] and to achieve spatial diversity through STC [23, 24]. Support of high mobility in MIMO-OFDM systems is critical for many applications (e.g., IEEE 802.16e). Similar to single-antenna OFDM, performance of MIMO-OFDM is also highly sensitive to channel time selectivity. Error performance of MIMO-OFDM systems in the presence of time-selective fading was analyzed in [25]. Besides, MIMO-

OFDM is highly vulnerable to phase noise. CPE estimation schemes for MIMO-OFDM systems were derived in [26] and in [27] a decision-directed approach for compensation of phase noise in MIMO-OFDM systems was studied. In OFDM systems with N_s subcarriers, the OFDM symbol duration could be N_s times of the data symbol period. Consequently, ITAI caused by channel time variations in space-time coded OFDM (ST-OFDM) systems is much more pronounced than in common STC systems.

1.2. Outline of the Dissertation

The objective of this dissertation is to address various aspects related to multi-antenna OFDM systems in the presence of phase noise and doubly-selective fading, which include performance analysis, channel estimation and equalization, receiver design and signal detection.

In Chapter 3, we study the impact of time-selective fading on quasi-orthogonal ST-OFDM systems over frequency-selective Rayleigh fading channels. We quantify the impact of Doppler frequency shift by deriving, via an analytical approach, the expressions of carrier-to-interference ratio (CIR) and SINR. We observe that system error performance is insensitive to changes in vehicle speeds and the channel power-delay profile, but very sensitive to changes in the number of subcarriers. We also evaluate the performance of five different detection schemes in the presence of time-selective fading. We show that, although there exist differences in their relative performances, all these detection schemes suffer from an irreducible error floor.

MIMO-OFDM systems are very vulnerable to time-selective fading as channel time variations destroy the orthogonality among subchannels, causing ICI. In Chapter 4, we apply frequency-domain correlative coding in MIMO-OFDM systems over doubly-selective fading channels to mitigate ICI. We derive an analytical expression of CIR

to quantify the impact of time-selective fading and demonstrate the effectiveness of correlative coding in mitigating ICI in MIMO-OFDM systems.

In quasi-orthogonal ST-OFDM systems, channel time variations cause not only ICI among different subcarriers in one OFDM block, but also ITAI. When applied in fast fading channels, common ST-OFDM receivers usually suffer from an irreducible error floor. In Chapter 5, we apply frequency-domain correlative coding combined with a modified decision-feedback (DF) detection scheme to effectively suppress the error floor of quasi-orthogonal ST-OFDM over fast fading channels. We also derive the analytical expressions of CIR and ITAI when frequency-domain correlative coding is applied at the transmitter to quantify the impact of time-varying fading. The effectiveness of the proposed scheme in mitigating the effects of channel time selectivity is demonstrated through comparison with existing schemes such as ZF, two-step ZF (TS-ZF), and sequential DF estimation.

In Chapter 6, we analyze the effects of phase noise to MIMO-OFDM systems over doubly-selective Rayleigh fading channels. Similar to single-antenna OFDM, MIMO-OFDM suffers from significant performance degradation due to phase noise and time-selective fading. We derive the expressions for CIR and SINR. After characterizing CPE caused by phase noise and ICI caused by phase noise as well as time-selective fading, we then derive a minimum mean-squared error (MMSE)-based scheme to mitigate the effect of both phase noise and time-selective fading. We also evaluate and compare the performances of various detection schemes combined with the proposed CPE mitigation scheme. Through numerical results, we examine the relative performances and the potential error floors of these detection schemes.

This dissertation is concluded in Chapter 7. Most of results presented in this dissertation have been published or accepted for publication in [28–32].

1.3. Notation Summary

In this dissertation, scalar variables are written as plain lower-case letters, vectors as bold-face lower-case letters, and matrices as bold-face upper-case letters. Some further used notations and commonly used acronyms are listed in the following:

$E[\cdot]$	Expectation
$var(\cdot)$	Variance
$cov(\cdot)$	Covariance
$(\cdot)^T$	Transpose
$(\cdot)^*$	Complex conjugate
$(\cdot)^H$	Hermitian transpose
$(\cdot)^{1/2}$	Matrix square-root
$(\cdot)^\dagger$	Pseudoinverse
$\lvert\cdot\rvert$	Absolute magnitude
$\lVert\cdot\rVert_F$	Frobenius norm
$\delta(\cdot)$	Dirac delta function
$tr(\cdot)$	Sum of diagonal elements
$J_0(\cdot)$	Zero-order Bessel function of the first kind
$vec(\boldsymbol{V})$	Vector obtained by vertically stacking the columns of matrix $\boldsymbol{V}$
$\otimes$	Kronecker product
$\boldsymbol{I}_N$	$N \times N$ identity matrix
$\{\boldsymbol{A}\}_{ij}$	(i,j)th element of matrix $\boldsymbol{A}$
AWGN	Additive white Gaussian noise
BER	Bit-error-rate
BPSK	Binary phase shift keying

CIR	Carrier-to-interference ratio
CP	Cyclic prefix
CPE	Common phase error
CSI	Channel state information
DTTB	Digital terrestrial TV broadcasting
DF	Decision-feedback
DFT	Discrete Fourier transform
DSL	Digital subscriber line
FEC	Forward error correction
IBI	Interblock interference
ICI	Intercarrier interference
IDFT	Inverse discrete Fourier transform
i.i.d.	Independent and identically distributed
ITAI	Intertransmit-antenna interference
ISI	Intersymbol interference
HIPERLAN-LAN	European high performance local area networks
LS	Least square
MIMO	Multiple-input multiple-output
ML	Maximum-likelihood
MMSE	Minimum mean-squared error
MRC	Maximum ratio combing
MSE	Mean-square error
OFDM	Orthogonal frequency division multiplexing
QPSK	Quaternary phase shift keying
rms	Root-mean square

SDFSE	Sequential DF sequence estimation
SER	Symbol-error-rate
SINR	Signal-to-interference-plus-noise ratio
SNR	Signal-to-noise ratio
ST-OFDM	Space-time coded OFDM
STBC	Space-time block code
STC	Space-time coding
STTC	Space-time trellis code
TS-ZF	Two-step zero-forcing
WLAN	Wireless local area networks
WMAN	Wireless metropolitan area networks
WSSUS	Wide sense stationary uncorrelated scattering
ZF	Zero-forcing

2. OVERVIEW

2.1. Multi-Antenna OFDM Systems Model

2.1.1. Space-Time Coded OFDM Transmitter

Consider a MIMO-OFDM system with N_t transmit antennas, N_r receive antennas, and N_s subcarriers. The channel is frequency-selective Rayleigh fading and is modeled as quasi-static, allowing it to be constant over an OFDM block and change independently from one block to another.

Input symbol sequence $\{a(0), a(1), \cdots, a(N_t N_s - 1)\}$ is serial-to-parallel converted into N_t sequences, each of length N_s, as

$$a_p(k) = a(k + (p-1)N_s);\ k = 0, \cdots, N_s - 1, p = 1, \cdots, N_t.$$

Each of the N_s sequences $\{a_1(k), a_2(k) \cdots, a_{N_t}(k)\},\ k = 0, \cdots, N_s - 1$, is mapped to a matrix $\mathbf{\Psi}_k$ of size $N_t \times N$ (N is the number of time burst defined in STC) by using the orthogonal space-time block coding scheme given in [5]

$$\{a_1(k), a_2(k) \cdots, a_{N_t}(k)\} \Rightarrow \mathbf{\Psi}_k,\ k = 0, \cdots, N_s - 1. \tag{2.1}$$

For instance, if we apply the Alamouti code [3] for a system with two transmit antennas, $\mathbf{\Psi}_k$ is obtained as

$$\mathbf{\Psi}_k = \begin{bmatrix} a_1(k) & -a_2^*(k) \\ a_2(k) & a_1^*(k) \end{bmatrix} \tag{2.2}$$

Then we take the inverse discrete Fourier transform (DFT) of $\{\mathbf{\Psi}_0, \cdots, \mathbf{\Psi}_{N_s-1}\}$ as

$$\boldsymbol{S}_m = \frac{1}{\sqrt{N_s}} \sum_{k=0}^{N_s-1} \mathbf{\Psi}_k \cdot e^{j\frac{2\pi}{N_s}mk},\ \ m = 0, \cdots, N_s - 1 \tag{2.3}$$

where $j = \sqrt{-1}$, to form the transmitted signals represented in a matrix form as

$$\boldsymbol{S} = [\boldsymbol{S}_0^T,\ \boldsymbol{S}_1^T,\ \cdots,\ \boldsymbol{S}_{N_s-1}^T]^T \tag{2.4}$$

where $\boldsymbol{S}_m$ is given by

$$\boldsymbol{S}_m = \begin{bmatrix} s_{1,0}(m) & \cdots & s_{1,(N-1)}(m) \\ \vdots & \ddots & \vdots \\ s_{N_t,0}(m) & \cdots & s_{N_t,(N-1)}(m) \end{bmatrix}. \tag{2.5}$$

It is easy to recognize that $\{s_{p,n}(m)\},\ p = 1,\ldots,N_t,\ n = 0,\ldots,N-1,\ m = 0,\ldots,N_s-1$, are transmitted in parallel using the N_s subcarriers and N_t antennas over N time intervals. Thus, each transmitted symbol is coded onto the space, time, and frequency dimensions through the ST-OFDM process.

2.1.2. MIMO Wireless Channel

In a frequency-selective fading channel with L resolvable paths, there exists mutual interference between adjacent OFDM blocks. This interblock interference (IBI) could be cancelled by adding a cyclic prefix (CP) of length c_p ($c_p \geq L$) to each transmitted block. At the receiver, the CP is discarded, leaving IBI-free information-bearing signals. The channel matrix $\boldsymbol{H}$ is block-circulant with $N_s \times N_s$ blocks expressed as

$$\boldsymbol{H} = \begin{bmatrix} \boldsymbol{H}(0) & \cdots & \mathbf{0} & \boldsymbol{H}(L-1) & \cdots & \boldsymbol{H}(1) \\ \vdots & & & \vdots & & \vdots \\ \boldsymbol{H}(L-1) & \cdots & \boldsymbol{H}(1) & \boldsymbol{H}(0) & \mathbf{0} & \cdots \\ \vdots & & & \vdots & & \vdots \\ \mathbf{0} & \cdots & \boldsymbol{H}(L-1) & \cdots & \boldsymbol{H}(1) & \boldsymbol{H}(0) \end{bmatrix} \tag{2.6}$$

where $\mathbf{0}$ is a zero matrix of size $N_r \times N_t$. Each nonzero block of $\boldsymbol{H}$ represents the MIMO spatial channel matrix of size $N_r \times N_t$ for a particular path l and is expressed as

$$\boldsymbol{H}(l) = \begin{bmatrix} h_{1,1}(l) & \cdots & h_{1,N_t}(l) \\ \vdots & \ddots & \vdots \\ h_{N_r,1}(l) & \cdots & h_{N_r,N_t}(l) \end{bmatrix},\ l = 0,\cdots,L-1 \tag{2.7}$$

where $h_{i,j}(l)$, $1 \leq i \leq N_r,\ 1 \leq j \leq N_t$, is zero-mean complex Gaussian with unit variance. In a practical scenario, insufficient spacing among antennas will cause spatial correlation. Thus, the channel matrix $\boldsymbol{H}(l)$ can be written in a general form as [33]

$$\boldsymbol{H}(l) = \boldsymbol{D}^{1/2}\boldsymbol{H}_w(l)\boldsymbol{B}^{1/2},\ \ l = 0, \cdots, L-1 \tag{2.8}$$

where $\boldsymbol{H}_w(l)$ is an $N_r \times N_t$ matrix whose elements are independent and identically distributed (i.i.d.) complex Gaussian random variables with zero mean and unit variance, and $\boldsymbol{D} = \boldsymbol{D}^{1/2}(\boldsymbol{D}^{1/2})^H$ and $\boldsymbol{B} = \boldsymbol{B}^{1/2}(\boldsymbol{B}^{1/2})^H$ are, respectively, the receive and the transmit correlation matrices. For example, the correlation matrices for a 2×2 MIMO system are written as [34]

$$\boldsymbol{D} = \begin{bmatrix} 1 & \rho \\ \rho^* & 1 \end{bmatrix} \tag{2.9a}$$

$$\boldsymbol{B} = \begin{bmatrix} 1 & \mu \\ \mu^* & 1 \end{bmatrix} \tag{2.9b}$$

where ρ and μ are the complex antenna correlation coefficients.

2.1.3. Space-Time Coded OFDM Receiver

The received signal matrix $\boldsymbol{R}$ can be expressed as

$$\boldsymbol{R} = \boldsymbol{H}\boldsymbol{S} + \boldsymbol{V} \tag{2.10}$$

where $\boldsymbol{V} = [\boldsymbol{V}_0^T, \boldsymbol{V}_1^T, \cdots, \boldsymbol{V}_{N_s-1}^T]^T$ is an additive white Gaussian noise (AWGN) matrix whose elements are i.i.d.. Thus, $E[vec(\boldsymbol{V}) \cdot vec(\boldsymbol{V})^H] = \sigma^2\boldsymbol{I}_{N_rN_sN}$, where σ^2 is the variance of the zero-mean noise samples when the transmitted symbol energy is normalized to unity. Since $\boldsymbol{H}$ has the block Toeplitz structure, it has the following eigen-decomposition

$$\boldsymbol{H} = \boldsymbol{U}_{N_r}^H\boldsymbol{\Lambda}\boldsymbol{U}_{N_t} \tag{2.11}$$

with

$$\boldsymbol{U}_{N_r} = \boldsymbol{U} \otimes \boldsymbol{I}_{N_r},\ \boldsymbol{U}_{N_r}\boldsymbol{U}_{N_r}^H = \boldsymbol{I}_{N_r N_s} \tag{2.12a}$$

$$\boldsymbol{U}_{N_t} = \boldsymbol{U} \otimes \boldsymbol{I}_{N_t},\ \boldsymbol{U}_{N_t}\boldsymbol{U}_{N_t}^H = \boldsymbol{I}_{N_t N_s} \tag{2.12b}$$

where $\boldsymbol{U}$ is the $N_s \times N_s$ unitary DFT matrix given by

$$\boldsymbol{U} = \frac{1}{\sqrt{N_s}} \begin{bmatrix} 1 & 1 & \cdots & 1 \\ \vdots & & \cdots & \vdots \\ 1 & e^{-j\frac{2\pi}{N_s}(N_s-1)} & \cdots & e^{-j\frac{2\pi}{N_s}(N_s-1)(N_s-1)} \end{bmatrix} \tag{2.13}$$

and $\boldsymbol{\Lambda}$ is a block diagonal matrix whose (k,k)th block is given by

$$\begin{aligned} \boldsymbol{\Lambda}_k &= \sum_{l=0}^{L-1} \boldsymbol{H}(l) \cdot e^{-j\frac{2\pi}{N_s}kl} \\ &= \boldsymbol{D}^{1/2} \left(\sum_{l=0}^{L-1} \boldsymbol{H}_w(l) \cdot e^{-j\frac{2\pi}{N_s}kl} \right) \boldsymbol{B}^{1/2},\ \ k = 0, \cdots, N_s - 1. \end{aligned} \tag{2.14}$$

At the receiver, a matrix $\boldsymbol{X}$ is generated by multiplying $\boldsymbol{R}$ with $\boldsymbol{U}_{N_r}$ as

$$\begin{aligned} \boldsymbol{X} &= [\boldsymbol{X}_0^T, \boldsymbol{X}_1^T, \cdots, \boldsymbol{X}_{N_s-1}^T]^T \\ &= \boldsymbol{U}_{N_r}\boldsymbol{R} \\ &= \boldsymbol{\Lambda}\boldsymbol{U}_{N_t}\boldsymbol{S} + \boldsymbol{U}_{N_r}\boldsymbol{V} \end{aligned} \tag{2.15}$$

where

$$\boldsymbol{X}_k = \boldsymbol{\Lambda}_k\boldsymbol{\Psi}_k + \boldsymbol{W}_k,\ k = 0, \cdots, N_s - 1 \tag{2.16}$$

and

$$\boldsymbol{W}_k = \frac{1}{\sqrt{N_s}} \sum_{m=0}^{N_s-1} \boldsymbol{V}_m \cdot e^{-j\frac{2\pi}{N_s}mk}. \tag{2.17}$$

Note that $\boldsymbol{W} = [\boldsymbol{W}_0^T, \boldsymbol{W}_1^T, \cdots, \boldsymbol{W}_{N_s-1}^T]^T$ has the same distribution as $\boldsymbol{V}$, i.e., all elements of $\boldsymbol{W}$ are i.i.d. with zero mean and variance σ^2.

It has been shown [14] that the maximum diversity order achievable in a MIMO system with N_t transmit antennas, N_r receive antennas, and L resolvable multipath

components is $N_t N_r L$. However, the conventional ST-OFDM scheme described above is suboptimal in that it is not capable of exploiting frequency diversity in a frequency-selective environment subject to the property of OFDM; it achieves a diversity order of only $N_r N_t$.

2.1.4. Achieving Full Diversity for Space-Time Coded OFDM

Due to the property of OFDM which converts the frequency-selective fading channel into flat fading channel, conventional ST-OFDM cannot achieve maximum diversity order. We then present a simple design of ST-OFDM to achieve full spatial and frequency diversities over frequency-selective fading channels.

Consider a multi-antenna OFDM system with N_t transmit antennas, N_r receive antennas, and N_s subcarriers over a frequency-selective Rayleigh fading channel with L resolvable paths. The channel is modeled as quasi-static, allowing it to be constant over an OFDM block and change independently from one block to another. The number of subcarriers N_s is chosen to be such that N_s/L is an integer. Input symbol sequence $\{a(0), a(1), \cdots, a((N_s/L)N_t - 1)\}$ is serial-to-parallel converted into N_t sequences of length N_s/L as

$$a_p(f) = a\left(f + \frac{p-1}{L}N_s\right) \tag{2.18}$$

where $p = 1, \cdots, N_t,\ f = 0, \cdots, N_s/L - 1$. Each of the $N_s/L - 1$ sequences $\{a_1(f), a_2(f) \cdots, a_{N_t}(f)\}, f = 0, \cdots, N_s/L - 1$, is mapped to a matrix $\mathbf{\Phi}_f$ by using the orthogonal space-time block coding technique given in [5] as

$$\{a_1(f), a_2(f) \cdots, a_{N_t}(f)\} \Rightarrow \mathbf{\Phi}_f,\ f = 0, \cdots, \frac{N_s}{L} - 1. \tag{2.19}$$

Matrix $\mathbf{\Phi}_f$ is of size $N_t \times N$, where N is the number of time burst defined in STC. We then construct N_s matrices of the same size as $\mathbf{\Phi}_f$ using the repetition coding technique

$$\mathbf{\Psi}_{l\frac{N_s}{L}+f} = \mathbf{\Phi}_f, \;\; f = 0, \cdots, N_s/L-1; \; l = 0, \cdots, L-1 \tag{2.20}$$

through which each $\mathbf{\Phi}_f$ is repeated L times, forming $\{\mathbf{\Psi}_0, \cdots, \mathbf{\Psi}_{N_s-1}\}$.

Following the analysis in the aforementioned sections of ST-OFDM systems over quasi-static channels, we obtain

$$\begin{aligned} \boldsymbol{X} &= [\boldsymbol{X}_0^T, \boldsymbol{X}_1^T, \cdots, \boldsymbol{X}_{N_s-1}^T]^T \\ &= \mathbf{\Lambda} \boldsymbol{U}_{N_t} \boldsymbol{U}_{N_t}^H \mathbf{\Psi} + \boldsymbol{U}_{N_r} \boldsymbol{V} \end{aligned} \tag{2.21}$$

where $\mathbf{\Psi} = [\mathbf{\Psi}_0^T, \mathbf{\Psi}_1^T, \cdots, \mathbf{\Psi}_{N_s-1}^T]^T$ and $\mathbf{\Psi}_l, \; l = 0, \cdots, N_s-1$, was defined in (2.20). Thus, we have

$$\boldsymbol{X}_k = \mathbf{\Lambda}_k \mathbf{\Psi}_k + \boldsymbol{W}_k, \; k = 0, \cdots, N_s - 1 \tag{2.22}$$

where

$$\boldsymbol{W}_k = \frac{1}{\sqrt{N_s}} \sum_{m=0}^{N_s-1} \boldsymbol{V}_m \cdot e^{-j\frac{2\pi}{N_s}mk}. \tag{2.23}$$

Substituting (2.20) into (2.22) yields

$$
\begin{aligned}
\boldsymbol{X}_0 &= \boldsymbol{\Lambda}_0\boldsymbol{\Phi}_0 + \boldsymbol{W}_0 \\
\boldsymbol{X}_1 &= \boldsymbol{\Lambda}_1\boldsymbol{\Phi}_1 + \boldsymbol{W}_1 \\
&\vdots \\
\boldsymbol{X}_{\frac{N_s}{L}-1} &= \boldsymbol{\Lambda}_{\frac{N_s}{L}-1}\boldsymbol{\Phi}_{\frac{N_s}{L}-1} + \boldsymbol{W}_{\frac{N_s}{L}-1} \\
\boldsymbol{X}_{\frac{N_s}{L}} &= \boldsymbol{\Lambda}_{\frac{N_s}{L}}\boldsymbol{\Phi}_0 + \boldsymbol{W}_{\frac{N_s}{L}} \\
\boldsymbol{X}_{\frac{N_s}{L}+1} &= \boldsymbol{\Lambda}_{\frac{N_s}{L}+1}\boldsymbol{\Phi}_1 + \boldsymbol{W}_{\frac{N_s}{L}+1} \\
&\vdots \\
\boldsymbol{X}_{\frac{2N_s}{L}-1} &= \boldsymbol{\Lambda}_{\frac{2N_s}{L}-1}\boldsymbol{\Phi}_{\frac{N_s}{L}-1} + \boldsymbol{W}_{\frac{2N_s}{L}-1} \\
&\vdots \\
\boldsymbol{X}_{\frac{L-1}{L}N_s} &= \boldsymbol{\Lambda}_{\frac{L-1}{L}N_s}\boldsymbol{\Phi}_0 + \boldsymbol{W}_{\frac{L-1}{L}N_s} \\
\boldsymbol{X}_{\frac{L-1}{L}N_s+1} &= \boldsymbol{\Lambda}_{\frac{L-1}{L}N_s+1}\boldsymbol{\Phi}_1 + \boldsymbol{W}_{\frac{L-1}{L}N_s+1} \\
&\vdots \\
\boldsymbol{X}_{N_s-1} &= \boldsymbol{\Lambda}_{N_s-1}\boldsymbol{\Phi}_{\frac{N_s}{L}-1} + \boldsymbol{W}_{N_s-1}.
\end{aligned}
$$

Each transmitted matrix $\boldsymbol{\Phi}_f,\ f = 0, \cdots, N_s/L - 1$, is received in L duplicates, each of which is multiplied by a channel matrix corresponding to a different subcarrier. The minimum distance between the indexes of any two subcarriers carrying the same transmitted signal $\boldsymbol{\Phi}_f$ is N_s/L. If maximum ratio combing (MRC) [35] is applied to combine the L duplicates, a maximum frequency diversity order of L can be achieved. In a practical system, the achievable frequency diversity order depends on the correlation among the L channel matrices.

To analyze the performance of the scheme, we consider, without loss of generality, detection of transmitted matrix $\boldsymbol{\Phi}_0$ only. For simplicity of illustration, we focus on a MIMO system with two transmit antennas and two receive antennas employing

the complex orthogonal STBC given in [3]. Thus

$$\mathbf{\Phi}_0 = \begin{bmatrix} a_1(0) & -a_2^*(0) \\ a_2(0) & a_1^*(0) \end{bmatrix}. \tag{2.24}$$

Let

$$\mathbf{\Lambda}_{k'} = \begin{bmatrix} \lambda_{11}(k') & \lambda_{12}(k') \\ \lambda_{21}(k') & \lambda_{22}(k') \end{bmatrix}, \quad k' = 0, \frac{N_s}{L}, \cdots, \frac{L-1}{L}N_s \tag{2.25}$$

and

$$\boldsymbol{W}_{k'} = \begin{bmatrix} w_{11}(k') & w_{12}(k') \\ w_{21}(k') & w_{22}(k') \end{bmatrix}, \; k' = 0, \frac{N_s}{L}, \cdots, \frac{L-1}{L}N_s. \tag{2.26}$$

Following the ML decoding procedure for orthogonal STBC described in [3] and MRC, we obtain the detected symbol for $a_1(0)$ in (2.24) as

$$\hat{a}_1(0) = a_1(0) + \frac{\sum_{k'}\sum_{i=1}^{2}[\lambda_{i1}^*(k')w_{i1}(k') + \lambda_{i2}(k')w_{i2}^*(k')]}{\sum_{k'}\sum_{i=1}^{2}\sum_{j=1}^{2}|\lambda_{ij}(k')|^2} \tag{2.27}$$

where the sum over k' is extended to all values of k' ($k' = 0, \frac{N_s}{L}, \cdots, \frac{L-1}{L}N_s$). It has been shown [14] that the maximum diversity order achievable in a MIMO system with N_t transmit antennas, N_r receive antennas, and L resolvable multipath components is N_tN_rL. The proposed scheme achieves full spatial and frequency diversities if channel coefficients $\lambda_{ij}(k'), k' = 0, \frac{N_s}{L}, \cdots, \frac{L-1}{L}N_s$, are mutually independent.

The analysis becomes more difficult in a practical scenario. This is because that channel matrices for different subcarriers are typically correlated and $\lambda_{ij}(k')$ for different values of k' may not have the same variance.

Consider a channel model with L resolvable multipath components given as (Eq. (2), [41])

$$h(\tau) = \sum_{l=0}^{L-1} \alpha_l \delta(\tau - \tau_l T_s) \tag{2.28}$$

where α_l is the zero-mean complex Gaussian random variable and τ_l is the delay of the lth path normalized with respect to the OFDM symbol duration T_s, which also equals the sampling period. The channel has a power-delay profile $\theta(\tau_l) = e^{-\tau_l/\tau_{rms}}$, where τ_{rms} represents the root-mean square (rms) delay spread. We assume that delays τ_l are independently and uniformly distributed over the CP c_p. Let the correlation matrix (frequency correlation) of the channel coefficients at the L different subcarriers that involve transmitted signal $\mathbf{\Phi}_0$ be

$$\boldsymbol{C}_{ij} = E[\boldsymbol{M}_{ij}\boldsymbol{M}_{ij}^H] = \boldsymbol{C} \tag{2.29}$$

where $\boldsymbol{M}_{ij} = [\lambda_{ij}(0), \lambda_{ij}(\frac{N_s}{L}), \cdots, \lambda_{ij}(\frac{L-1}{L}N_s)]^T,\ i = 1, 2,\ j = 1, 2$, and correlation characteristics are assumed independent of antenna indexes. Each of the off-diagonal entries of $\boldsymbol{C}$ is a function of the distance between two different subcarriers, ω ($\frac{N_s}{L} \leq \omega \leq \frac{L-1}{L}N_s$), and is expressed as (Appendix A, [41])

$$c(\omega) = \frac{1 - e^{-P(1/\tau_{rms} + 2\pi j\omega/N_s)}}{\tau_{rms}(1 - e^{-P/\tau_{rms}})(\frac{1}{\tau_{rms}} + 2\pi j\frac{\omega}{N_s})}. \tag{2.30}$$

Note that here both τ_{rms} and ω are represented in terms of number of samples, rather than actual values in seconds or radians/s.

Performance of the proposed scheme for a MIMO-OFDM system with $N_t = 2$, $N_r = 2$, and $N_s = 128$ is simulated. Within each OFDM block, the Alamouti code [3] with quaternary phase shift keying (QPSK) is applied. Two cases are simulated: 1) $c_p = L = 2$, $\tau_0 = 0, \tau_1 = 2$, and 2) $c_p = L = 3$, $\tau_0 = 0, \tau_1 = 2, \tau_2 = 3$. Symbol-error-rate (SER) performance of the proposed scheme with different values of τ_{rms} is shown in Fig. 2.1. For comparison, SER curves of three baseline systems (conventional ST-OFDM without frequency diversity, with frequency diversity 2, and with frequency diversity 3, all with full spatial diversity) are also included in the same figure. It is observed that with the same set of values of L, c_p, and τ_l, performance of the proposed

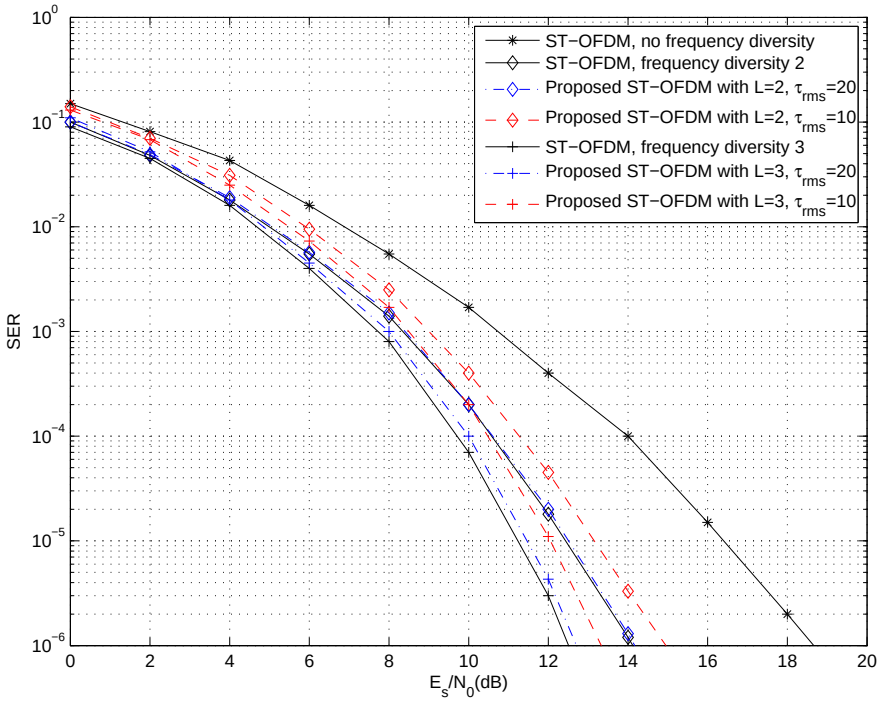

FIGURE 2.1. Error performance of the repetition coding scheme.

scheme depends on the value of τ_{rms}. A smaller τ_{rms} results in a larger difference in the power of different channel coefficients $\lambda_{ij}(k')$, which causes a higher SER. Also, a large value of $|c(\omega)|$ between two subcarriers carrying the same transmitted signal results in a loss of frequency diversity. With $\tau_{rms} = 20$, the proposed scheme performs very close to the baseline systems. It is also found that the proposed scheme will lose full frequency diversity as the ratio τ_l/τ_{rms} increases.

It should be mentioned that the increase in diversity is achieved at the expense of data throughput loss with a factor of $\frac{L-1}{L}$. Nevertheless, the scheme analyzed is very simple to implement and no feedback of channel state information (CSI) is needed to exploit frequency diversity in a frequency-selective environment. Thus it could be very useful when system diversity order is a more important design consideration.

2.2. Phase Noise Model

Phase noise $\phi(t)$, generated at both transmitter and receiver oscillators, may be described as a continuous Brownian motion process or a random Wiener process with zero mean and variance $2\pi\beta t$, where β denotes the two-sided 3-dB linewidth of the Lorentzian power density spectrum of the free-running carrier generator [36]. As a random Wiener process, phase noise has independent Gaussian increments and its power is a monotonically increasing function of time. This indicates that its power could be infinitely large as time increases. However, if restricted to a finite period, phase noise can be modeled as a filtered Gaussian random variable [37].

If discrete phase noise model is of interest, we need to consider discretized Brownian motion $\phi(n) = \phi(nT_s)$, where T_s is the data symbol period. Thus we have $\phi(n+1) = \phi(n) + \varsigma(n)$, where $\varsigma(n) \sim \mathcal{N}(0, 2\pi\beta T_s)$ is a Gaussian random variable with zero mean and variance $\sigma_\varsigma^2 = 2\pi\beta T_s$.

3. IMPACT OF TIME-SELECTIVE FADING ON SPACE-TIME CODED OFDM SYSTEMS

3.1. Introduction

Mobile wireless channels exhibit time-varying multipath fading, and the rapidity of which can be quantified by the Doppler shift. OFDM is effective in avoiding ISI that multipath delay might cause. However, it is sensitive to time-selective fading which destroys the orthogonality among different subcarriers in one OFDM symbol, causing ICI [15, 16]. STC is a technique to achieve transmit diversity in a multi-antenna system by coding across both space and time domains [4]. STBC was originally proposed in [3] for systems with two transmit antennas. The orthogonal design was then generalized to systems with an arbitrary number of transmit antennas [5]. Quasi-orthogonal STC design with rate one but partial diversity was investigated in [6, 7]. Recently, quasi-orthogonal STBC with constellation rotation was proposed in [8, 9] to provide full diversity. STBCs are typically designed assuming a quasi-static channel. Time-selective fading will cause ITAI in orthogonal codes. For quasi-orthogonal codes, channel time variations cause ITAI among all symbols, and the pairwise ML decoding scheme [8] becomes suboptimal. To mitigate ITAI caused by channel time variations, many schemes have been studied, which include a simplified linear quasi-ML decoder [10], a low-complexity receiver using the conventional ML decoding method [11], and a TS-ZF scheme [12].

Multiple antennas can be combined with OFDM to achieve spatial diversity and/or to increase spectral efficiency through spatial multiplexing [14]. For a multi-antenna OFDM system in a frequency-selective environment, STC schemes must be extended to include the frequency element, forming ST-OFDM [23, 24]. Similar to single-antenna OFDM, ST-OFDM is also sensitive to the Doppler shift and frequency

errors which destroy the orthogonality among subcarriers, causing ICI [25]. In an OFDM system with N_s subcarriers, the OFDM symbol duration could be N_s times of the data symbol period. Consequently, ITAI caused by channel time variations in an ST-OFDM system is much more pronounced than in a common STC system.

While the problems caused by time-selective fading in ST-OFDM have been recognized, the exact quantitative impact of which has not been well understood yet. In this chapter, we analyze, via mainly an analytical approach, the impact of both ICI and ITAI to the performance of quasi-orthogonal ST-OFDM systems in the presence of time-selective Rayleigh fading. We also compare five detection schemes - the ZF scheme [38], the TS-ZF scheme [12], the MMSE scheme [38], the decorrelating DF scheme [39], and the MMSE-DF scheme [40] - and evaluate their SER floors.

3.2. System Model

We focus on a space-time block coded multi-antenna OFDM system with P transmit antennas, one receive antenna, and N_s subcarriers in a time-selective Rayleigh fading environment. Input symbols $\{a(i)\}$ are assumed to have the following properties

$$E[a(i)] = 0$$
$$E[a(i)a^*(j)] = \begin{cases} 1, & i = j \\ 0, & i \neq j \end{cases}.$$

The input sequence $\{a(i),\ i = 0, \cdots, N_sP - 1\}$ is serial-to-parallel converted into P sequences, each of length N_s, as

$$a_p(k) = a(k + (p-1)N_s),\ p = 1, \cdots, P,\ k = 0, \cdots, N_s - 1. \tag{3.1}$$

Each of the N_s sequences $\{a_1(k), \cdots, a_P(k)\},\ k = 0, \cdots, N_s - 1$, is mapped to a matrix $\mathbf{\Psi}_k$ of size $P \times P$ by using a quasi-orthogonal space-time block coding scheme

(e.g., the 4×4 quasi-orthogonal scheme given in [8]). Then we take the inverse DFT (IDFT) of $\{\boldsymbol{\Psi}_0, \cdots, \boldsymbol{\Psi}_{N_s-1}\}$, forming the transmitted signals as[1]

$$\boldsymbol{S}_m = \frac{1}{\sqrt{N_s}} \sum_{k=0}^{N_s-1} \boldsymbol{\Psi}_k \cdot e^{j\frac{2\pi}{N_s}mk}, \;\; m = 0, \cdots, N_s-1. \tag{3.2}$$

Note that $\boldsymbol{S}_m$ is a $P \times P$ matrix, which represents the transmitted signals on the mth subcarrier. If we define

$$\boldsymbol{\Psi} = [\boldsymbol{\Psi}_0^T, \; \cdots, \; \boldsymbol{\Psi}_{N_s-1}^T]^T, \quad (N_sP \times P) \tag{3.3a}$$

$$\boldsymbol{S} = [\boldsymbol{S}_0^T, \; \cdots, \; \boldsymbol{S}_{N_s-1}^T]^T, \quad (N_sP \times P) \tag{3.3b}$$

then $\boldsymbol{S}$ can be written as

$$\boldsymbol{S} = (\boldsymbol{U} \otimes \boldsymbol{I}_P)^H \boldsymbol{\Psi} \tag{3.4}$$

where $\boldsymbol{U}$ is the unitary DFT matrix with $\{\boldsymbol{U}\}_{ij} = 1/\sqrt{N_s}e^{(-2\pi\sqrt{-1}/N_s)ij}$, $0 \le i, j \le N_s-1$. In frequency-selective fading channels with L resolvable paths, there exists IBI. To minimize this IBI, a CP of length c_p ($c_p \ge L$) is added to each OFDM symbol. At the receiver, the CP is discarded, leaving IBI-free, information-bearing signals. Combined with the characteristics of time-selective fading, the $N_s \times N_sP$ spatiotemporal channel

---

[1]Note that this is not the only way to construct ST-OFDM. We adopted it because of its mathematical convenience. Implementation of this scheme requires $P \times P$ IDFT operations. If IDFT is done before STBC mapping, then only P IDFT operations are needed.

matrix $\boldsymbol{H}_t$ is expressed as[2]

$$\boldsymbol{H}_t = \begin{bmatrix} \boldsymbol{h}_{t,0}^T(0) & \cdots & \mathbf{0}^T & \boldsymbol{h}_{t,L-1}^T(0) & \cdots & \boldsymbol{h}_{t,1}^T(0) \\ \vdots & & & \vdots & & \vdots \\ \boldsymbol{h}_{t,L-1}^T(L-1) & \cdots & \boldsymbol{h}_{t,1}^T(L-1) & \boldsymbol{h}_{t,0}^T(L-1) & \cdots & \mathbf{0}^T \\ \vdots & & & \vdots & & \vdots \\ \mathbf{0}^T & \cdots & \boldsymbol{h}_{t,L-1}^T(N_s-1) & \cdots & \boldsymbol{h}_{t,1}^T(N_s-1) & \boldsymbol{h}_{t,0}^T(N_s-1) \end{bmatrix} \tag{3.5}$$

where L is less than or equal to N_s, $\mathbf{0}$ is a $P \times 1$ zero vector, and each nonzero block of $\boldsymbol{H}_t$ contains the $P \times 1$ channel vector $\boldsymbol{h}_{t,l}(n)$ for a particular path l at time nT_s (T_s is the data symbol period) expressed as

$$\boldsymbol{h}_{t,l}(n) = [h_{t,1,l}(n), \cdots, h_{t,P,l}(n)]^T, \ \ l = 0, \cdots, L-1, \ n = 0, \cdots, N_s - 1. \tag{3.6}$$

In the case of quasi-static fading[3] that allows the channel coefficients to be constant over an OFDM symbol and change independently from one symbol to another, $\boldsymbol{H}_t$ has a block-circulant structure. Without loss of generality, we omit the index of OFDM symbol period t in the following discussion.

Assuming a wide sense stationary uncorrelated scattering (WSSUS) channel [25], all elements of $\boldsymbol{h}_l(n)$ are modeled as independent complex Gaussian random variables with zero mean and equal variance. Let the power of the first path $\boldsymbol{h}_0(n)$ be normalized, i.e., all elements of $\boldsymbol{h}_0(n)$ have unit variance. The model of the channel with L resolvable multipath components can be expressed as (Eq. (2), [41])

$$h(\tau) = \sum_{l=0}^{L-1} \rho_l \delta(\tau - \tau_l T_s) \tag{3.7}$$

---

[2]The index in the parenthesis following $\boldsymbol{h}_{t,l}$ is the time index.

[3]Quasi-static fading models are appropriate to describe slow fading channels.

where ρ_l is the zero-mean complex Gaussian random variable, and τ_l is the delay of the lth path normalized with respect to T_s. The delays $\{\tau_l\}$ are assumed to be uniformly distributed over the CP c_p. The channel has an exponential power-delay profile $\theta(\tau_l) = e^{-\tau_l/\tau_{rms}}$, where τ_{rms} represents the rms delay spread, which is also normalized with respect to T_s. Since the channel is time-varying, the relationship between the channel coefficients for path l of antenna p at times nT_s and $(n+m)T_s$ can be described by using the auto-regressive model as [10, 12]

$$h_{p,l}(n+m) = \alpha_m h_{p,l}(n) + \beta_{p,l}(n+m) \tag{3.8}$$

where

$$\alpha_m = \frac{E\left[h_{p,l}(n) \cdot h^*_{p,l}(n+m)\right]}{e^{-\frac{\tau_l}{\tau_{rms}}}} = J_0(2\pi m f_d T_s) \tag{3.9}$$

where f_d is the Doppler shift, $J_0(\cdot)$ is the zero-order Bessel function of the first kind, and $\beta_{p,l}(n)$ are independent (for different indices p, l, and n) complex Gaussian random variables with zero mean and variance

$$\sigma^2_\beta = \begin{cases} 1-\alpha_m^2, & l = 0 \\ e^{-\frac{\tau_l}{\tau_{rms}}}(1-\alpha_m^2), & l \neq 0. \end{cases} \tag{3.10}$$

The received signals can be expressed in an $N_s \times P$ matrix as

$$\boldsymbol{R} = \boldsymbol{H}\boldsymbol{S} + \boldsymbol{V} \tag{3.11}$$

where $\boldsymbol{V} = [\boldsymbol{v}_0, \cdots, \boldsymbol{v}_{N_s-1}]^T$ $(N_s \times P)$ is the AWGN matrix whose elements are i.i.d.. Hence

$$E[vec(\boldsymbol{V}) \cdot vec(\boldsymbol{V})^H] = \sigma^2 \boldsymbol{I}_{N_s P} \tag{3.12}$$

where σ^2 is the variance of the zero-mean noise samples when the transmitted symbol energy is normalized to unity.

In the special case of a quasi-static fading, $\boldsymbol{h}_l(n) = \boldsymbol{h}_l,\ n = 0, \cdots, N_s - 1$. Thus, $\boldsymbol{H}$ becomes a block-circulant matrix and has the following eigen-decomposition

$$\boldsymbol{H} = \boldsymbol{U}^H \boldsymbol{\Lambda} (\boldsymbol{U} \otimes \boldsymbol{I}_P) \tag{3.13}$$

where $N_s \times N_s P$ matrix $\boldsymbol{\Lambda} = diag[\boldsymbol{\lambda}_0^T, \cdots, \boldsymbol{\lambda}_{N_s-1}^T]$ is a block diagonal matrix whose (k,k)th block is given by

$$\boldsymbol{\lambda}_k = \sum_{l=0}^{L-1} \boldsymbol{h}_l \cdot e^{-j\frac{2\pi}{N_s}kl},\ k = 0, \cdots, N_s - 1. \tag{3.14}$$

Analysis of the receiver under quasi-static fading is straightforward. The received $\boldsymbol{R}$ is processed by multiplying it with $\boldsymbol{U}$, forming $N_s \times P$ matrix $\boldsymbol{X}$ as

$$\begin{aligned} \boldsymbol{X} &= [\boldsymbol{x}_0, \cdots, \boldsymbol{x}_{N_s-1}]^T \\ &= \boldsymbol{U}\boldsymbol{R} \\ &= \boldsymbol{\Lambda}\boldsymbol{\Psi} + \boldsymbol{U}\boldsymbol{V}. \end{aligned} \tag{3.15}$$

Let $\boldsymbol{x}_k = [x_1(k), \cdots, x_P(k)]^T$, $\boldsymbol{w}_k = [w_1(k), \cdots, w_P(k)]^T$, and $\boldsymbol{W} = \boldsymbol{U}\boldsymbol{V} = [\boldsymbol{w}_0, \cdots, \boldsymbol{w}_{N_s-1}]^T$ $(N_s \times P)$. From Eq. (3.15), $\boldsymbol{x}_k$ can be obtained as

$$\boldsymbol{x}_k^T = \boldsymbol{\lambda}_k^T \boldsymbol{\Psi}_k + \boldsymbol{w}_k^T,\ k = 0, \cdots, N_s - 1 \tag{3.16}$$

where

$$\boldsymbol{w}_k = \frac{1}{\sqrt{N_s}} \sum_{m=0}^{N_s-1} \boldsymbol{v}_m \cdot e^{-j\frac{2\pi}{N_s}mk}. \tag{3.17}$$

Note that $\boldsymbol{W}$ has the same first and second order statistics as $\boldsymbol{V}$, i.e., all elements of $\boldsymbol{W}$ are i.i.d. with zero mean and variance σ^2. It is clear from Eq. (3.16) that ICI does not exist in the ST-OFDM system over quasi-static channels.

The P symbols in each column of $\boldsymbol{\Psi}_k$ are transmitted from the P transmit antennas simultaneously during every OFDM symbol period. If the channel is time-invariant over P consecutive OFDM symbol periods, the pairwise ML scheme [8] can be used to detect pairs of transmitted symbols, instead of symbol by symbol, and there is no error floor in BER performance.

3.3. Impact of Time-Varying Fading

3.3.1. CIR and SINR in the Presence of Time-Varying Fading

For OFDM systems over fast fading channels, channel estimation is generally carried out by transmitting pilot symbols in given positions of the frequency-time grid [42, 43]. We assume hereafter that CSI is known at the receiver. In the presence of time-selective fading, $\boldsymbol{H}$ is no longer a block-circulant matrix. Consequently, $\boldsymbol{G} = \boldsymbol{U}\boldsymbol{H}(\boldsymbol{U} \otimes \boldsymbol{I}_P)^H$ is no longer a block diagonal matrix as $\boldsymbol{\Lambda}$ given in Eq. (3.13). This shows that time-selective fading causes ICI, which is represented by the off-diagonal blocks of $\boldsymbol{G}$. For this more general case, we can rewrite Eq. (3.15) as

$$\boldsymbol{X} = [\boldsymbol{x}_0, \cdots, \boldsymbol{x}_{N_s-1}]^T = \boldsymbol{G}\boldsymbol{\Psi} + \boldsymbol{W} \tag{3.18}$$

where

$$\boldsymbol{x}_k^T = \boldsymbol{g}_{k,k}^T \boldsymbol{\Psi}_k + \sum_{k'=0,k'\neq k}^{N_s-1} \boldsymbol{g}_{k,k'}^T \boldsymbol{\Psi}_{k'} + \boldsymbol{w}_k^T, \;\; k = 0, \cdots, N_s - 1 \tag{3.19}$$

and $\boldsymbol{g}_{k,k'} = [g_{k,k'}^{(1)}, \cdots, g_{k,k'}^{(P)}]^T$, $k, k' = 0, \cdots, N_s - 1$, is the (k, k')th block of $\boldsymbol{G}$. Apparently, the second term on the right-hand side of Eq. (3.19) represents ICI.

To make the rest of the analysis in this chapter clearer and easier to understand, we focus on using the 4×4 (i.e., $P = 4$) quasi-orthogonal STBC with constellation rotation given in [8], which is replicated here as

$$\boldsymbol{\Psi}_k = \begin{bmatrix} a_1(k) & -a_2^*(k) & e^{j\phi}a_3(k) & -e^{-j\phi}a_4^*(k) \\ a_2(k) & a_1^*(k) & e^{j\phi}a_4(k) & e^{-j\phi}a_3^*(k) \\ e^{j\phi}a_3(k) & -e^{-j\phi}a_4^*(k) & a_1(k) & -a_2^*(k) \\ e^{j\phi}a_4(k) & e^{-j\phi}a_3^*(k) & a_2(k) & a_1^*(k) \end{bmatrix} \tag{3.20}$$

where the rotation angle ϕ depends on the signal constellation. The analysis procedures and conclusions drawn for this specific case can be easily extended to different number of antennas and code structures (e.g., the 8×8 code given in [8]).

ICI can be well quantified by using CIR [44]. In order to quantify the effects of time-varying fading, we derive CIR as a function of the number of subcarriers and the normalized Doppler shift (f_dT_s). Let us define three vectors:

$$\boldsymbol{y}_k = [x_1(k), x_2^*(k), x_3(k), x_4^*(k)]^T$$
$$\boldsymbol{z}_k = [w_1(k), w_2^*(k), w_3(k), w_4^*(k)]^T$$
$$\boldsymbol{\psi}_k = [a_1(k), a_2(k), e^{j\phi}a_3(k), e^{j\phi}a_4(k)]^T.$$

From Eq. (3.19), $\boldsymbol{y}_k$ can be expressed as

$$\boldsymbol{y}_k = \boldsymbol{M}_{k,k}\boldsymbol{\psi}_k + \sum_{k'=0,k'\neq k}^{N_s-1} \boldsymbol{M}_{k,k'}\boldsymbol{\psi}_{k'} + \boldsymbol{z}_k \tag{3.21}$$

where

$$\boldsymbol{M}_{k,k'} = \begin{bmatrix} \boldsymbol{M}_{k,k'}^{(1,2)}(0) & \boldsymbol{M}_{k,k'}^{(3,4)}(0) \\ \boldsymbol{M}_{k,k'}^{(3,4)}(2(N_s+c_p)) & \boldsymbol{M}_{k,k'}^{(1,2)}(2(N_s+c_p)) \end{bmatrix}, \quad k,k' = 0,\cdots N_s-1 \tag{3.22}$$

with

$$\boldsymbol{M}_{k,k'}^{(i,j)}(n) = \begin{bmatrix} g_{k,k'}^{(i)}(n) & g_{k,k'}^{(j)}(n) \\ g_{k,k'}^{(j)*}(n+N_s+c_p) & -g_{k,k'}^{(i)*}(n+N_s+c_p) \end{bmatrix}. \tag{3.23}$$

By letting $g_{k,k'}^{(p)}(0) = g_{k,k'}^{(p)},\ p = 1,\cdots,4$, we have

$$g_{k,k'}^{(p)}(q(N_s+c_p)) = J_0(2\pi f_d(N_s+c_p)T_s)g_{k,k'}^{(p)}[(q-1)(N_s+c_p)] + \varepsilon_{k,k'}^{(p)}(q(N_s+c_p)) \tag{3.24}$$

where $\{\varepsilon_{k,k'}^{(p)}(q(N_s+c_p)),\ q=1,2,3\}$ are independent complex Gaussian random variables with zero mean and variance

$$\sigma_{\varepsilon_{k,k'}}^2 = (1 - J_0^2(2\pi f_d(N_s+c_p)T_s)) \cdot var(g_{k,k'}^{(p)}). \tag{3.25}$$

Note that the spaced-time correlation function Eq. (3.9) is for channel coefficients in the time domain. In obtaining Eq. (3.24) in the frequency domain, we have applied the time-frequency relationship $\boldsymbol{G} = \boldsymbol{U}\boldsymbol{H}(\boldsymbol{U}\otimes\boldsymbol{I}_P)^H$ and Eqs. (3.8) and (3.9).

Let $\boldsymbol{\Upsilon}$ be an $N_s \times N_s$ matrix given by

$$\boldsymbol{\Upsilon} = \begin{bmatrix} var(g_{0,0}^{(p)}) & \cdots & var(g_{0,N_s-1}^{(p)}) \\ \vdots & \ddots & \vdots \\ var(g_{N_s-1,0}^{(p)}) & \cdots & var(g_{N_s-1,N_s-1}^{(p)}) \end{bmatrix}. \tag{3.26}$$

As shown in APPENDIX A, for a particular antenna index p, $\boldsymbol{\Upsilon}$ has a circulant structure as

$$\boldsymbol{\Upsilon} = \begin{bmatrix} \gamma_0 & \gamma_1 & \cdots & \gamma_{N_s-1} \\ \gamma_{N_s-1} & \gamma_0 & \cdots & \gamma_{N_s-2} \\ \vdots & \vdots & & \vdots \\ \gamma_1 & \gamma_2 & \cdots & \gamma_0 \end{bmatrix}. \tag{3.27}$$

Since elements of $\boldsymbol{g}_{k,k'}$ are i.i.d. Gaussian random variables [25], Eq. (3.27) applies to all antennas. It is also shown in the APPENDIX A that $\gamma_{k'}$ defined in Eq. (3.27) has a closed-form expression as

$$\gamma_{k'} = \frac{1}{N_s^2} \sum_{l=0}^{L-1} \left[N_s + 2 \sum_{i=1}^{N_s-1} (N_s - i)\, \alpha_i \cos\left(\frac{2\pi}{N_s} k' i\right) \right] e^{-\frac{\tau_l}{\tau_{rms}}},\ k' = 0, \cdots, N_s - 1. \tag{3.28}$$

With Eq. (3.28), $g_{k,k'}^{(p)}(q(N_s + c_p))$ in Eq. (3.24) can be obtained by substituting $\gamma_{k'}$ into Eq. (3.25). As a result of channel time-variations, $\gamma_{k'} \neq 0$ for $k' \neq 0$, which causes ICI. In the presence of time-varying fading, CIR for quasi-orthogonal STBC given in Eq. (3.20) applied in an OFDM system is obtained as

$$
\begin{aligned}
CIR &= \frac{E\left[\|\boldsymbol{M}_{k,k}\boldsymbol{\psi}_k\|_F^2\right]}{E\left[\|\sum_{k'=0,k'\neq k}^{N_s-1}\boldsymbol{M}_{k,k'}\boldsymbol{\psi}_{k'}\|_F^2\right]} \\
&= \frac{tr\left\{E\left[\boldsymbol{M}_{k,k}\boldsymbol{\psi}_k\boldsymbol{\psi}_k^H\boldsymbol{M}_{k,k}^H\right]\right\}}{tr\left\{E\left[\left(\sum_{k'=0,k'\neq k}^{N_s-1}\boldsymbol{M}_{k,k'}\boldsymbol{\psi}_{k'}\right)\left(\sum_{k'=0,k'\neq k}^{N_s-1}\boldsymbol{M}_{k,k'}\boldsymbol{\psi}_{k'}\right)^H\right]\right\}} \\
&= \frac{E\left[\sum_{q=0}^{3}\sum_{p=1}^{4}|g_{k,k}^{(p)}(q(N_s+c_p))|^2\right]}{E\left[\sum_{k'=0,k'\neq k}^{N_s-1}\sum_{q=0}^{3}\sum_{p=1}^{4}|g_{k,k'}^{(p)}(q(N_s+c_p))|^2\right]} \\
&= \frac{\gamma_0}{\sum_{k'=1}^{N_s-1}\gamma_{k'}} = \frac{\sum_{l=0}^{L-1}\left[N_s+2\sum_{i=1}^{N_s-1}(N_s-i)\,\alpha_i\right]e^{-\frac{\tau_l}{\tau_{rms}}}}{\sum_{k'=1}^{N_s-1}\sum_{l=0}^{L-1}\left[N_s+2\sum_{i=1}^{N_s-1}(N_s-i)\alpha_i\cos\left(\frac{2\pi}{N_s}k'i\right)\right]e^{-\frac{\tau_l}{\tau_{rms}}}} \\
&= \frac{N_s+2\sum_{i=1}^{N_s-1}(N_s-i)J_0(2\pi i f_d T_s)}{\sum_{k'=1}^{N_s-1}\left[N_s+2\sum_{i=1}^{N_s-1}(N_s-i)J_0(2\pi i f_d T_s)\cos\left(\frac{2\pi}{N_s}k'i\right)\right]}.
\end{aligned}
\tag{3.29}
$$

In deriving the 4th equality of Eq. (3.29), we have applied the property that $g_{k,k'}^{(p)}(q(N_s+c_p)), p=1,\cdots,4$, have the same variance. Note that CIR is independent of the channel power-delay profile and the number of resolvable paths. Furthermore, SINR of this quasi-orthogonal ST-OFDM system is obtained as

$$
\begin{aligned}
SINR &= \frac{E\left[\|\boldsymbol{M}_{k,k}\boldsymbol{\psi}_k\|_F^2\right]}{E\left[\|\sum_{k'=0,k'\neq k}^{N_s-1}\boldsymbol{M}_{k,k'}\boldsymbol{\psi}_{k'}+\boldsymbol{z}_k\|_F^2\right]} \\
&= \frac{tr\left\{E\left[\boldsymbol{M}_{k,k}\boldsymbol{\psi}_k\boldsymbol{\psi}_k^H\boldsymbol{M}_{k,k}^H\right]\right\}}{tr\left\{E\left[\left(\sum_{k'=0,k'\neq k}^{N_s-1}\boldsymbol{M}_{k,k'}\boldsymbol{\psi}_{k'}\right)\left(\sum_{k'=0,k'\neq k}^{N_s-1}\boldsymbol{M}_{k,k'}\boldsymbol{\psi}_{k'}\right)^H+\boldsymbol{z}_k\boldsymbol{z}_k^H\right]\right\}} \\
&= \frac{4\gamma_0}{4\sum_{k'=1}^{N_s-1}\gamma_{k'}+\sigma^2}
\end{aligned}
\tag{3.30}
$$

where $\gamma_{k'}$ was given in Eq. (3.28). Moreover, the channel time variations over four consecutive OFDM symbols as seen in the 4×4 matrix $\boldsymbol{M}_{k,k'}$ given in Eq. (3.22) introduce, as mentioned in Section 3.1, additional ITAI among elements of $\boldsymbol{\psi}_k$.

3.3.2. Detection

In a quasi-static fading channel, the received signal can be directly processed by a space-time decoder. In a time-varying fading channel, detection could be done as follows. Let ICI and noise terms in Eq. (3.21) be represented by a single variable $\boldsymbol{d}_k$ as

$$
\boldsymbol{d}_k = \sum_{k'=0,k'\neq k}^{N_s-1}\boldsymbol{M}_{k,k'}\boldsymbol{\psi}_{k'}+\boldsymbol{z}_k. \tag{3.31}
$$

Various schemes have been proposed for detection of quasi-orthogonal STBC over time-selective fading channels. For example, a TS-ZF detector was proposed in [12], assuming perfect CSI at the receiver. The main objective of this scheme is to lower the error floor due to ITAI caused by channel time selectivity. However, quasi-orthogonal ST-OFDM systems over time-selective multipath fading channels not only suffer from ITAI, but also ICI, especially when N_s is large. Thus, the TS-ZF scheme will not be very effective for the system being addressed in this chapter.

In a simpler ZF detector, $\boldsymbol{y}_k$ is processed as

$$\boldsymbol{\Theta}_k \boldsymbol{y}_k = \boldsymbol{\Theta}_k \boldsymbol{M}_{k,k} \boldsymbol{\psi}_k + \boldsymbol{\Theta}_k \boldsymbol{d}_k \tag{3.32}$$

where $\boldsymbol{\Theta}_k = \boldsymbol{M}_{k,k}^{-1}$. Then the least square (LS) criterion can be used to detect the transmitted signal as

$$\widehat{a}_p(k) = \begin{cases} \underbrace{\operatorname{argmin}}_{a(i)\in\boldsymbol{\mathcal{A}}} |[\boldsymbol{\Theta}_k]_p \boldsymbol{y}_k - a(i)|^2, \ p = 1, 2 \\ \underbrace{\operatorname{argmin}}_{a(i)\in\boldsymbol{\mathcal{A}}} |[\boldsymbol{\Theta}_k]_p \boldsymbol{y}_k - e^{j\phi} a(i)|^2, \ p = 3, 4 \end{cases} \tag{3.33}$$

where $\boldsymbol{\mathcal{A}}$ is the symbol alphabet and $[\boldsymbol{\Theta}_k]_p$ is the pth row of $\boldsymbol{\Theta}_k$.

When the MMSE detection scheme is applied, the cost function $E\left[\|\boldsymbol{\psi}_k - \acute{\boldsymbol{W}}_k^H \boldsymbol{y}_k\|_F^2\right]$ is minimized by finding an appropriate coefficient matrix $\acute{\boldsymbol{W}}_k$. With some algebraic manipulations, it is shown that the optimal matrix is given by

$$\acute{\boldsymbol{W}}_k = \left(\boldsymbol{M}_{k,k} \boldsymbol{M}_{k,k}^H + \acute{\boldsymbol{N}}_k\right)^{-1} \boldsymbol{M}_{k,k} \tag{3.34}$$

where

$$\acute{\boldsymbol{N}}_k = \begin{bmatrix} 4\sum_{k'=1}^{N_s-1} \gamma_{k'} + \sigma^2 & 4\acute{J}_1 \sum_{k'=1}^{N_s-1} \gamma_{k'} & 4\acute{J}_2 \sum_{k'=1}^{N_s-1} \gamma_{k'} & 4\acute{J}_3 \sum_{k'=1}^{N_s-1} \gamma_{k'} \\ 4\acute{J}_1 \sum_{k'=1}^{N_s-1} \gamma_{k'} & 4\sum_{k'=1}^{N_s-1} \gamma_{k'} + \sigma^2 & 4\acute{J}_1 \sum_{k'=1}^{N_s-1} \gamma_{k'} & 4\acute{J}_2 \sum_{k'=1}^{N_s-1} \gamma_{k'} \\ 4\acute{J}_2 \sum_{k'=1}^{N_s-1} \gamma_{k'} & 4\acute{J}_1 \sum_{k'=1}^{N_s-1} \gamma_{k'} & 4\sum_{k'=1}^{N_s-1} \gamma_{k'} + \sigma^2 & 4\acute{J}_1 \sum_{k'=1}^{N_s-1} \gamma_{k'} \\ 4\acute{J}_3 \sum_{k'=1}^{N_s-1} \gamma_{k'} & 4\acute{J}_2 \sum_{k'=1}^{N_s-1} \gamma_{k'} & 4\acute{J}_1 \sum_{k'=1}^{N_s-1} \gamma_{k'} & 4\sum_{k'=1}^{N_s-1} \gamma_{k'} + \sigma^2 \end{bmatrix} \tag{3.35}$$

with $\acute{J}_i = J_0(2\pi f_d i(N_s + c_p)T_s), \ i = 1, 2, 3$. Thus the MMSE criterion is given by

$$\hat{\boldsymbol{\psi}}_k = \acute{\boldsymbol{W}}_k^H \boldsymbol{y}_k = \boldsymbol{M}_{k,k}^H \left(\boldsymbol{M}_{k,k} \boldsymbol{M}_{k,k}^H + \acute{\boldsymbol{N}}_k\right)^{-1} \boldsymbol{y}_k. \tag{3.36}$$

The decorrelating DF and the MMSE-DF schemes have been shown to provide better performances than the ZF and the MMSE schemes [45]. In the decorrelating DF detection, $\boldsymbol{y}_k$ is premultiplied by $\boldsymbol{\mathcal{L}}^{-1}\boldsymbol{M}_{k,k}^H$ as

$$\begin{aligned}\widetilde{\boldsymbol{y}}_k &= \boldsymbol{\mathcal{L}}^{-1}\boldsymbol{M}_{k,k}^H\boldsymbol{y}_k \\ &= \boldsymbol{\mathcal{L}}^{-1}\boldsymbol{M}_{k,k}^H\boldsymbol{M}_{k,k}\boldsymbol{\psi}_k + \boldsymbol{\mathcal{L}}^{-1}\boldsymbol{M}_{k,k}^H\boldsymbol{d}_k \\ &= \boldsymbol{\mathcal{L}}^H\boldsymbol{\psi}_k + \boldsymbol{e}_k \end{aligned} \tag{3.37}$$

where $\boldsymbol{\mathcal{L}}^H$ is an upper triangular matrix obtained by using the Cholesky decomposition as

$$\boldsymbol{\mathcal{R}} \;=\; \boldsymbol{M}_{k,k}^H\boldsymbol{M}_{k,k} \;=\; \boldsymbol{\mathcal{L}}\boldsymbol{\mathcal{L}}^H.$$

The pth component of $\widetilde{\boldsymbol{y}}_k$ is given by

$$[\widetilde{\boldsymbol{y}}_k]_p = \boldsymbol{\mathcal{L}}_{p,p}^H[\boldsymbol{\psi}_k]_p + \sum_{i=p+1}^{4}\boldsymbol{\mathcal{L}}_{p,i}^H[\boldsymbol{\psi}_k]_i + [\boldsymbol{e}_k]_p \tag{3.38}$$

which contains only interference from $(4-p)$ signals. The last component $[\widetilde{\boldsymbol{y}}_k]_4$ contains no interference, so a decision for this transmitted signal can be made first: $\widehat{a}_4(k) = \text{dec}\{e^{-j\phi}[\widetilde{\boldsymbol{y}}_k]_4\}$, where dec$(\cdot)$ is the slice function corresponding to the specific modulation scheme applied. The next signal can be detected by subtracting the interference contribution from the fourth signal using the previous decision as $\widehat{a}_3(k) = \text{dec}\{e^{-j\phi}([\widetilde{\boldsymbol{y}}_k]_3 - \boldsymbol{\mathcal{L}}_{3,4}^H\widehat{a}_4(k)e^{j\phi})\}$. This procedure is repeated until all signals are detected. The MMSE-DF scheme is the one that minimizes the average energy of $[\widetilde{\boldsymbol{y}}_k]_p - a_p(k),\ p = 1,2$ and $[\widetilde{\boldsymbol{y}}_k]_p - e^{j\phi}a_p(k),\ p = 3,4$ under the assumption that previously detected signals in the feedback filter are correct. Details of this scheme can be found in [40, 46].

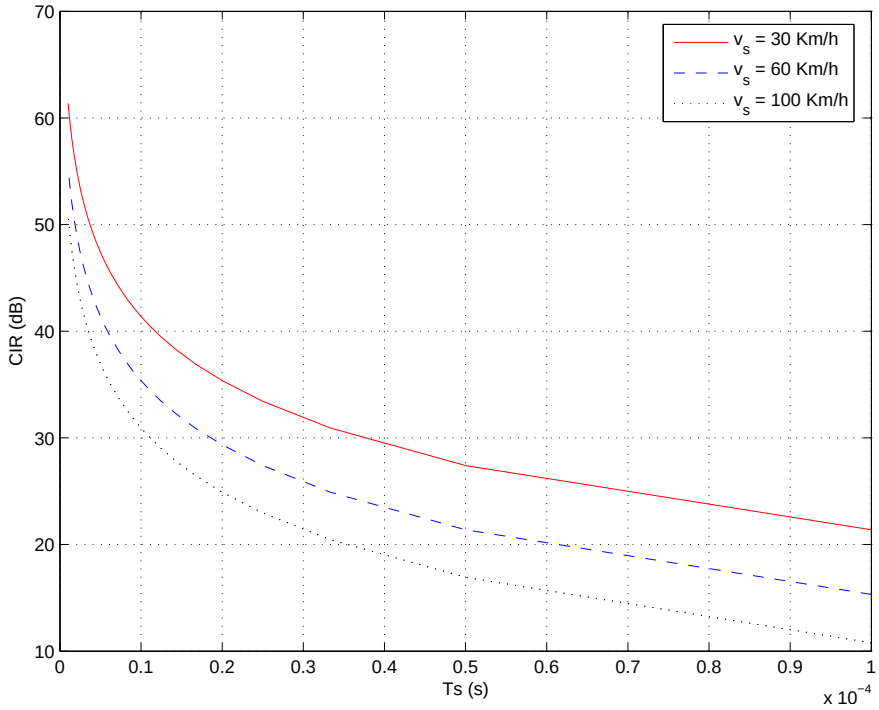

FIGURE 3.1. CIR comparisons with different fading rates ($N_s = 12$).

3.4. Numerical Results and Discussion

In simulations, we assume a system with four transmit antennas and one receive antenna, employing QPSK modulation. The 4×4 quasi-orthogonal STBC given in [8] and replicated in Eq. (3.20) is applied ($\phi = \pi/4$ used in simulation). The time-selective Rayleigh fading channel is assumed to have three resolvable multipath components, and the channel Doppler shift is calculated based on a carrier frequency of $f_c = 2$GHz.

Fig. 3.1 shows the impact of data symbol period T_s ($N_s = 12$) and vehicle speed on CIR by using the analytical expression given in Eq. (3.29). Note, again, that CIR does not depend on the channel power-delay profile of the channel. CIR curves are compared for three different vehicle speeds chosen as $v_s = 30, 60,$ and 100Km/h,

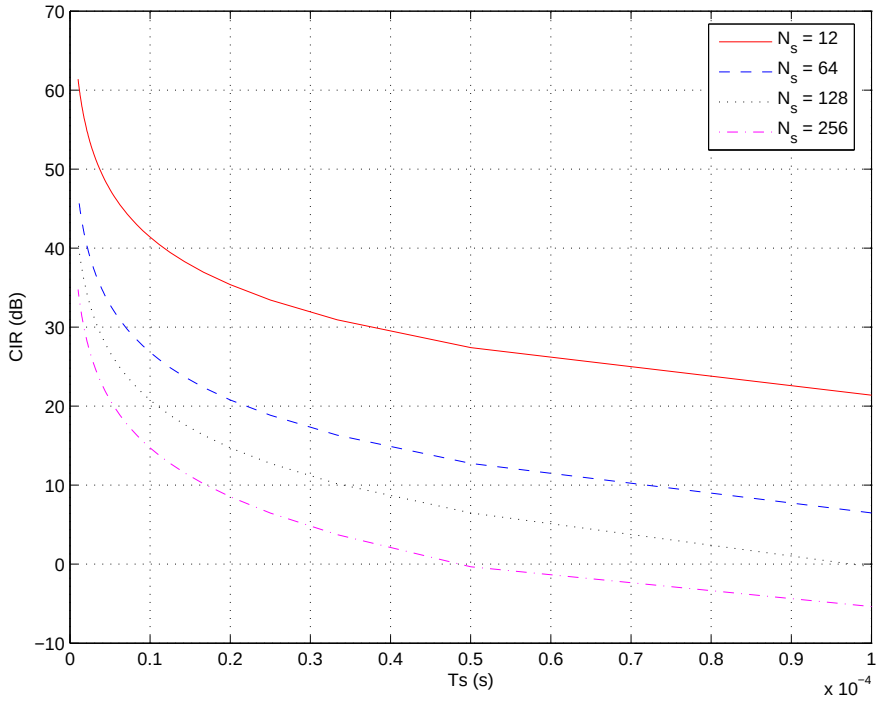

FIGURE 3.2. CIR comparisons with different number of subcarriers ($v_s = 30$Km/h).

which are typical for urban and suburban environments. It is clearly observed that CIR is inversely proportional to T_s and vehicle speed, which makes sense, as a larger T_s or v_s makes the quasi-orthogonal ST-OFDM system more vulnerable to time variations of the channel coefficients.

In Fig. 3.2, CIR curves of the system under $v_s = 30$Km/h for different number of subcarriers in one OFDM symbol ($N_s = 12,\ 64,\ 128,$ and 256) are obtained. It is observed that given the same data symbol duration T_s, CIR decreases significantly as the number of subcarriers increases.

Shown in Fig. 3.3 are the simulated SER performances of the system when a ZF detection scheme is employed. The power-delay profile related parameters are $\tau_0 = 0$, $\tau_1 = 2$, $\tau_2 = 3$, and $\tau_{rms} = 20$. The OFDM symbol is assumed to have $N_s = 12$

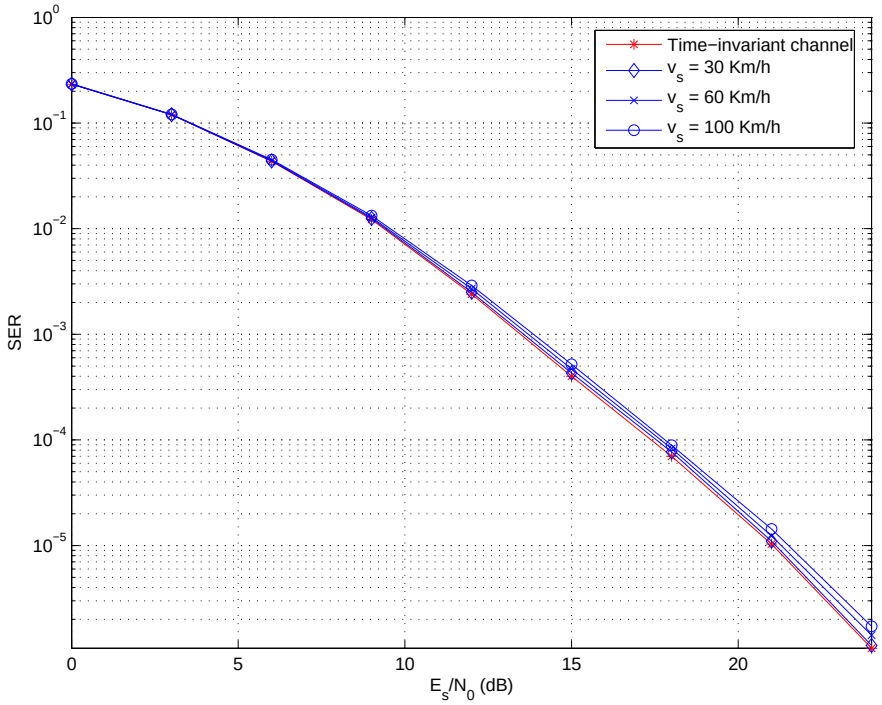

FIGURE 3.3. SER versus E_s/N_0 for quasi-orthogonal ST-OFDM systems with different fading rates ($N_s = 12$, $T_s = 5 \times 10^{-7} s$).

subcarriers, and data symbol period is $T_s = 1/(2 \times 10^6)$ seconds. Performances with different vehicle speeds ($v_s = 30, 60,$ and 100Km/h) are compared. In the same figure, the curve of the quasi-orthogonal ST-OFDM system over a time-invariant multipath fading channel is used as the baseline performance. When the number of subcarriers is small ($N_s = 12$ in Fig. 3.3), the system performs almost the same for any of the vehicle speeds applied, and they all approach the baseline performance. As the number of subcarriers increases, however, system performance deteriorates dramatically. This is clearly shown in Fig. 3.4, where the vehicle speed is $v_s = 30$Km/h and all other parameters are the same as those applied to generate Fig. 3.3. From the SER versus E_s/N_0 curves with $N_s = 12,\ 64,\ 128,$ and 256, it is observed that the error floor

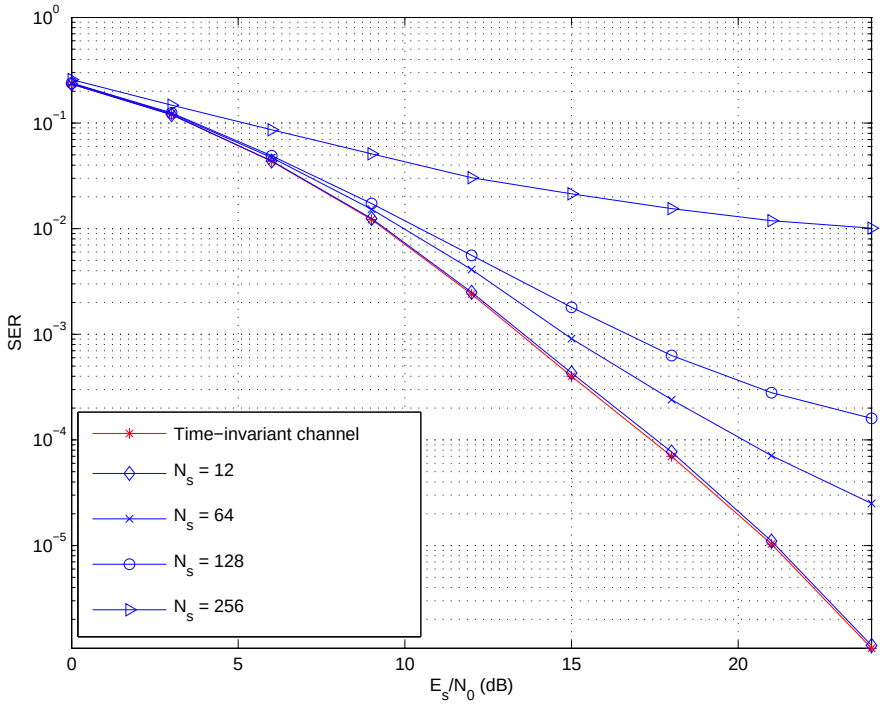

FIGURE 3.4. SER versus E_s/N_0 for quasi-orthogonal ST-OFDM systems with different number of subcarriers ($v_s = 30$Km/h, $T_s = 5 \times 10^{-7} s$).

increases as N_s increases. The main reason is that a larger number of subcarriers within one OFDM symbol not only causes a more severe ICI, but also increases the time interval ($(N_s + c_p)T_s$) in Eq. (3.25), causing a greater amount of ITAI within one STBC matrix.

In Figs. 3.3 and 3.4, the same exponential power-delay profile is applied. Fig. 3.5 shows the impact of different power-delay profiles on the SER performance. Three cases are simulated: (1) a uniform power-delay profile as defined in [41], Appendix A, which results unit variance of all elements of $\boldsymbol{H}$; (2) $\tau_0 = 0, \tau_1 = 2, \tau_2 = 3$; and (3) $\tau_0 = 0, \tau_1 = 7, \tau_2 = 10$. Other parameters applied are $\tau_{rms} = 10$ for cases (2) and (3), $v_s = 30$Km/h, $N_s = 12$, and $T_s = 1/(2 \times 10^6)$ s. For comparison, the baseline

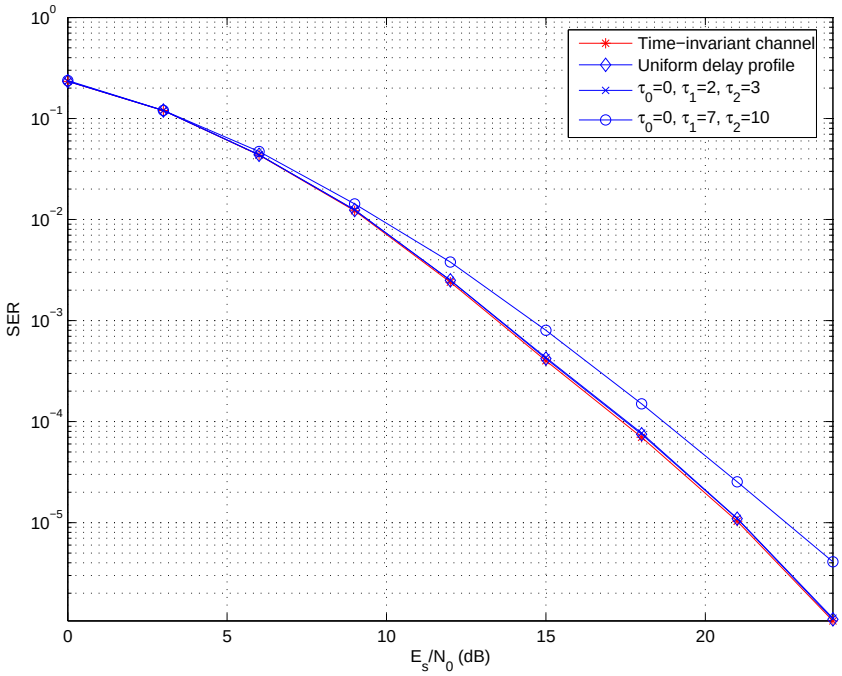

FIGURE 3.5. SER versus E_s/N_0 for quasi-orthogonal ST-OFDM systems with different power-delay profiles ($N_s = 12$, $\tau_{rms} = 10$, $v_s = 30$Km/h).

performance curve shown in Figs. 3.3 and 3.4 is also shown in Fig. 3.5. For the set of channel parameters chosen, it seems that the channel profile only affects the system performance slightly.

In Fig. 3.6, we compare the performances of five different detection methods: the ZF, the TS-ZF, the MMSE, the decorrelating DF (also known as the ZF-DF) and the MMSE-DF schemes. Other than that $N_s = 128$, all other parameters are the same as those applied for Fig. 3.4. The ML scheme is used as the benchmark for other detection schemes. Since these schemes are not specifically optimized for ST-OFDM systems over time-varying fading channels for which ICI should be dealt with, error floors are observed for all of them. To effectively cancel the error floor, the receiver must deal with both ICI and ITAI. We believe that frequency-domain correlative coding

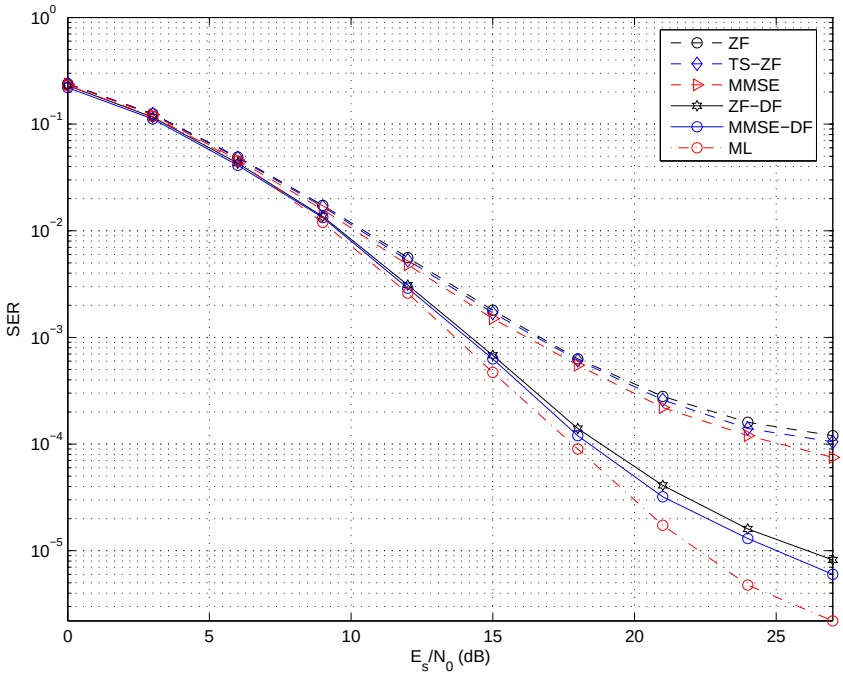

FIGURE 3.6. SER versus E_s/N_0 for quasi-orthogonal ST-OFDM systems with different detection schemes ($N_s = 128, v_s = 30$Km/h, $T_s = 5 \times 10^{-7} s$).

[47] combined with a sequential nulling and cancellation process [48] could be one of such schemes, although discussions of its details are beyond the scope of this chapter.

As a result of dividing the total bandwidth into many narrowband subcarriers, each subcarrier in an OFDM system suffers from flat fading, and system performance degradation is dominated by the weakest subcarrier. To protect data against deep fades an individual subcarrier may experience, an effective technique is to employ forward error correction (FEC) codes, which is often combined with an interleaver before modulation of input data onto subcarriers. This will effectively spread the same information bit onto many subcarriers which may experience fading of low correlations. The receiver must perform channel decoding after the normal detector (e.g., the ZF or MMSE detector). Fig. 3.7 shows the simulated BER curves of the quasi-orthogonal

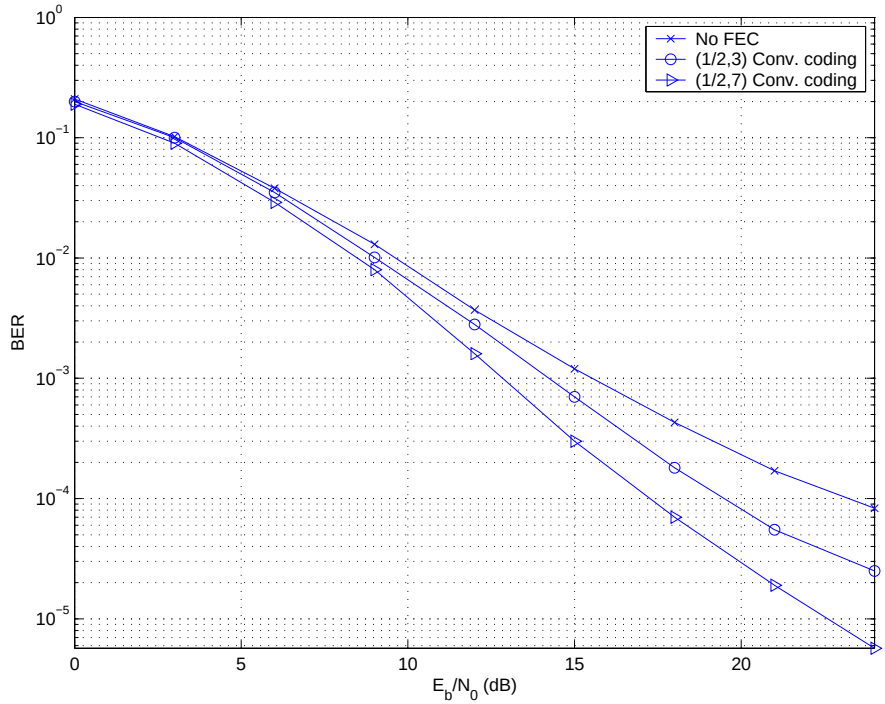

FIGURE 3.7. BER versus E_b/N_0 for quasi-orthogonal ST-OFDM systems with different FEC schemes ($N_s = 128, v_s = 30$Km/h, $T_s = 5 \times 10^{-7} s$).

ST-OFDM system with rate 1/2 convolutional codes of different constraint lengths (3 and 7). $N_s = 128$ is adopted and all other parameters are the same as those applied for Fig. 3.4. Although, as expected, the outer channel encoding improves system performance, there is still a need of other techniques to effectively eliminate the error floor caused by time-selective fading.

We have assumed perfect CSI for all numerical results so far. In practical systems, however, there exist channel estimation errors. It is beyond the scope of this chapter to discuss channel estimation schemes for time-varying fading channels. To assess its impact, channel estimation error is emulated by introducing an error with a normalized average mean-square error (MSE) defined as MSE $=$

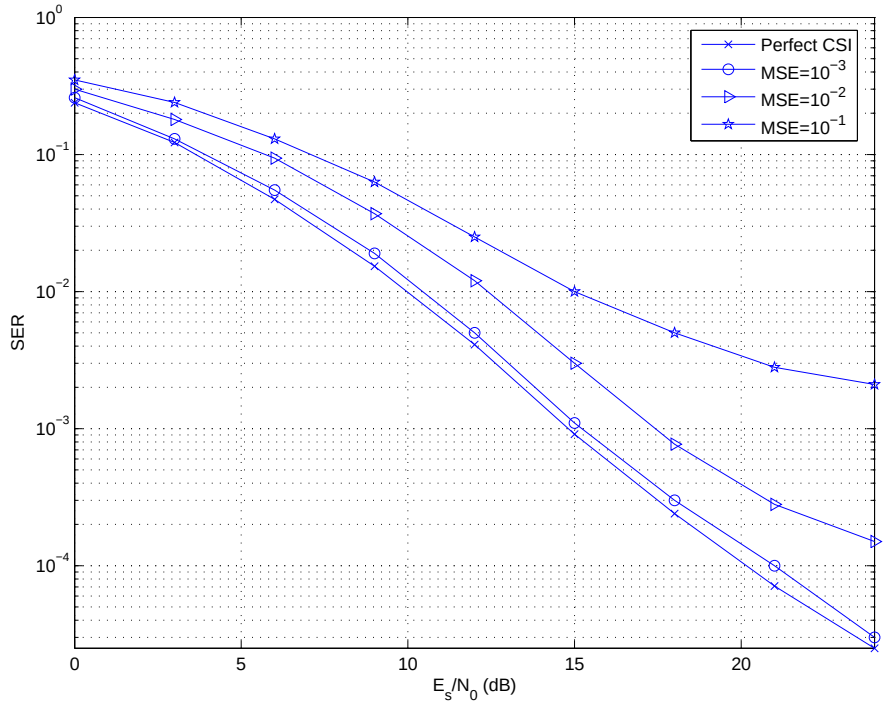

FIGURE 3.8. SER versus E_s/N_0 for quasi-orthogonal ST-OFDM systems with different MSE ($N_s = 64, v_s = 30$Km/h, $T_s = 5 \times 10^{-7}s$).

$E\left[\|\hat{\boldsymbol{H}} - \boldsymbol{H}\|_F^2\right] / E\left[\|\boldsymbol{H}\|_F^2\right]$. The performance results of quasi-orthogonal ST-OFDM systems with various MSE values are shown in Fig. 3.8, where $N_s = 64$ and other parameters are the same as those applied in Fig. 3.4. It is observed that when the MSE value of channel estimation errors is small (e.g., 10^{-3}), the performance degradation is negligible.

3.5. Conclusions

We have analyzed the impact of channel time selectivity on the performance of quasi-orthogonal ST-OFDM systems. Specifically, we have quantified ICI and evaluated ITAI caused by channel time variations. Performances of five detection schemes

are compared, and it seems that none of them can effectively eliminate the error floor of ST-OFDM in a time-selective environment. It is also observed that an increase in Doppler shift, symbol duration, or number of OFDM subcarriers lowers the achievable CIR. With a symbol duration of $T_s = 5 \times 10^{-7}$ s and a small N_s (e.g., 12), system SER performance is quite insensitive to changes in vehicle speeds and the channel power-delay profile. However, with the same T_s and even a low vehicle speed (e.g., 30Km/h), SER performance is very sensitive to changes in the number of subcarriers.

4. FREQUENCY-DOMAIN CORRELATIVE CODING FOR MIMO-OFDM SYSTEMS OVER FAST FADING CHANNELS

4.1. Introduction

OFDM, though effective in avoiding ISI due to multipath delay, is sensitive to time-selective fading, which destroys the orthogonality among different subcarriers in one OFDM symbol and thus causes ICI [15, 16]. If not compensated for, ICI will result in an error floor, which increases as Doppler shift and symbol duration increase. To combat ICI caused by time-selective fading or frequency offset in single-antenna OFDM systems, various methods [47, 49–51], including frequency-domain correlative fading [47] and partial response coding [51], have been studied. The scheme in [47] can be viewed as a special type of frequency-domain partial response coding with correlation polynomial $F(D) = 1 - D$.

To improve spectral efficiency, MIMO antennas can be combined with OFDM to achieve spatial multiplexing [14], which forms MIMO-OFDM. Supports of high mobility (e.g., IEEE 802.16e) in MIMO-OFDM systems are critical for many applications. Similar to single-antenna OFDM, MIMO-OFDM is also sensitive to channel time selectivity.

In this chapter, we apply frequency-domain correlative coding originally proposed in [47] for single-antenna OFDM systems to MIMO-OFDM to improve system robustness to time-selective fading. While the analysis in [47] considered a simple case in which ICI is caused by a single parameter - the frequency offset normalized to the subcarrier separation, we consider a more comprehensive and realistic scenario which includes not only the spatial elements, but also the time-varying and frequency-selective aspects of the channel. We focus on deriving, via a rigorous analytical approach, a tractable, closed-form expression of CIR as a function of channel Doppler shift, num-

ber of subcarriers, OFDM symbol duration, and the power-delay profile of the multi-path fading channel. With the CIR expression derived, we can quantify the impact of time-selective fading and the improvement due to correlative coding in MIMO-OFDM.

4.2. System Model

Consider a MIMO-OFDM system with N_t transmit antennas, N_r receive antennas, and N_s subcarriers which employs binary phase shift keying (BPSK) modulation. Input symbols $a_i \in \{1, -1\}$ are assumed to be i.i.d. with normalized energy. The correlative coding to encode a_i is achieved through the frequency-domain polynomial $F(D) = 1 - D$ [47], which generates a new sequence $b_i = a_i - a_{i-1}$ with $E[b_i] = 0$ and

$$E[b_i b_j^*] = \begin{cases} 2E[a_i^2] = 2, & i = j \\ -E[a_i^2] = -1, & |i - j| = 1 \\ 0, & \text{otherwise.} \end{cases} \tag{4.1}$$

It is well known that the general form of MIMO-OFDM over slowly fading channels (i.e., the channel is time-invariant over several OFDM symbol periods) can be expressed as [14]

$$\boldsymbol{y}_k = \boldsymbol{\Lambda}_k \boldsymbol{x}_k + \boldsymbol{n}_k \tag{4.2}$$

where $\boldsymbol{x}_k$ and $\boldsymbol{y}_k$ represent, respectively, the transmitted and received data for all antennas on subcarrier k, $\boldsymbol{\Lambda}_k$ is an $N_r \times N_t$ matrix whose (i, j)th element, $\{\boldsymbol{\Lambda}_k\}_{ij}$, denotes the channel frequency response between transmit antenna j and receive antenna i, and $\boldsymbol{n}_k$ is an $N_r \times 1$ vector denoting the zero-mean AWGN with covariance $\sigma_n^2 \boldsymbol{I}_{N_r}$ for all antennas on subcarrier k.

4.3. Effects of Time-Selective Fading

In a time-selective fading environment, the $N_sN_r \times N_sN_t$ spatiotemporal channel matrix $\boldsymbol{H}$ in one OFDM symbol period is expressed as

$$\boldsymbol{H} = \begin{bmatrix} \boldsymbol{H}_0(0) & \cdots & \boldsymbol{H}_{L-1}(0) & \cdots & \boldsymbol{H}_1(0) \\ \vdots & & \ddots & & \vdots \\ \mathbf{0} & \cdots & \boldsymbol{H}_{L-1}(N_s-1) & \cdots & \boldsymbol{H}_0(N_s-1) \end{bmatrix} \tag{4.3}$$

where L is the number of resolvable paths and $\mathbf{0}$ is an $N_r \times N_t$ zero matrix. Each nonzero block of $\boldsymbol{H}$ contains the $N_r \times N_t$ channel matrix $\boldsymbol{H}_l(n)$ for path l at time nT_s (T_s is the data symbol period).

Assuming a WSSUS channel, all elements of $\boldsymbol{H}_l(n)$ are modeled as independent complex Gaussian random variables with zero mean and equal variance. The channel is assumed to have an exponential power-delay profile $\theta(\tau_l) = e^{-\tau_l/\tau_{rms}}$ [41], where τ_l is the delay of the lth path and τ_{rms} is the rms delay spread. Since the channel is time-variant, the relationship between the channel coefficients for path l at times nT_s and $(n+m)T_s$ can be described as [12]

$$\{\boldsymbol{H}_l(n+m)\}_{ij} = \alpha_m\{\boldsymbol{H}_l(n)\}_{ij} + \beta_{l,ij}(n+m) \tag{4.4}$$

where

$$\alpha_m = \frac{E\left[\{\boldsymbol{H}_l(n)\}_{ij}\{\boldsymbol{H}_l(n+m)\}_{ij}^*\right]}{e^{-\tau_l/\tau_{rms}}} = J_0(2\pi m f_d T_s) \tag{4.5}$$

f_d is the maximum Doppler shift and $\beta_{l,ij}(n)$ are independent complex Gaussian random variables with zero mean and variance $e^{-\frac{\tau_l}{\tau_{rms}}}(1-\alpha_m^2)$. It is observed that the channel matrix $\boldsymbol{H}$ in (4.3) is no longer a block-circulant matrix as the case of slowly fading channels. Consequently, $\boldsymbol{G} = (\boldsymbol{U} \otimes \boldsymbol{I}_{N_r})\boldsymbol{H}(\boldsymbol{U} \otimes \boldsymbol{I}_{N_t})^H$ is no longer a block diagonal matrix, where $\boldsymbol{U}$ is the unitary DFT matrix with $\{\boldsymbol{U}\}_{ij} = 1/\sqrt{N_s}e^{(-2\pi\sqrt{-1}/N_s)ij}$,

$0 \leq i, j \leq N_s - 1$. This shows that time-selective fading causes ICI, which is represented by the off-diagonal blocks of $\boldsymbol{G}$. Let $\boldsymbol{G}_{ij}$ denote the (i, j)th block of $\boldsymbol{G}$. Eq. (4.2) can be rewritten as

$$\boldsymbol{y}_k = \boldsymbol{G}_{kk}\boldsymbol{x}_k + \sum_{\substack{k'=0 \\ k' \neq k}}^{N_s-1} \boldsymbol{G}_{kk'}\boldsymbol{x}_{k'} + \boldsymbol{n}_k, \; k = 0, \cdots, N_s - 1. \tag{4.6}$$

Let $\boldsymbol{\Upsilon}_{ij}$ be an $N_s \times N_s$ matrix given by

$$\boldsymbol{\Upsilon}_{ij} = \begin{bmatrix} var(\{\boldsymbol{G}_{00}\}_{ij}) & \cdots & var(\{\boldsymbol{G}_{0,N_s-1}\}_{ij}) \\ \vdots & \ddots & \vdots \\ var(\{\boldsymbol{G}_{N_s-1,0}\}_{ij}) & \cdots & var(\{\boldsymbol{G}_{N_s-1,N_s-1}\}_{ij}) \end{bmatrix}, \; 1 \leq i \leq N_r, 1 \leq j \leq N_t. \tag{4.7}$$

As shown in APPENDIX A, $\boldsymbol{\Upsilon}_{ij}$ has a circulant structure, i.e.,

$$\{\boldsymbol{\Upsilon}_{ij}\}_{i'j'} = \gamma_{[j'-i']} = \frac{1}{N_s^2} \sum_{l=0}^{L-1} \left\{ N_s + 2 \sum_{i=1}^{N_s-1} (N_s - i) \, J_0(2\pi i f_d T_s) \cos\left(\frac{2\pi}{N_s}[j' - i']i\right) \right\} \times e^{-\frac{\tau_l}{\tau_{rms}}}, \; 1 \leq i', j' \leq N_s \tag{4.8}$$

where $[n]$ denotes n modulo N_s. CIR of the kth subcarrier for MIMO-OFDM systems over time-selective fading channels is given by

$$
\begin{aligned}
C_{corr}^{(k)} &= \frac{E\left[\{\boldsymbol{G}_{kk}\}_{ij} b_k b_k^* \{\boldsymbol{G}_{kk}\}_{ij}^*\right]}{\sum_{\substack{k'=0 \\ k'\neq k}}^{N_s-1} \sum_{\substack{k''=0 \\ k''\neq k}}^{N_s-1} E\left[\{\boldsymbol{G}_{kk'}\}_{ij} b_{k'} b_{k''}^* \{\boldsymbol{G}_{kk''}\}_{ij}^*\right]} \\
&= \frac{2\gamma_0}{\sum_{k'=1}^{N_s-1} 2\gamma_{k'} - \sum_{\substack{k'=0 \\ k'\neq k,k-1}}^{N_s-2} E\left[\{\boldsymbol{G}_{kk'}\}_{ij} \{\boldsymbol{G}_{k,k'+1}\}_{ij}^* + \{\boldsymbol{G}_{k,k'+1}\}_{ij} \{\boldsymbol{G}_{kk'}\}_{ij}^*\right]} \\
&= \frac{\frac{2}{N_s^2} \sum_{l=0}^{L-1} \left\{ N_s + 2 \sum_{i=1}^{N_s-1} (N_s - i)\, J_0(2\pi i f_d T_s) \right\} e^{-\frac{\tau_l}{\tau_{rms}}}}{\frac{2}{N_s^2} \sum_{k'=1}^{N_s-1} \sum_{l=0}^{L-1} \left\{ N_s + 2 \sum_{i=1}^{N_s-1} (N_s - i) J_0(2\pi i f_d T_s) \cos\left(\frac{2\pi}{N_s} k' i\right) \right\} e^{-\frac{\tau_l}{\tau_{rms}}} - \theta}
\end{aligned}
\tag{4.9}
$$

where $\theta = \sum_{k'=0, k'\neq k, k-1}^{N_s-2} \Omega_{k'}$. As shown in APPENDIX A, $\Omega_{k'}$ is given as

$$
\begin{aligned}
\Omega_{k'} =& \frac{1}{N_s^2} \sum_{l=0}^{L-1} \sum_{r=0}^{N_s-1} \sum_{s=0}^{N_s-1} J_0(2\pi |r-s| f_d T_s) e^{-\frac{\tau_l}{\tau_{rms}}} \Big(e^{-(2\pi\sqrt{-1}/N_s) t_{kk'rs}^{(1)}} \\
&+ e^{-(2\pi\sqrt{-1}/N_s) t_{kk'rs}^{(-1)}} \Big).
\end{aligned}
\tag{4.10}
$$

Without correlative coding, the CIR expression given in Eq. (4.9) simplifies to

$$
\begin{aligned}
C &= \frac{E\left[\{\boldsymbol{G}_{kk}\}_{ij} a_k a_k^* \{\boldsymbol{G}_{kk}\}_{ij}^*\right]}{\sum_{\substack{k'=0 \\ k'\neq k}}^{N_s-1} \sum_{\substack{k''=0 \\ k''\neq k}}^{N_s-1} E\left[\{\boldsymbol{G}_{kk'}\}_{ij} a_{k'} a_{k''}^* \{\boldsymbol{G}_{kk''}\}_{ij}^*\right]} \\
&= \frac{N_s + 2 \sum_{i=1}^{N_s-1} (N_s - i) J_0(2\pi i f_d T_s)}{\sum_{k'=1}^{N_s-1} \left\{ N_s + 2 \sum_{i=1}^{N_s-1} (N_s - i) J_0(2\pi i f_d T_s) \cos\left(\frac{2\pi}{N_s} k' i\right) \right\}}.
\end{aligned}
\tag{4.11}
$$

Note that in this case CIR is the same for all subcarriers and is independent of the channel power-delay profile as well as the number of resolvable paths. Obviously, $C_{corr}^{(k)} \geq C, \forall k$. Therefore, correlative coding effectively increases CIR. Noteworthily,

from (4.9), it is easy to see that although $C_{corr}^{(k)}$ is different for different subcarriers, the difference diminishes as N_s increases. As indicated in [47], when frequency-domain correlative coding with $F(D) = 1 - D$ is used, the signals modulated on subcarriers are identical with alternate mark inversion code and $\{a_i\}$ can be recovered by using a ML sequence detector [52].

4.4. Numerical Results and Discussion

In obtaining the numerical results, we consider a system with two transmit antennas and two receive antennas which employs BPSK modulation and adopt the "SUI-5" channel model [13]. The time-selective Rayleigh fading channel is assumed to have three resolvable multipath components occurring at 0, 5, and $10\mu s$. These paths are modeled as independent complex Gaussian random variables and the rms delay spread of the channel is $3.05\mu s$. The maximum Doppler shift is calculated based on a carrier frequency of $f_c = 2$GHz.

CIR levels versus T_s calculated using Eqs. (4.9) and (4.11) are plotted in Fig. 4.1, where the vehicle speed applied is $v_s = 100$Km/h. CIR curves of the MIMO-OFDM system with different number of subcarriers in one OFDM symbol ($N_s = 8,\ 24,$ and 128) are compared. As shown in Fig. 1, frequency-domain correlative coding incorporated in this letter can effectively increase CIR and the improvement is proportional to the number of subcarriers. With $N_s = 128$, the improvement is observed to be as high as 3.0dB. The BER performances of MIMO-OFDM systems with and without frequency-domain correlative coding are compared in Fig. 4.2, where $T_s = 5 \times 10^{-7} s$ and $v_s = 100$Km/h are applied. The ML detection scheme [14] is used when correlative coding is applied. The improvement in the BER performance is also found proportional to the number of subcarriers.

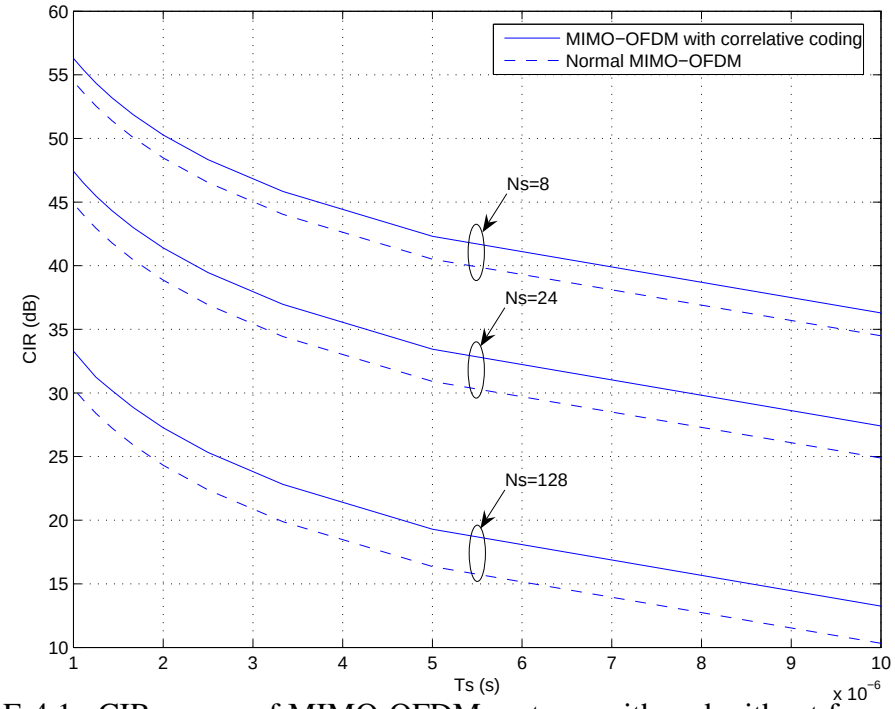

FIGURE 4.1. CIR curves of MIMO-OFDM systems with and without frequency-domain correlative coding.

4.5. Conclusions

We have applied frequency-domain correlative coding to mitigate the effect of time-selective fading to the performance of MIMO-OFDM systems. We derived the analytical expression of CIR as a function of the maximum Doppler shift and power-delay profile of the channel, the number of subcarriers, and the OFDM symbol duration. The CIR expression can be used to quantify the amount of ICI caused by channel time variations. Numerical results indicate that a simple correlative coding scheme with correlation polynomial $F(D) = 1 - D$ can effectively increase CIR of a 128-subcarrier MIMO-OFDM system by as much as 3.0dB, and the improvement further increases as the number of subcarriers becomes larger.

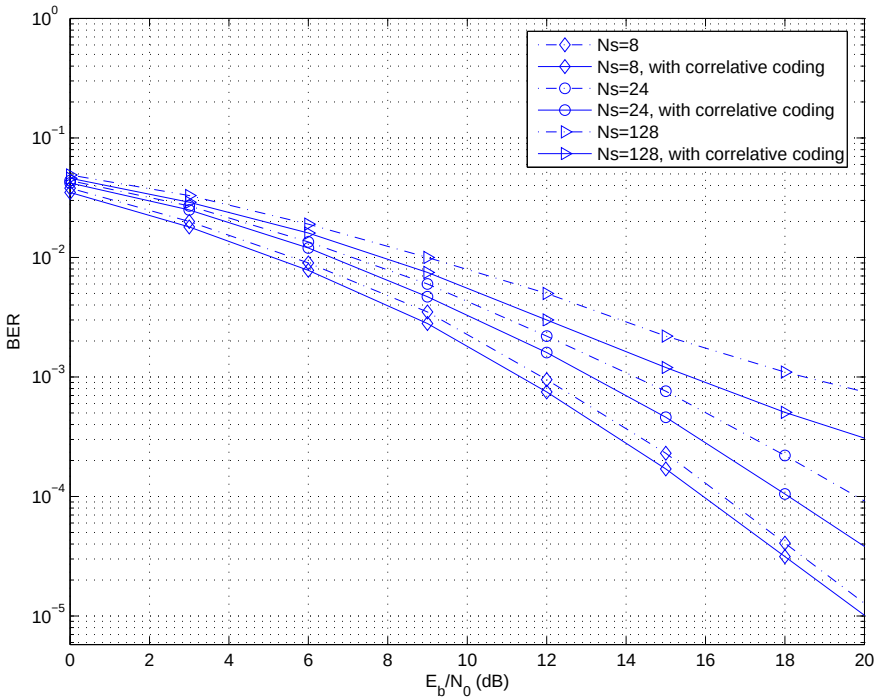

FIGURE 4.2. BER versus E_b/N_0 for MIMO-OFDM systems with and without frequency-domain correlative coding.

5. DECISION-FEEDBACK RECEIVER FOR SPACE-TIME CODED OFDM USING CORRELATIVE CODING

5.1. Introduction

One of the disadvantages of OFDM is that it is sensitive to time-selective fading inherent in mobile communication systems. Time-selective fading causes ICI. Multiple antennas can be combined with OFDM to increase diversity gain and to improve spectral efficiency. Performance of MIMO-OFDM systems in time-selective fading environments was analyzed in [25].

Orthogonal STBCs were first proposed in [3] for systems with two transmit antennas and later generalized to systems with an arbitrary number of transmit antennas [5]. Quasi-orthogonal STBCs with rate one [6, 7, 53] could be applied to provide partial diversity. STBCs are typically designed assuming a quasi-static channel, and time-selective fading will cause ITAI among all symbols for quasi-orthogonal codes[1]. Therefore, the pairwise ML decoding scheme [6] becomes suboptimal. To mitigate ITAI caused by channel time variations, many schemes have been studied [10–12].

For ST-OFDM systems over fast fading channels, it is necessary to consider the impact of ICI and ITAI simultaneously. ITAI caused by channel time variations in ST-OFDM systems is much more pronounced than in common STC systems. In [54], a sequential DF sequence estimation (SDFSE) scheme with an adaptive threshold was proposed to mitigate the performance degradation in orthogonal ST-OFDM systems with two transmit antennas over time-selective fading channels. However, this scheme does not seem to be very effective in eliminating the error floor. To mitigate ICI caused

---

[1]With quasi-static fading models, ITAI exists only between pairs of symbols with the 4×4 codes given in [6].

by channel frequency errors in single-antenna OFDM systems, a simple design using frequency-domain correlative coding was analyzed in [47]. For MIMO-OFDM systems, ITAI can be effectively cancelled through a sequential nulling and cancellation process [48, 55] if the number of transmit antennas is less than or equal to the number of receive antennas. Later, a modified decorrelating DF detection scheme was studied in [56] to reduce the complexity and to improve the numerical stability of such schemes.

To effectively mitigate the error floor due to channel time selectivity for ST-OFDM systems, the receiver must deal with both ICI and ITAI. In this chapter, we propose a scheme that combines frequency-domain correlative coding and a modified DF receiver for quasi-orthogonal ST-OFDM systems in time-varying fading environments. We show that the proposed scheme is much more effective in lowering the error floor than existing schemes such as the TS-ZF scheme [12] and the SDFSE scheme [54].

5.2. System Model

Consider a space-time block coded multi-antenna OFDM system with P transmit antennas, one receive antenna, and N_s subcarriers that employs BPSK modulation. Input symbols $a_i \in \{1, -1\}$ are assumed i.i.d.. The correlative coding to encode a_i is achieved through the frequency-domain polynomial $F(D) = 1 - D$ [47], which generates a new sequence $b_i = a_i - a_{i-1}$. The encoded sequence $\{b_i,\ i = 0, \cdots, N_sP - 1\}$ is then serial-to-parallel converted into P sequences, each of length N_s, as

$$b_k^{(p)} = b_{k+(p-1)N_s},\ \ p = 1, \cdots, P,\ k = 0, \cdots, N_s - 1. \tag{5.1}$$

Each of the N_s sequences $\{b_k^{(1)}, \cdots, b_k^{(P)}\},\ k = 0, \cdots, N_s - 1$, is mapped to a matrix $\mathbf{\Psi}_k$ of size $P \times P$ by using a quasi-orthogonal space-time block coding scheme (e.g., the 4×4 quasi-orthogonal scheme given in [6]). The transmitted signals are obtained by taking the IDFT of $\{\mathbf{\Psi}_0, \cdots, \mathbf{\Psi}_{N_s-1}\}$.

In frequency-selective fading channels with L resolvable paths, a CP of length c_p ($c_p \geq L$) is added at the beginning of each transmitted OFDM block. Combined with the characteristics of time-selective fading, the $N_s \times N_s P$ spatiotemporal channel matrix $\boldsymbol{H}_t$ during the tth OFDM block period is expressed as Eq. (3.5) in Chapter 3 with each non-zero block of $\boldsymbol{H}_t$ contains the $P \times 1$ channel vector $\boldsymbol{h}_{t,l}(n)$ for path l at time nT_s expressed as

$$\boldsymbol{h}_{t,l}(n) = [h_{t,l}^{(1)}(n), \cdots, h_{t,l}^{(P)}(n)]^T, \ l = 0, \cdots, L-1, \ n = 0, \cdots, N_s - 1. \tag{5.2}$$

If fading is assumed to be quasi-static, $\boldsymbol{H}_t$ has a block-circulant structure. Without loss of generality, we omit the index of OFDM block period t in the following discussion.

In the special case of quasi-static fading, channel matrix $\boldsymbol{H}$ has the following eigen-decomposition

$$\boldsymbol{H} = \boldsymbol{U}^H \boldsymbol{\Lambda} (\boldsymbol{U} \otimes \boldsymbol{I}_P) \tag{5.3}$$

where $\boldsymbol{U}$ is the unitary DFT matrix whose (i,j)th element is given by $u_{ij} = 1/\sqrt{N_s} e^{(-2\pi\sqrt{-1}/N_s)ij}$, $0 \leq i, j \leq N_s - 1$, $\boldsymbol{\Lambda} = diag[\boldsymbol{\lambda}_0^T, \cdots, \boldsymbol{\lambda}_{N_s-1}^T]$ is an $N_s \times N_s P$ block diagonal matrix whose (k,k)th block is given by

$$\boldsymbol{\lambda}_k = \sum_{l=0}^{L-1} \boldsymbol{h}_l \cdot e^{-\frac{2\pi\sqrt{-1}}{N_s} kl}, \ k = 0, \cdots, N_s - 1. \tag{5.4}$$

Thus the received signals can be obtained as

$$\boldsymbol{x}_k^T = [x_k^{(1)}, \cdots, x_k^{(P)}] = \boldsymbol{\lambda}_k^T \boldsymbol{\Psi}_k + \boldsymbol{w}_k^T, \ k = 0, \cdots, N_s - 1 \tag{5.5}$$

where $\boldsymbol{w}_k$ is a circularly symmetric zero-mean white complex Gaussian noise vector. It is clear from (5.5) that ICI does not exist in the ST-OFDM system over quasi-static channels.

The P symbols in each column of $\boldsymbol{\Psi}_k$ are transmitted from the P transmit antennas simultaneously during every OFDM block period. If the channel is time-invariant

over P consecutive OFDM blocks, the pairwise ML scheme [6] can be used to detect pairs of transmitted symbols, instead of symbol by symbol, and there is no error floor in BER performance.

5.3. The Impact of Time-Varying Fading and Decision-Feedback Receiver Design

5.3.1. ICI and ITAI Caused by Time-Varying Fading

In the presence of time-selective fading, $\boldsymbol{H}$ is no longer a block-circulant matrix. Assuming a WSSUS channel [25], all elements of $\boldsymbol{h}_l(n)$ are modeled as independent complex Gaussian random variables with zero mean and equal variance. The channel is assumed to have an exponential power delay profile $\theta(\tau_l) = e^{-\tau_l/\tau_{rms}}$ [41], where τ_l is the delay of the lth path and τ_{rms} represents the root-mean square delay spread. Since the channel is time-variant, the relationship between the channel coefficients for path l of antenna p at times nT_s and $(n+m)T_s$ can be described as

$$h_l^{(p)}(n+m) = \alpha_m h_l^{(p)}(n) + \beta_l^{(p)}(n+m) \tag{5.6}$$

where

$$\alpha_m = \frac{E\left[h_l^{(p)}(n) \cdot h_l^{(p)*}(n+m)\right]}{e^{-\frac{\tau_l}{\tau_{rms}}}} = J_0(2\pi m f_d T_s) \tag{5.7}$$

where f_d is the Doppler shift and $\beta_l^{(p)}(n)$ are independent complex Gaussian random variables with zero mean and variance

$$\sigma_\beta^2 = \begin{cases} 1-\alpha_m^2, & l=0 \\ e^{-\frac{\tau_l}{\tau_{rms}}}(1-\alpha_m^2), & l \neq 0. \end{cases} \tag{5.8}$$

Consequently, $\boldsymbol{G} = \boldsymbol{U}\boldsymbol{H}(\boldsymbol{U} \otimes \boldsymbol{I}_P)^H$ is no longer a block diagonal matrix as $\boldsymbol{\Lambda}$ given in (5.3). This shows that time-selective fading causes ICI, which is represented

by the off-diagonal blocks of $\boldsymbol{G}$. For this more general case, the received signals are given by

$$\boldsymbol{x}_k^T = \boldsymbol{g}_{kk}^T \boldsymbol{\Psi}_k + \sum_{k'=0,k'\neq k}^{N_s-1} \boldsymbol{g}_{kk'}^T \boldsymbol{\Psi}_{k'} + \boldsymbol{w}_k^T, \;\; k = 0, \cdots, N_s - 1 \tag{5.9}$$

where $\boldsymbol{g}_{kk'} = [g_{kk'}^{(1)}, \cdots, g_{kk'}^{(P)}]^T, \; k, k' = 0, \cdots, N_s - 1$, is the (k, k')th block of $\boldsymbol{G}$. Apparently, the second term on the right-hand side of (5.9) represents ICI. To make the following analysis clearer and easier to understand, we focus on the 4×4 (i.e., $P = 4$) quasi-orthogonal STBC given in [6], which is replicated here as

$$\boldsymbol{\Psi}_k = \begin{bmatrix} b_k^{(1)} & -b_k^{(2)*} & -b_k^{(3)*} & b_k^{(4)} \\ b_k^{(2)} & b_k^{(1)*} & -b_k^{(4)*} & -b_k^{(3)} \\ b_k^{(3)} & -b_k^{(4)*} & b_k^{(1)*} & -b_k^{(2)} \\ b_k^{(4)} & b_k^{(3)*} & b_k^{(2)*} & b_k^{(1)} \end{bmatrix}. \tag{5.10}$$

To decode $\boldsymbol{\Psi}_k$, (5.9) is processed as

$$\boldsymbol{y}_k = \boldsymbol{M}_{kk} \boldsymbol{\psi}_k + \sum_{k'=0,k'\neq k}^{N_s-1} \boldsymbol{M}_{kk'} \boldsymbol{\psi}_{k'} + \boldsymbol{z}_k \tag{5.11}$$

where $\boldsymbol{\psi}_k = [b_k^{(1)}, b_k^{(2)}, b_k^{(3)}, b_k^{(4)}]^T$, $\boldsymbol{y}_k = [x_k^{(1)}, x_k^{(2)*}, x_k^{(3)*}, x_k^{(4)}]^T$, $\boldsymbol{z}_k$ is the noise term with the same mean and variance as $\boldsymbol{w}_k$, and the equivalent channel matrix is expressed as

$$\boldsymbol{M}_{kk'} = \begin{bmatrix} \boldsymbol{M}_{kk'}^{(1,2)}(0) & \boldsymbol{M}_{kk'}^{(3,4)}(0) \\ \boldsymbol{M}_{kk'}^{(3,4)*}(2\ell) & -\boldsymbol{M}_{kk'}^{(1,2)*}(2\ell) \end{bmatrix}, \;\; k, k' = 0, \cdots \; N_s - 1 \tag{5.12}$$

with

$$\boldsymbol{M}_{kk'}^{(i,j)}(n) = \begin{bmatrix} g_{kk'}^{(i)}(n) & g_{kk'}^{(j)}(n) \\ g_{kk'}^{(j)*}(n+\ell) & -g_{kk'}^{(i)*}(n+\ell) \end{bmatrix} \tag{5.13}$$

where $\ell = N_s + c_p$. By letting $g_{kk'}^{(p)}(0) = g_{kk'}^{(p)}, \; p = 1, \cdots, 4$, and using the same auto-regressive model as applied in (5.6), we have

$$g_{kk'}^{(p)}(q\ell) = J_0(2\pi f_d \ell T_s) g_{kk'}^{(p)}((q-1)\ell) + \varepsilon_{kk'}^{(p)}(q\ell) \tag{5.14}$$

where the index in the parenthesis following $g_{kk'}^{(p)}$ is the time index and $\{\varepsilon_{kk'}^{(p)}(q\ell)\}$ are independent complex Gaussian random variables with zero mean and variance

$$\sigma_{\varepsilon}^2 = (1 - J_0^2(2\pi f_d \ell T_s)) \cdot var(g_{kk'}^{(p)}). \tag{5.15}$$

Let $\boldsymbol{\Upsilon}$ be an $N_s \times N_s$ matrix given by

$$\boldsymbol{\Upsilon} = \begin{bmatrix} var(g_{00}^{(p)}) & \cdots & var(g_{0,N_s-1}^{(p)}) \\ \vdots & \ddots & \vdots \\ var(g_{N_s-1,0}^{(p)}) & \cdots & var(g_{N_s-1,N_s-1}^{(p)}) \end{bmatrix}. \tag{5.16}$$

As shown in APPENDIX A, for a particular antenna index p, $\boldsymbol{\Upsilon}$ has a circulant structure expressed as

$$\boldsymbol{\Upsilon} = \begin{bmatrix} \gamma_0 & \gamma_1 & \cdots & \gamma_{N_s-1} \\ \gamma_{N_s-1} & \gamma_0 & \cdots & \gamma_{N_s-2} \\ \vdots & \vdots & & \vdots \\ \gamma_1 & \gamma_2 & \cdots & \gamma_0 \end{bmatrix}. \tag{5.17}$$

Since elements of $\boldsymbol{g}_{kk'},\ k, k' = 0, \cdots, N_s - 1$, are i.i.d. Gaussian random variables [25], (5.17) applies to all antennas. It is also shown in APPENDIX A that γ_k defined in (5.17) has a closed-form expression as

$$\gamma_k = \frac{1}{N_s^2} \sum_{l=0}^{L-1} \left\{ N_s + 2 \sum_{i=1}^{N_s-1} (N_s - i)\, J_0(2\pi i f_d T_s) \cos\left(\frac{2\pi}{N_s} ki\right) \right\} e^{-\frac{\tau_l}{\tau_{rms}}}. \tag{5.18}$$

With (5.18), $g_{kk'}^{(p)}(q\ell)$ in (5.14) can be obtained by substituting γ_k into (5.15). As a result of channel time variations, $\gamma_k \neq 0$ for $k \neq 0$, which causes ICI. Noteworthily, as mentioned in [47], the frequency-domain correlative coding method incorporated in this chapter can effectively enhance system CIR without reducing its bandwidth efficiency.

In addition to ICI, channel time variations in $\boldsymbol{M}_{kk}$ introduce additional ITAI among elements of $\boldsymbol{\psi}_k$, which is illustrated as below. If the channel is time-invariant,

time indexes of elements in $\boldsymbol{M}_{kk}$ can be omitted and

$$\boldsymbol{M}_{kk}^{H}\boldsymbol{M}_{kk} = \begin{bmatrix} c & 0 & 0 & d \\ 0 & c & -d & 0 \\ 0 & -d & c & 0 \\ d & 0 & 0 & c \end{bmatrix} \tag{5.19}$$

where $c = \sum_{p=1}^{4} |g_{kk}^{(p)}|^2$ and $d = g_{kk}^{(1)} g_{kk}^{(4)*} + g_{kk}^{(1)*} g_{kk}^{(4)} - g_{kk}^{(2)} g_{kk}^{(3)*} - g_{kk}^{(2)*} g_{kk}^{(3)}$. Apparently, there is no interference between pairs $(b_k^{(1)}, b_k^{(4)})$ and $(b_k^{(2)}, b_k^{(3)})$ [6]. When the channel exhibits channel-varying fading, however, (5.19) does not hold and $\boldsymbol{M}_{kk}^{H}\boldsymbol{M}_{kk}$ should be expressed as

$$\boldsymbol{M}_{kk}^{H}\boldsymbol{M}_{kk} = \begin{bmatrix} \varrho_{11} & \varrho_{12} & \varrho_{13} & \varrho_{14} \\ \varrho_{21} & \varrho_{22} & \varrho_{23} & \varrho_{24} \\ \varrho_{31} & \varrho_{32} & \varrho_{33} & \varrho_{34} \\ \varrho_{41} & \varrho_{42} & \varrho_{43} & \varrho_{44} \end{bmatrix}. \tag{5.20}$$

Elements of the first row of the above matrix are expressed as

$$\varrho_{11} = |g_{kk}^{(1)}(0)|^2 + |g_{kk}^{(2)}(\ell)|^2 + |g_{kk}^{(3)}(2\ell)|^2 + |g_{kk}^{(4)}(3\ell)|^2 \tag{5.21a}$$

$$\varrho_{12} = g_{kk}^{(1)*}(0) g_{kk}^{(2)}(0) - g_{kk}^{(1)*}(\ell) g_{kk}^{(2)}(\ell) + g_{kk}^{(3)}(2\ell) g_{kk}^{(4)*}(2\ell) - g_{kk}^{(3)}(3\ell) g_{kk}^{(4)*}(3\ell) \tag{5.21b}$$

$$\varrho_{13} = g_{kk}^{(1)*}(0) g_{kk}^{(3)}(0) - g_{kk}^{(1)*}(2\ell) g_{kk}^{(3)}(2\ell) + g_{kk}^{(2)}(\ell) g_{kk}^{(4)*}(\ell) - g_{kk}^{(2)}(3\ell) g_{kk}^{(4)*}(3\ell) \tag{5.21c}$$

$$\varrho_{14} = g_{kk}^{(1)*}(0) g_{kk}^{(4)}(0) + g_{kk}^{(1)}(3\ell) g_{kk}^{(4)*}(3\ell) - g_{kk}^{(2)}(\ell) g_{kk}^{(3)*}(\ell) - g_{kk}^{(2)*}(2\ell) g_{kk}^{(3)}(2\ell). \tag{5.21d}$$

The non-zero items ϱ_{12} and ϱ_{13} represent ITAI to pair $(1, 4)$ from pair $(2, 3)$.

5.3.2. Decision-Feedback Receiver Design

In a quasi-static fading channel, the received signal can be directly processed by a space-time decoder, whereas in a time-varying fading channel, the detection becomes

more complex if ICI and ITAI are to be dealt with simultaneously. The TS-ZF detector [12] aims at lowering the error floor due to ITAI. This scheme will not be very effective for quasi-orthogonal ST-OFDM systems over time-varying channels as ICI could be severe especially when N_s is large.

The SDFSE with an adaptive threshold [54] for two-antenna, orthogonal ST-OFDM systems is expected to perform better than the TS-ZF scheme. But this scheme also suffers from an irreducible error floor. We apply a modified DF scheme for detection of ST-OFDM systems with correlative coding. Without loss of generality, we still focus on the code given in (5.10) in describing the proposed receiver. The ICI and noise terms in (5.11) are represented by a single variable $\boldsymbol{d}_k$ as

$$\boldsymbol{d}_k = \sum_{k'=0,k'\neq k}^{N_s-1} \boldsymbol{M}_{kk'}\boldsymbol{\psi}_{k'} + \boldsymbol{z}_k. \tag{5.22}$$

Then we pre-multiply $\boldsymbol{y}_k$ by $\boldsymbol{\mathcal{L}}^{-1}\boldsymbol{M}_{kk}^H$, which yields

$$\widetilde{\boldsymbol{y}}_k = \boldsymbol{\mathcal{L}}^{-1}\boldsymbol{M}_{kk}^H\boldsymbol{y}_k = \boldsymbol{\mathcal{L}}^H\boldsymbol{\psi}_k + \boldsymbol{e}_k \tag{5.23}$$

where $\boldsymbol{e}_k = \boldsymbol{\mathcal{L}}^{-1}\boldsymbol{M}_{kk}^H\boldsymbol{d}_k$ and $\boldsymbol{\mathcal{L}}^H$ is an upper triangular matrix obtained by using the Cholesky decomposition as $\boldsymbol{\mathcal{R}} = \boldsymbol{M}_{kk}^H\boldsymbol{M}_{kk} = \boldsymbol{\mathcal{L}}\boldsymbol{\mathcal{L}}^H$. The pth component of $\widetilde{\boldsymbol{y}}_k$ is given by

$$[\widetilde{\boldsymbol{y}}_k]_p = \boldsymbol{\mathcal{L}}_{pp}^H[\boldsymbol{\psi}_k]_p + \sum_{i=p+1}^{4} \boldsymbol{\mathcal{L}}_{pi}^H[\boldsymbol{\psi}_k]_i + [\boldsymbol{e}_k]_p. \tag{5.24}$$

The transmitted symbols are detected as

$$\begin{aligned}
\widehat{b}_k^{(4)} &= \text{dec}\{[\widetilde{\boldsymbol{y}}_k]_4\} \\
\widehat{b}_k^{(p)} &= \text{dec}\left\{[\widetilde{\boldsymbol{y}}_k]_p - \sum_{i=p+1}^{4} \boldsymbol{\mathcal{L}}_{pi}^H\widehat{b}_k^{(i)}\right\}, \quad p = 1,2,3
\end{aligned}$$

where $\text{dec}(\cdot)$ is the slice function corresponding to $(1-D)$ correlative coding [47]. Finally, $\{a_i\}$ can be recovered by using a ML sequence detector [52].

It is well known that performance of the DF scheme described above can be significantly improved if signals are ranked according to their relative strength[2] and then followed by a successive cancellation process [48, 55]. The decorrelating DF detection scheme [56] for spatial multiplexing systems requires that the number of receive antennas be greater than or equal to the number of transmit antennas. Since the equivalent channel matrix $\boldsymbol{\mathcal{L}}^H$ in (5.23) is a 4×4 matrix, this DF scheme can be employed for detection of quasi-orthogonal ST-OFDM systems in time-varying environments. The detection begins with (5.23) by decoding the strongest signal first, followed by a cancellation process, which is summarized as follows. Let $\boldsymbol{\mathcal{L}}^{(u)}|_{u=4} = \boldsymbol{\mathcal{L}}$. The following procedures are repeated for $u = 4$ to 1:

1. *Find the column of* $(\boldsymbol{\mathcal{L}}^{(u)})^{-1}$ *which has the smallest column norm, and exchange it with the last column via a unitary transformation* $\boldsymbol{\mathcal{P}}$ *as* $(\boldsymbol{\mathcal{L}}^{(u)})^{-1}\boldsymbol{\mathcal{P}}$.

2. *Find a unitary matrix* $\boldsymbol{\mathcal{O}}$ *which transforms* $\boldsymbol{\mathcal{L}}^{(u)*}\boldsymbol{\mathcal{P}}$ *to an upper triangular matrix* $\boldsymbol{\mathcal{O}}\boldsymbol{\mathcal{L}}^{(u)*}\boldsymbol{\mathcal{P}}$. *Then, compute the lower triangular matrix* $\boldsymbol{\mathcal{O}}(\boldsymbol{\mathcal{L}}^{(u)})^{-1}\boldsymbol{\mathcal{P}}$.

3. *Perform DF detection based on (5.23) using the reordered matrices.*

Because this modified DF detection scheme guarantees that the detected signal has the highest SNR at every step, it should achieve a better BER performance than conventional DF schemes.

---

[2]The strongest signal refers to the signal with the highest signal-to-noise ratio (SNR), and the weakest signal refers to the signal with the lowest SNR.

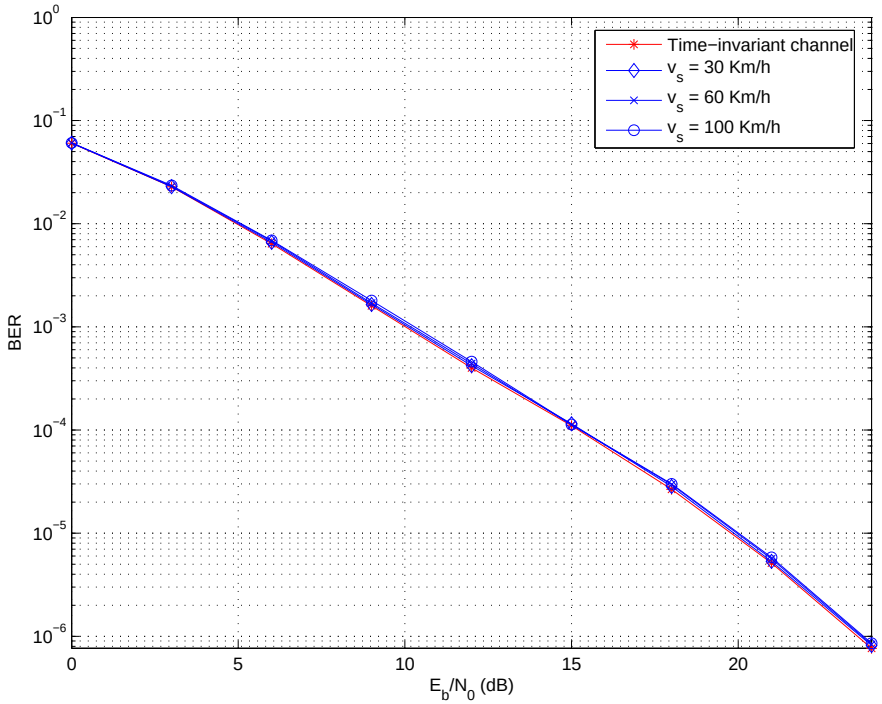

FIGURE 5.1. BER versus E_b/N_0 for quasi-orthogonal ST-OFDM systems with different fading rates ($N_s = 16$, $T_s = 10^{-6}$s).

5.4. Numerical Results and Discussion

Simulations are carried out based on the "SUI-5" channel model [13], which is one of six channel models adopted by IEEE 802.16a for evaluating broadband wireless systems in 2-11 GHz bands. We consider a system with four transmit antennas and one receive antenna which employs BPSK modulation and the 4×4 quasi-orthogonal STBC given in (5.10). The time-selective Rayleigh fading channel is assumed to have three resolvable multipath components, each of which at 0, 5, and $10\mu s$ is modeled as an independent complex gaussian random variable, the rms delay spread is $3.05\mu s$, and the Doppler shift of the channel is calculated based on a carrier frequency of $f_c = 2$GHz.

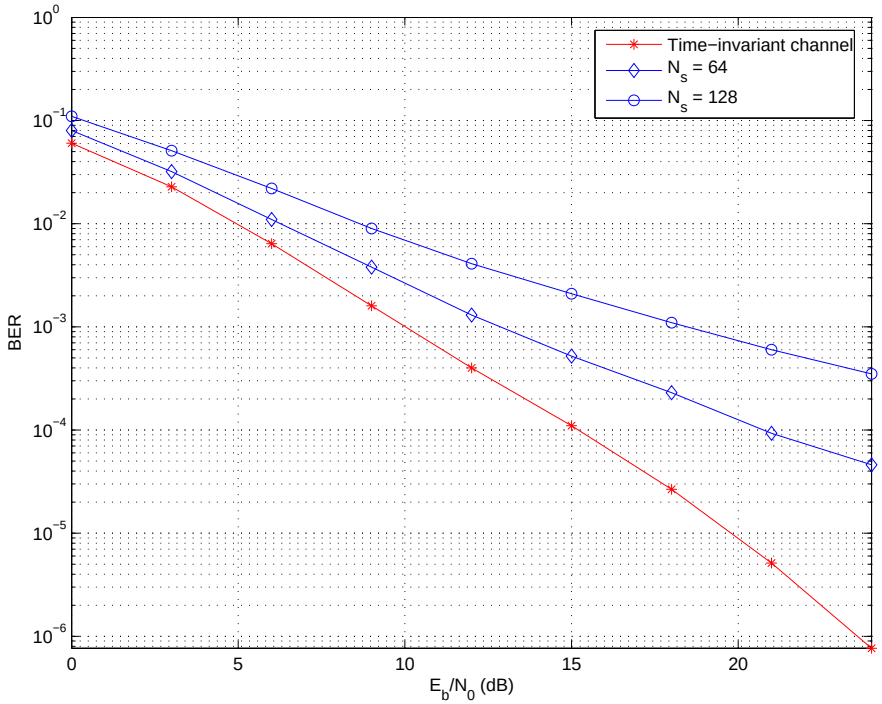

FIGURE 5.2. BER versus E_b/N_0 for quasi-orthogonal ST-OFDM systems with different number of subcarriers ($v_s = 100$Km/h, $T_s = 10^{-6}$s).

Fig. 5.1 shows the simulated BER performance of the system when the modified DF scheme is employed. The OFDM symbol is assumed to have $N_s = 16$ subcarriers, and each data symbol period is $T_s = 10^{-6}$ seconds. Performances with different vehicle speeds, $v_s = 30, 60,$ and 100Km/h, are compared. In the same figure, the curve of the quasi-orthogonal ST-OFDM system over a time-invariant multipath fading channel is used as the baseline performance. When the number of subcarriers is small ($N_s = 16$ in Fig. 5.1), the system performs almost the same for any of the vehicle speeds, all of which approach the baseline performance.

As the number of subcarriers increases, however, system performance deteriorates rapidly. This is clearly shown in Fig. 5.2, where the vehicle speed is

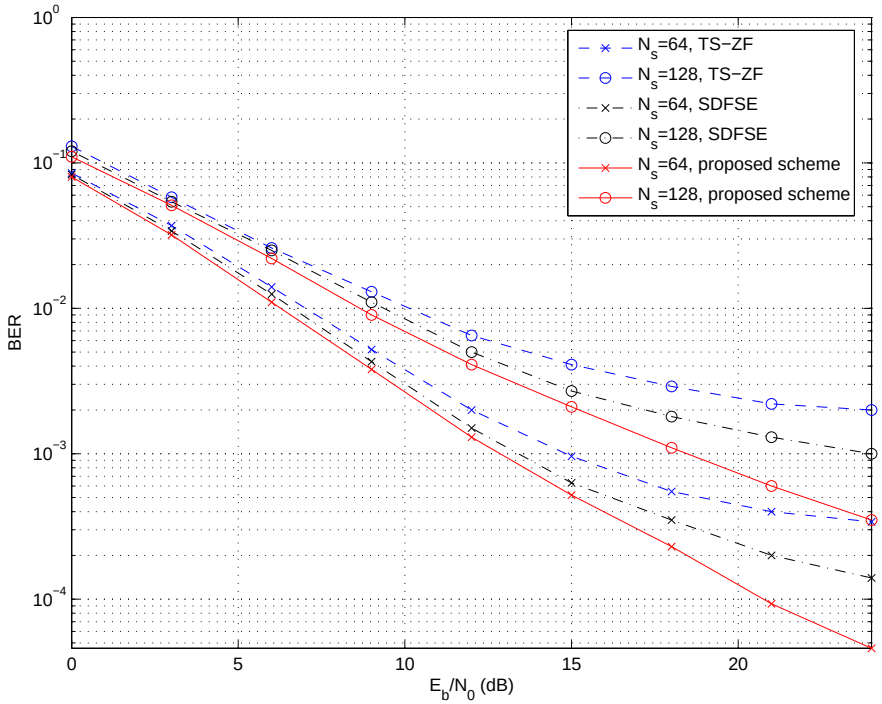

FIGURE 5.3. Error performances of the quasi-orthogonal ST-OFDM system with different detection schemes

$v_s = 100$Km/h and all other parameters are the same as those applied to generate Fig. 5.1. From the BER versus E_b/N_0 curves with $N_s = 64$ and 128, the error floor becomes larger as N_s increases. The main reason is that a larger number of subcarriers within one OFDM block not only causes a more severe ICI but also increases the time interval in (5.15), causing a greater amount of ITAI within one STBC matrix.

In Fig. 5.3, we compare the performances of three different schemes: the TS-ZF, the SDFSE, and the proposed scheme which uses frequency-domain correlative coding and the modified DF detection scheme. All parameters are the same as those applied for Fig. 5.2. It is observed that the proposed scheme effectively eliminates

the error floor of the quasi-orthogonal ST-OFDM system, whereas the TS-ZF and the SDFSE schemes both suffer from an error floor.

The required number of metric calculations for an quasi-orthogonal STBC codeword (4 consecutive OFDM symbol periods) with the TS-ZF scheme is proportional to QN_s [12], where Q is the constellation size. The number of metric calculations for the same codeword with the SDFSE scheme is approximately equal to $Q^{2q}N_s$ [54], where $2q$ is the number of subchannels that cause inter-codeword couplings. The computational complexity of the proposed scheme is approximately P^3N_s. With a typical set of system parameters (e.g., $Q = 2$, $P = 4$, and $q = 3$), the TS-ZF scheme has the lowest complexity, and the SDFSE scheme with an adaptive threshold and the proposed scheme have comparable complexities.

5.5. Conclusions

We have studied a scheme that combines frequency-domain correlative coding with a modified DF receiver for quasi-orthogonal ST-OFDM systems over time-selective fading channels. We have analyzed the impact of channel time selectivity on the performance of such systems. Performances of three detection schemes are compared, and it is found that the proposed scheme can effectively eliminate the error floor of quasi-orthogonal ST-OFDM systems in fast fading environments.

6. MIMO-OFDM SYSTEMS IN THE PRESENCE OF PHASE NOISE AND DOUBLY-SELECTIVE FADING

6.1. Introduction

OFDM is considered a promising transmission technique for wideband wireless communications. One of the disadvantages of OFDM is its sensitivity to phase noise, which is a random process caused by the fluctuation of the transmitter and receiver oscillators [36]. It is widely accepted that phase noise in OFDM has two major effects [18, 37]: CPE, a constant rotation to the signal constellation, and ICI due to the loss of orthogonality among subcarriers caused by the fast changes of the oscillator phase. The CPE term is the same for all subcarriers within one OFDM symbol interval and changes slowly from one symbol to another. If phase noise level is low, CPE approximately equals the mean of the phase deviation of an oscillator within one OFDM symbol. The ICI term is a random process. Schemes which compensate phase noise in OFDM systems have been proposed in [20,24]. In [22], the SINR expression for single-antenna OFDM systems with various phase noise levels and different number of subcarriers was derived.

MIMO antennas have been combined with OFDM to improve spectral efficiency through spatial multiplexing [14]. Similar to single-antenna OFDM, MIMO-OFDM is also highly sensitive to phase noise. CPE estimation schemes for MIMO-OFDM systems were derived in [26] and in [27] a decision-directed approach for compensation of phase noise in MIMO-OFDM systems was studied. Besides phase noise, time-selective fading also destroys the orthogonality among different subcarriers within one OFDM symbol and causes ICI [15, 16]. Similar to single-antenna OFDM, MIMO-OFDM is also vulnerable to channel time selectivity. Error performance of

MIMO-OFDM systems in the presence of time-selective fading without considering phase noise was analyzed in [25].

Although the issue caused by phase noise and time-selective fading in MIMO-OFDM has been recognized, the exact quantitative effect of the combination of the two has not been well addressed. Phase noise mitigation for MIMO-OFDM in fast time-varying fading environments has not been well studied either. In this chapter, we analyze, via mainly an analytical approach, the impact of phase noise to the performance of MIMO-OFDM systems over doubly-selective Rayleigh fading channels.After characterizing CPE caused by phase noise and ICI caused by phase noise and time-selective fading, we derive an MMSE-based mitigation scheme to effectively minimize the impact of phase noise. We also compare four detection schemes, ZF, MMSE, decorrelating DF and MMSE-DF schemes, and evaluate their SER performance.

6.2. System Model

Consider a MIMO-OFDM system with N_t transmit antennas, N_r receive antennas, and N_s subcarriers in a doubly-selective Rayleigh fading environment. Input data are assumed to be independent variables with zero mean and unit variance. The time domain data sequence is obtained by taking the IDFT of the data block for each transmit antenna. A CP with a length longer than the channel length is inserted at the beginning of each of the data sequences. The data sequences with a CP are then transmitted through N_t independent antennas. At each receive antenna, the CP is removed and a DFT unit is applied. Let $\boldsymbol{x}_k = [x_{k1}, \cdots, x_{kN_t}]^T$ and $\boldsymbol{y}_k = [y_{k1}, \cdots, y_{kN_r}]^T$ denote, respectively, the transmitted and received data for all antennas on subcarrier k, where $0 \leq k \leq N_s - 1$. The general form of the received signal in MIMO-OFDM over slowly fading channels (the channel is time-invariant over several OFDM symbol

periods) is expressed as

$$\boldsymbol{y}_k = \boldsymbol{\Delta}_k \boldsymbol{x}_k + \boldsymbol{n}_k \tag{6.1}$$

where $\boldsymbol{\Delta}_k$ is an $N_r \times N_t$ matrix whose (i,j)th component, $\{\boldsymbol{\Delta}_k\}_{ij}$, denotes the channel frequency response between the jth transmit antenna and the ith receive antenna and $\boldsymbol{n}_k$ is an $N_r \times 1$ Gaussian noise vector on subcarrier k. Elements of $\boldsymbol{n}_k$ have zero mean and variance σ^2.

Phase noise $\phi(t)$ may be described as a continuous Brownian motion process with zero mean and variance $2\pi\beta t$, where β denotes the two-sided 3-dB linewidth of the Lorentzian power density spectrum of the *free-running* carrier generator [36]. For the analysis in this chapter, we need to consider discretized Brownian motion $\phi(n) = \phi(nT_s)$, where T_s is the data symbol period. Thus we have $\phi(n+1) = \phi(n) + \varsigma(n)$, where $\varsigma(n) \sim \mathcal{N}(0, 2\pi\beta T_s)$ is a Gaussian random variable with zero mean and variance $\sigma_\varsigma^2 = 2\pi\beta T_s$. If we assume that only one oscillator is used to support multiple antennas, Eq. (6.1) needs to be modified to take into account the effects of phase noise as [22]

$$\boldsymbol{y}_k = \boldsymbol{\Delta}_k \boldsymbol{x}_k I(0) + \sum_{\substack{k'=0 \\ k' \neq k}}^{N_s-1} \boldsymbol{\Delta}_{k'} \boldsymbol{x}_{k'} I(k'-k) + \boldsymbol{n}_k \tag{6.2}$$

where

$$I(f) = \frac{1}{N_s} \sum_{n=0}^{N_s-1} e^{j\frac{2\pi f n}{N_s} + j\phi(n)}. \tag{6.3}$$

Note that CPE and ICI due to phase noise are represented by $I(0)$ and the second term on the right-hand side of Eq. (6.2), respectively.

6.3. The Impact of ICI Caused by Phase Noise and Time-Varying Fading

In the presence of phase noise and time-selective fading, the effective $N_s N_r \times N_s N_t$ spatiotemporal channel matrix $\boldsymbol{H}_t$ during the tth OFDM symbol period with the

effects of phase noise taken into consideration is expressed as [29] $\boldsymbol{H}_t =$

$$\begin{bmatrix} \boldsymbol{H}_{t,0}(0)e^{j\phi(0)} & \cdots & \mathbf{0} & \cdots & \boldsymbol{H}_{t,1}(0)e^{j\phi(0)} \\ \vdots & & \vdots & & \vdots \\ \boldsymbol{H}_{t,L-1}(L-1)e^{j\phi(L-1)} & \cdots & \boldsymbol{H}_{t,0}(L-1)e^{j\phi(L-1)} & \cdots & \mathbf{0} \\ \vdots & & \vdots & & \vdots \\ \mathbf{0} & \cdots & \boldsymbol{H}_{t,L-1}(N_s-1)e^{j\phi(N_s-1)} & \cdots & \boldsymbol{H}_{t,0}(N_s-1)e^{j\phi(N_s-1)} \end{bmatrix} \tag{6.4}$$

where L is the number of resolvable paths and $\mathbf{0}$ is an $N_r \times N_t$ zero matrix. Each non-zero block of $\boldsymbol{H}_t$ contains the $N_r \times N_t$ channel matrix $\boldsymbol{H}_{t,l}(n)$ for path l at time nT_s. Note that the index in the parenthesis following $\boldsymbol{H}_{t,l}$ is the time index. For simplicity of notation, we will omit the time index t which represents the OFDM symbol period hereafter.

Assuming a WSSUS channel [25], all elements of $\boldsymbol{H}_l(n)$ are modeled as independent complex Gaussian random variables with zero mean and equal variance. The channel is assumed to have an exponential power delay profile $\theta(\tau_l) = e^{-\tau_l/\tau_{rms}}$ [41], where τ_l is the delay of the lth path and τ_{rms} represents the rms delay spread. Since the channel is time-variant, the relationship between the channel coefficients for path l at times nT_s and $(n+m)T_s$ can be described as [12]

$$\{\boldsymbol{H}_l(n+m)\}_{ij} = \alpha_m\{\boldsymbol{H}_l(n)\}_{ij} + \rho_{l,ij}(n+m) \tag{6.5}$$

where

$$\alpha_m = \frac{E\left[\{\boldsymbol{H}_l(n)\}_{ij} \cdot \{\boldsymbol{H}_l(n+m)\}_{ij}^*\right]}{e^{-\frac{\tau_l}{\tau_{rms}}}} = J_0(2\pi m f_d T_s) \tag{6.6}$$

f_d is the maximum Doppler shift and $\{\rho_{l,ij}(n)\}$ are independent complex Gaussian random variables with zero mean and variance $e^{-\frac{\tau_l}{\tau_{rms}}}(1-\alpha_m^2)$.

Had the system been phase noise free and the channel been time-invariant, $\boldsymbol{H}$ given in Eq. (6.4) would have had the eigen-decomposition $\boldsymbol{H} = (\boldsymbol{U} \otimes \boldsymbol{I}_{N_r})^H \boldsymbol{\Lambda}(\boldsymbol{U} \otimes$

$\boldsymbol{I}_{N_t}$), where $\boldsymbol{U}$ is the unitary DFT matrix with $\{\boldsymbol{U}\}_{ij} = 1/\sqrt{N_s}e^{(-2\pi\sqrt{-1}/N_s)ij}$, $0 \leq i, j \leq N_s - 1$, and $\boldsymbol{\Lambda}$ is a block diagonal matrix whose (k,k)th block equals $\boldsymbol{\Delta}_k$ [25]. This establishes the relationship between the channel frequency response given in Eqs. (6.1) and (6.2) and the channel coefficients in the time domain.

With the effective channel matrix given in Eq. (6.4), we let $\boldsymbol{G} = (\boldsymbol{U} \otimes \boldsymbol{I}_{N_r})\boldsymbol{H}(\boldsymbol{U} \otimes \boldsymbol{I}_{N_t})^H$, which is no longer a block diagonal matrix. This shows that phase noise and time-selective fading cause ICI, which is represented by the off-diagonal blocks of $\boldsymbol{G}$. Let $\boldsymbol{G}_{ij}$ denote the (i,j)th block of $\boldsymbol{G}$. The ideal model given in Eq. (6.1) needs to be generalized to reflect the impacts of both time-selective fading and phase noise as

$$\boldsymbol{y}_k = \boldsymbol{G}_{kk}\boldsymbol{x}_k + \sum_{\substack{k'=0 \\ k' \neq k}}^{N_s-1} \boldsymbol{G}_{kk'}\boldsymbol{x}_{k'} + \boldsymbol{n}_k,\ k = 0, \cdots, N_s - 1. \tag{6.7}$$

Let $\boldsymbol{\Upsilon}_{ij}$ be an $N_s \times N_s$ matrix given by

$$\boldsymbol{\Upsilon}_{ij} = \begin{bmatrix} var(\{\boldsymbol{G}_{00}\}_{ij}) & \cdots & var(\{\boldsymbol{G}_{0,N_s-1}\}_{ij}) \\ \vdots & \ddots & \vdots \\ var(\{\boldsymbol{G}_{N_s-1,0}\}_{ij}) & \cdots & var(\{\boldsymbol{G}_{N_s-1,N_s-1}\}_{ij}) \end{bmatrix}. \tag{6.8}$$

As shown in APPENDIX B, $\boldsymbol{\Upsilon}_{ij}$ has a circulant structure expressed as

$$\boldsymbol{\Upsilon}_{ij} = \begin{bmatrix} \gamma_0 & \gamma_1 & \cdots & \gamma_{N_s-1} \\ \gamma_{N_s-1} & \gamma_0 & \cdots & \gamma_{N_s-2} \\ \vdots & \vdots & & \vdots \\ \gamma_1 & \gamma_2 & \cdots & \gamma_0 \end{bmatrix},\ 1 \leq i \leq N_r, 1 \leq j \leq N_t. \tag{6.9}$$

Since elements of $\boldsymbol{G}_{ij}$ are i.i.d. Gaussian random variables [25], Eq. (6.9) applies to all antennas. It is also shown in APPENDIX B that γ_k defined in Eq. (6.9) can be expressed in closed-form as

$$\gamma_k = \frac{1}{N_s^2}\sum_{l=0}^{L-1}\left\{N_s + 2\sum_{i=1}^{N_s-1}(N_s - i)J_0(2\pi i f_d T_s)\cos\left(\frac{2\pi}{N_s}ki\right)e^{-\pi\beta T_s i}\right\}e^{-\frac{\tau_l}{\tau_{rms}}}. \tag{6.10}$$

In order to quantify the combined effects of both phase noise and time-selective fading, we derive CIR as a function of the two-sided 3-dB linewidth β, the number of subcarriers, and the normalized Doppler shift ($f_d T_s$). In the presence of phase noise and time-selective fading, CIR of the kth subcarrier for MIMO-OFDM systems is expressed as

$$
\begin{aligned}
CIR &= \frac{E\left[\left\|\boldsymbol{G}_{kk}\boldsymbol{x}_k\right\|_F^2\right]}{E\left[\left\|\sum\limits_{\substack{k'=0\\k'\neq k}}^{N_s-1}\boldsymbol{G}_{kk'}\boldsymbol{x}_{k'}\right\|_F^2\right]} \\
&= \frac{tr\left\{E\left[\boldsymbol{G}_{kk}\boldsymbol{x}_k\boldsymbol{x}_k^H\boldsymbol{G}_{kk}^H\right]\right\}}{tr\left\{E\left[\left(\sum\limits_{\substack{k'=0\\k'\neq k}}^{N_s-1}\boldsymbol{G}_{kk'}\boldsymbol{x}_{k'}\right)\left(\sum\limits_{\substack{k'=0\\k'\neq k}}^{N_s-1}\boldsymbol{G}_{kk'}\boldsymbol{x}_{k'}\right)^H\right]\right\}} \\
&= \frac{\gamma_0}{\sum\limits_{k'=1}^{N_s-1}\gamma_{k'}} = \frac{\sum\limits_{l=0}^{L-1}\left\{N_s+2\sum\limits_{i=1}^{N_s-1}(N_s-i)\alpha_i e^{-\pi\beta T_s i}\right\}e^{-\frac{\tau_l}{\tau_{rms}}}}{\sum\limits_{k'=1}^{N_s-1}\sum\limits_{l=0}^{L-1}\left\{N_s+2\sum\limits_{i=1}^{N_s-1}(N_s-i)\alpha_i\cos\left(\frac{2\pi}{N_s}k'i\right)e^{-\pi\beta T_s i}\right\}e^{-\frac{\tau_l}{\tau_{rms}}}} \\
&= \frac{N_s+2\sum\limits_{i=1}^{N_s-1}(N_s-i)J_0(2\pi i f_d T_s)e^{-\pi\beta T_s i}}{\sum\limits_{k'=1}^{N_s-1}\left\{N_s+2\sum\limits_{i=1}^{N_s-1}(N_s-i)J_0(2\pi i f_d T_s)\cos\left(\frac{2\pi}{N_s}k'i\right)e^{-\pi\beta T_s i}\right\}}.
\end{aligned}
\tag{6.11}
$$

Note that CIR is independent of the channel power-delay profile and the number of resolvable paths, and is the same for all subcarriers. Furthermore, the SINR expression of MIMO-OFDM systems in the presence of phase noise and time-selective fading is given as

$$
\begin{aligned}
SINR &= \frac{E\left[\|\boldsymbol{G}_{kk}\boldsymbol{x}_k\|_F^2\right]}{E\left[\left\|\sum\limits_{\substack{k'=0\\k'\neq k}}^{N_s-1}\boldsymbol{G}_{kk'}\boldsymbol{x}_{k'}+\boldsymbol{n}_k\right\|_F^2\right]} \\
&= \frac{tr\left\{E\left[\boldsymbol{G}_{kk}\boldsymbol{x}_k\boldsymbol{x}_k^H\boldsymbol{G}_{kk}^H\right]\right\}}{tr\left\{E\left[\left(\sum\limits_{\substack{k'=0\\k'\neq k}}^{N_s-1}\boldsymbol{G}_{kk'}\boldsymbol{x}_{k'}\right)\left(\sum\limits_{\substack{k'=0\\k'\neq k}}^{N_s-1}\boldsymbol{G}_{kk'}\boldsymbol{x}_{k'}\right)^H+\boldsymbol{n}_k\boldsymbol{n}_k^H\right]\right\}} \\
&= \frac{N_t\gamma_0}{N_t\sum\limits_{k'=1}^{N_s-1}\gamma_{k'}+\sigma^2}
\end{aligned}
\tag{6.12}
$$

where $\gamma_{k'}$ was given in Eq. (6.10).

6.4. Phase Noise Suppression and Data Detection

As mentioned in Section 6.3, Eqs. (6.1) and (6.2) do not hold for MIMO-OFDM systems in the presence of phase noise and time-selective fading. From Eq. (6.5), we have

$$
\sum_{n=0}^{N_s-1}\{\boldsymbol{H}_l(n)\}_{ij}e^{j\phi(n)} = \{\boldsymbol{H}_l(0)\}_{ij}\sum_{m=0}^{N_s-1}\alpha_m e^{j\phi(m)} + \sum_{n=1}^{N_s-1}\rho_{l,ij}(n)e^{j\phi(n)}. \tag{6.13}
$$

Hence

$$
\begin{aligned}
&\{\boldsymbol{G}_{kk}\}_{ij} \\
=&\sum_{l=0}^{L-1}\sum_{n=0}^{N_s-1}u_{kn}u_{k,[n-l]}^*\{\boldsymbol{H}_l(n)\}_{ij}e^{j\phi(n)} \\
=&\frac{1}{N_s}\sum_{l=0}^{L-1}e^{-j\frac{2\pi}{N_s}kl}\sum_{n=0}^{N_s-1}\{\boldsymbol{H}_l(n)\}_{ij}e^{j\phi(n)} \\
=&\frac{1}{N_s}\sum_{l=0}^{L-1}e^{-j\frac{2\pi}{N_s}kl}\{\boldsymbol{H}_l(0)\}_{ij}\sum_{m=0}^{N_s-1}\alpha_m e^{j\phi(m)} + \frac{1}{N_s}\sum_{l=0}^{L-1}e^{-j\frac{2\pi}{N_s}kl}\sum_{n=1}^{N_s-1}\rho_{l,ij}(n)e^{j\phi(n)}
\end{aligned}
\tag{6.14}
$$

where u_{kn} and $u^*_{k,[n-l]}$ are defined in APPENDIX B. Thus, Eq. (6.7) can be modified as

$$\boldsymbol{y}_k = \boldsymbol{C}_{kk}\boldsymbol{x}_k \frac{1}{N_s}\sum_{m=0}^{N_s-1}\alpha_m e^{j\phi(m)} + \boldsymbol{P}_{kk}\boldsymbol{x}_k + \sum_{\substack{k'=0\\k'\neq k}}^{N_s-1}\boldsymbol{G}_{kk'}\boldsymbol{x}_{k'} + \boldsymbol{n}_k \tag{6.15}$$

where

$$\{\boldsymbol{C}_{kk}\}_{ij} = \sum_{l=0}^{L-1} e^{-j\frac{2\pi}{N_s}kl}\{\boldsymbol{H}_l(0)\}_{ij} \tag{6.16a}$$

$$\{\boldsymbol{P}_{kk}\}_{ij} = \frac{1}{N_s}\sum_{l=0}^{L-1} e^{-j\frac{2\pi}{N_s}kl}\sum_{n=1}^{N_s-1}\rho_{l,ij}(n)e^{j\phi(n)}. \tag{6.16b}$$

Note that $\frac{1}{N_s}\sum_{m=0}^{N_s-1}\alpha_m e^{j\phi(m)}$ in Eq. (6.15) is similar to $I(0)$ in Eq. (6.2), which is the CPE term. The term $\boldsymbol{P}_{kk}\boldsymbol{x}_k$ carries data symbols, but the distortion $\boldsymbol{P}_{kk}$ is a function of the phase noise process, which is costly to estimate. Additionally, when N_s is large, this term is very small due to the scaling factor $1/N_s$. Therefore, the term $\boldsymbol{P}_{kk}\boldsymbol{x}_k$ will be treated as noise for the derivation of MMSE-based phase noise mitigation and the third term on the right-hand side of Eq. (6.15) is the ICI term caused by both phase noise and time-selective fading.

For OFDM systems over fast fading channels, channel estimates are generally obtained by transmitting pilot symbols at certain positions of the frequency-time grid [20, 22, 42, 43]. When significant phase noise is also present, a joint scheme to simultaneously estimate CPE and CSI is needed. Such a joint estimation appears to be very challenging because of the mutual coupling effects of phase noise and channel fading processes as seen from (6.15), and is out of the scope of this chapter. We thus assume perfect CSI at the receiver, but unknown CPE to make the analytical derivation tractable. Therefore, the CPE term $C(0) = \frac{1}{N_s}\sum_{m=0}^{N_s-1}\alpha_m e^{j\phi(m)}$ must be estimated. In the following discussion, pilot signals are transmitted to estimate CPE. We rewrite Eq. (6.15) as

$$\boldsymbol{y}_{k\in N_p} = \boldsymbol{s}_{k\in N_p}C(0) + \boldsymbol{e}_{k\in N_p} \tag{6.17}$$

where $\boldsymbol{s}_k = \boldsymbol{C}_{kk}\boldsymbol{x}_k$, $\boldsymbol{e}_k = \boldsymbol{P}_{kk}\boldsymbol{x}_k + \sum_{k'=0,k'\neq k}^{N_s-1} \boldsymbol{G}_{kk'}\boldsymbol{x}_{k'} + \boldsymbol{n}_k$, and N_p stands for the set of pilot signals, which will be omitted in the analysis of MMSE for simplicity of notation. Let $\acute{\boldsymbol{N}}_k = E\left[\boldsymbol{e}_k\boldsymbol{e}_k^H\right]$. As shown in APPENDIX C, $\acute{\boldsymbol{N}}_k$ can be expressed as

$$\begin{aligned}\acute{\boldsymbol{N}}_k &= E\left[\boldsymbol{e}_k\boldsymbol{e}_k^H\right] \\ &= \left\{\frac{N_t}{N_s^2}\sum_{l=0}^{L-1} e^{-\frac{\tau_l}{\tau_{rms}}} \sum_{n=1}^{N_s-1}\left(1 - J_0^2(2\pi n f_d T_s)\right) + N_t\sum_{k'=1}^{N_s-1}\gamma_{k'} + \sigma^2\right\}\boldsymbol{I}_{N_r}. \quad (6.18)\end{aligned}$$

The results given in Eqs. (6.17) and (6.18) allow us to estimate the CPE term. When an MMSE scheme is applied, the cost function $E\left[\|C(0) - \acute{\boldsymbol{W}}_k^H\boldsymbol{y}_k\|_F^2\right]$ is minimized by finding an appropriate coefficient matrix $\acute{\boldsymbol{W}}_k$. With some algebraic manipulations, the optimal matrix in the MMSE sense is determined to be

$$\acute{\boldsymbol{W}}_k = \left(\boldsymbol{s}_k\boldsymbol{s}_k^H + \acute{\boldsymbol{N}}_k\right)^{-1}\boldsymbol{s}_k. \quad (6.19)$$

Thus, the MMSE estimate of CPE is given by

$$\hat{C}(0) = \acute{\boldsymbol{W}}_k^H\boldsymbol{y}_k = \boldsymbol{s}_k^H\left(\boldsymbol{s}_k\boldsymbol{s}_k^H + \acute{\boldsymbol{N}}_k\right)^{-1}\boldsymbol{y}_k. \quad (6.20)$$

CPE is the same for each subcarrier within one OFDM symbol. The effects of phase noise, time-selective fading, and the channel delay spread are jointly minimized through a single parameter $\hat{C}(0)$, which is a function of $\{\beta T_s, f_d T_s, \tau_{rms}, N_s, N_t, \sigma\}$. In what follows, we analyze a few existing detection schemes which incorporate the MMSE estimate of CPE derived in this chapter, that is, $\hat{C}(0)$ given in Eq. (6.20).

From the analysis above, we can relate the transmitted signals and received signals of the kth subcarrier as

$$\boldsymbol{y}_k = \boldsymbol{C}_{kk}\hat{C}(0)\boldsymbol{x}_k + \boldsymbol{e}_k. \quad (6.21)$$

When a simple ZF detection scheme is applied, $\boldsymbol{y}_k$ is processed as

$$\boldsymbol{\Theta}_k\boldsymbol{y}_k\hat{C}^{-1}(0) = \boldsymbol{\Theta}_k\boldsymbol{C}_{kk}\boldsymbol{x}_k + \boldsymbol{\Theta}_k\boldsymbol{e}_k\hat{C}^{-1}(0) \quad (6.22)$$

where $\boldsymbol{\Theta}_k = \boldsymbol{C}_{kk}^{\dagger}$. Note that when $N_r \geq N_t$ and a linear detection scheme is adopted, a diversity order of $N_r - N_t + 1$ can be achieved. Based on Eq. (6.22), the LS criterion can be used to detect the transmitted signal as

$$\hat{x}_{kp} = \underbrace{\operatorname{argmin}}_{x(i)\in\boldsymbol{\mathcal{A}}} |[\boldsymbol{\Theta}_k]_p \boldsymbol{y}_k \hat{C}^{-1}(0) - x(i)|^2, \;\; p = 1, \cdots, N_t \tag{6.23}$$

where $\boldsymbol{\mathcal{A}}$ is the symbol alphabet and $[\boldsymbol{\Theta}_k]_p$ is the pth row of $\boldsymbol{\Theta}_k$.

When the MMSE detection scheme is considered, $E\left[\|\boldsymbol{x}_k - \acute{\boldsymbol{M}}_k^H \boldsymbol{y}_k\|_F^2\right]$ is minimized by finding an matrix $\acute{\boldsymbol{M}}_k$, which is easily obtained as

$$\acute{\boldsymbol{M}}_k = \left(\boldsymbol{C}_{kk}\boldsymbol{C}_{kk}^H |\hat{C}(0)|^2 + \acute{\boldsymbol{N}}_k\right)^{-1} \boldsymbol{C}_{kk}\hat{C}(0) \tag{6.24}$$

where $\acute{\boldsymbol{N}}_k$ was given in Eq. (6.18). Thus the MMSE criterion yields

$$\begin{aligned} \hat{\boldsymbol{x}}_k &= \acute{\boldsymbol{M}}_k^H \boldsymbol{y}_k \\ &= \boldsymbol{C}_{kk}^H \hat{C}^*(0) \left(\boldsymbol{C}_{kk}\boldsymbol{C}_{kk}^H |\hat{C}(0)|^2 + \acute{\boldsymbol{N}}_k\right)^{-1} \boldsymbol{y}_k. \end{aligned} \tag{6.25}$$

The decorrelating DF and the MMSE-DF schemes have been shown to provide better performance than the ZF and the MMSE schemes [45]. In the decorrelating DF detection, $\boldsymbol{y}_k$ is premultiplied by $\boldsymbol{\mathcal{L}}^{-1}\boldsymbol{C}_{kk}^H \hat{C}^{-1}(0)$ as

$$\begin{aligned} \widetilde{\boldsymbol{y}}_k &= \boldsymbol{\mathcal{L}}^{-1}\boldsymbol{C}_{kk}^H \hat{C}^{-1}(0)\boldsymbol{y}_k \\ &= \boldsymbol{\mathcal{L}}^{-1}\boldsymbol{C}_{kk}^H \boldsymbol{C}_{kk}\boldsymbol{x}_k + \boldsymbol{\mathcal{L}}^{-1}\boldsymbol{C}_{kk}^H \hat{C}^{-1}(0)\boldsymbol{e}_k \\ &= \boldsymbol{\mathcal{L}}^H \boldsymbol{x}_k + \boldsymbol{d}_k \end{aligned} \tag{6.26}$$

where $\boldsymbol{\mathcal{L}}^H$ is an upper triangular matrix obtained by using the Cholesky decomposition as

$$\boldsymbol{\mathcal{R}} \;=\; \boldsymbol{C}_{kk}^H \boldsymbol{C}_{kk} \;=\; \boldsymbol{\mathcal{L}}\boldsymbol{\mathcal{L}}^H.$$

The pth component of $\widetilde{\boldsymbol{y}}_k$ is given by

$$\widetilde{y}_{kp} = \{\boldsymbol{\mathcal{L}}^H\}_{pp} x_{kp} + \sum_{i=p+1}^{N_t} \{\boldsymbol{\mathcal{L}}^H\}_{pi} x_{ki} + d_{kp}. \tag{6.27}$$

Finally, the transmitted symbols are detected as

$$\hat{x}_{kN_t} = \text{dec}\left(\widetilde{y}_{kN_t}\right)$$
$$\hat{x}_{kp} = \text{dec}\left(\widetilde{y}_{kp} - \sum_{i=p+1}^{N_t} \{\boldsymbol{\mathcal{L}}^H\}_{pi}\hat{x}_{ki}\right), \;\; p = 1, \cdots, N_t - 1$$

where dec$(\cdot)$ is the slice function corresponding to the specific modulation applied. The MMSE-DF scheme is the one that minimizes the average energy of $\widetilde{y}_{kp} - x_{kp}, \; p = 1, \cdots, N_t$, under the assumption that previously detected signals in the feedback filter are correct. Details of this scheme can be found in [40, 46].

6.5. Numerical Results and Discussion

Simulations are carried out based on the "SUI-5" channel model [13], which is one of six channel models adopted by IEEE 802.16a for evaluating broadband wireless systems in the 2-11GHz band. We consider a system with two transmit antennas and three receive antennas which employs QPSK modulation. The doubly-selective Rayleigh fading channel is assumed to have three resolvable multipath components. These paths are modeled as independent complex Gaussian random variables and have relative delays of $0\mu s$, $5\mu s$, and $10\mu s$. The rms delay spread of the channel is $3.05\mu s$ and the maximum Doppler shift of the channel is calculated based on a carrier frequency of $f_c = 2$GHz.

Fig. 6.1 shows the CIR values as a function of data symbol period T_s, the 3-dB phase noise linewidth β, and the number of subcarriers N_s within one OFDM symbol. These curves are obtained by using the analytical expression given in Eq. (6.11) and simulations based on the maximum Doppler shift under a vehicle speed of $v_s = 100$Km/h. Simulation results match well with the theoretical results. CIR is found to be inversely proportional to T_s, N_s, and β; thus, increasing β or T_s makes the

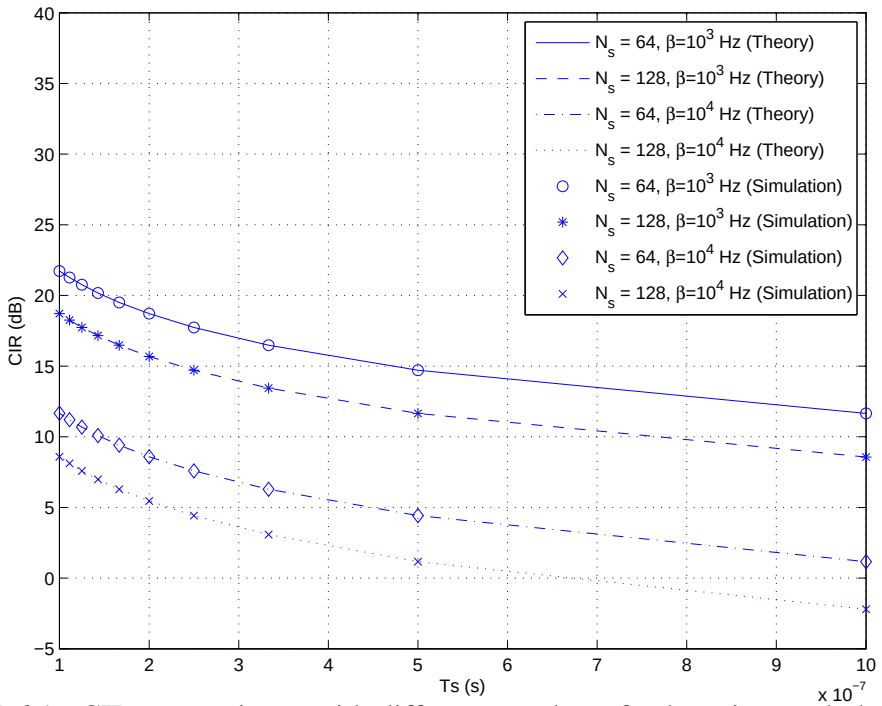

FIGURE 6.1. CIR comparisons with different number of subcarriers and phase noise linewidth ($v_s = 100$Km/h).

MIMO-OFDM system more vulnerable to phase noise or time variations of the channel coefficients.

In Fig. 6.2, SINR versus E_s/N_0 curves under different values of βT_s and v_s are obtained by using Eq. (6.12) and computer simulations. The OFDM symbol is assumed to have $N_s = 256$ subcarriers, and data symbol period is $T_s = 10^{-6}$ seconds. It is observed that SINR is inversely proportional to βT_s. With a fixed but large value of βT_s (e.g., 10^{-3}), however, the difference between SINR curves corresponding to different vehicle speeds diminishes. This is because when βT_s is large, ICI is dominated by phase noise. On the other hand, with a smaller βT_s value such as $\beta T_s = 10^{-4}$, increasing the Doppler shift (or vehicle speed) clearly lowers the SINR value.

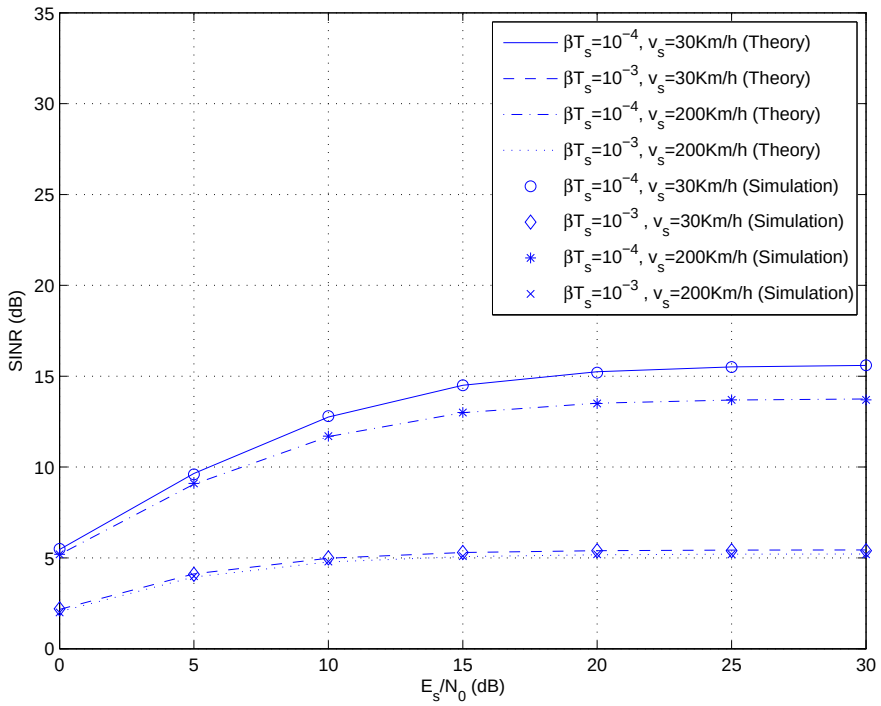

FIGURE 6.2. SINR versus E_s/N_0 for MIMO-OFDM with different vehicle speed and phase noise variance ($N_s = 256, T_s = 10^{-6}s$).

Fig. 6.3 shows the SER performance of the proposed MMSE-based phase noise suppression scheme together with those of a phase-noise-free system and a system without phase noise correction when the MMSE detection scheme given by Eq. (6.25) is considered. System parameters chosen are: $N_s = 128$, $T_s = 10^{-7}s$, $\beta = 10$Hz, and $v_s = 30$Km/h. It is observed that without phase noise correction, even a very mild amount of phase noise ($\beta T_s = 10^{-6}$) causes a high error floor. On the other hand, the proposed scheme significantly reduces the effect of phase noise. Note that performance of the proposed scheme does not approach that of the phase-noise-free system because this scheme mitigates only CPE, and it does not eliminate ICI, which is caused by both phase noise and time-selective fading.

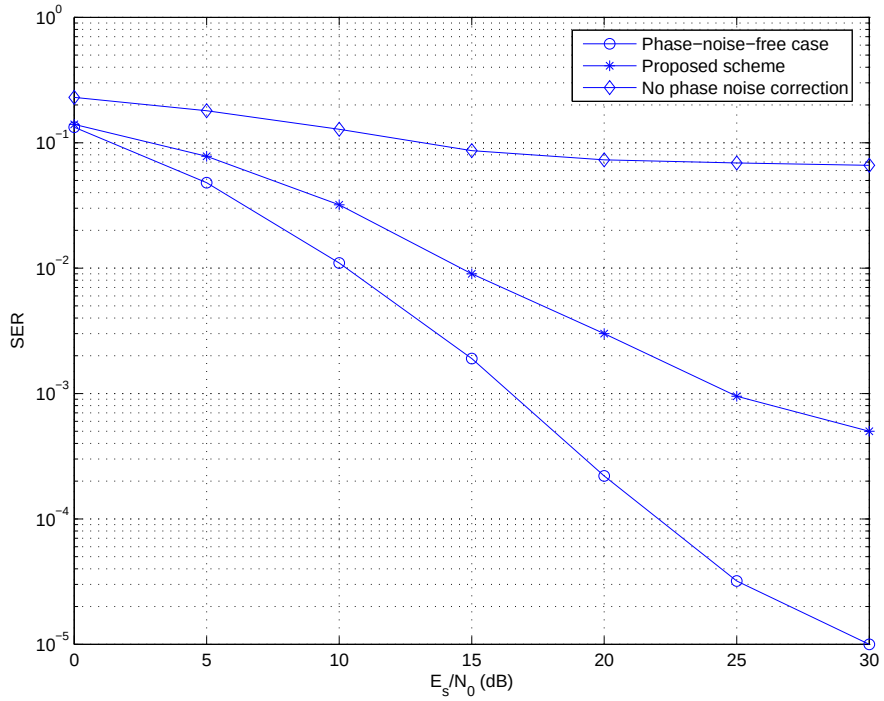

FIGURE 6.3. SER versus E_s/N_0 for MIMO-OFDM with phase noise $\beta T_s = 10^{-6}$ ($N_s = 128, T_s = 10^{-7}s, v_s = 30$Km/h).

Shown in Fig. 6.4 are the simulated SER performances of the system when the proposed MMSE-based phase noise suppression scheme given by Eq. (6.20) and the MMSE detection scheme described by Eq. (6.25) are employed. Other parameters chosen are: $N_s = 64$, $T_s = 10^{-7}s$, and $v_s = 100$Km/h. Performances with different values of the 3-dB phase noise variance ($\beta T_s = 10^{-7},\ 10^{-6},\ 3 \times 10^{-6},$ and 10^{-5}) are compared. The performance curve of a phase-noise-free MIMO-OFDM system is used as the baseline performance. It appears that the scheme works effectively only when βT_s is small.

In Fig. 6.5, we compare the performances of four different detection methods: the ZF, MMSE, decorrelating DF, and MMSE-DF schemes when the MMSE-based

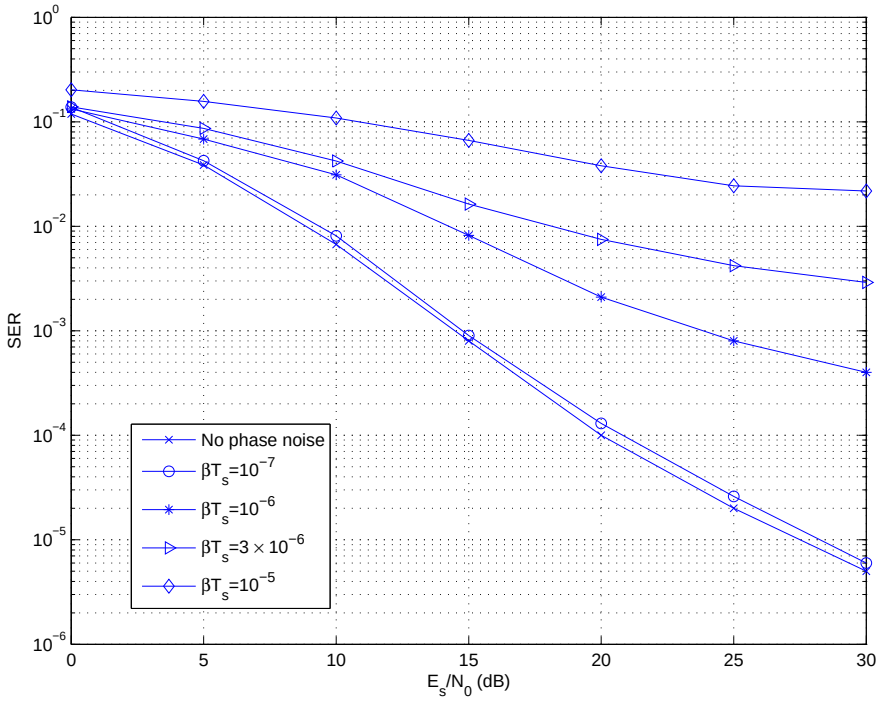

FIGURE 6.4. SER versus E_s/N_0 for MIMO-OFDM with different phase noise variance ($N_s = 64, T_s = 10^{-7}s, v_s = 100$Km/h).

phase noise suppression scheme given by Eq. (6.20) is applied. Other than that $\beta = 30$Hz, all other parameters are the same as those applied for Fig. 6.4. Performance of the MLscheme is used as the benchmark for other detection schemes. Since these schemes are not specifically optimized for MIMO-OFDM systems with phase noise over fast time-varying fading channels for which ICI should be dealt with, error floors are observed for all cases. Note that from Eqs. (6.10) and (6.11), the energy of ICI due to the phase noise and time-selective fading is found to spread over all subcarriers, which is different from the assumption in [57] that most of ICI on each subcarrier comes from several neighboring subcarriers. Consequently, ICI suppression for the scenario studied in this chapter becomes more challenging than the case dealt with in [57].

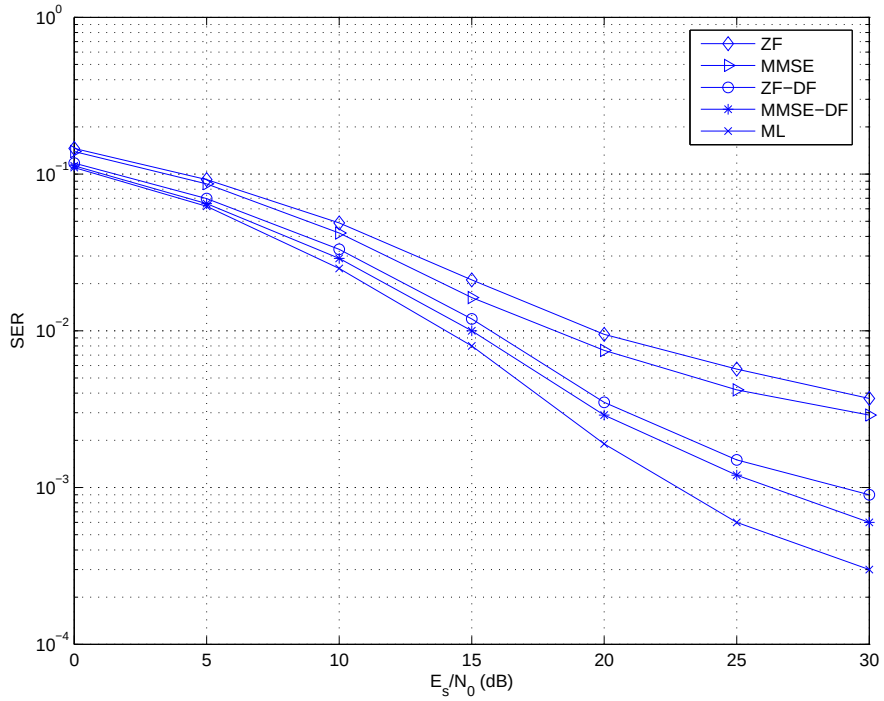

FIGURE 6.5. SER versus E_s/N_0 for MIMO-OFDM with different detection schemes ($\beta T_s = 3 \times 10^{-6}$, $N_s = 64$, $v_s = 100$Km/h).

We have assumed perfect CSI for all numerical results so far. In practical systems, however, there exist channel estimation errors. It is beyond the scope of this chapter to discuss channel estimation schemes for time-selective fading channels. To access its impact, channel estimation error is emulated by introducing an error with a normalized average MSE defined as $MSE = E\left[\|\hat{\breve{\boldsymbol{H}}} - \breve{\boldsymbol{H}}\|_F^2\right] / E\left[\|\breve{\boldsymbol{H}}\|_F^2\right]$, where $\breve{\boldsymbol{H}}$ has the same form as Eq. (6.4), except that phase noise terms and OFDM symbol index are neglected. The performance results of MIMO-OFDM systems with various MSE values are shown in Fig. 6.6, where all parameters, except $\beta = 10$Hz, are the same as those applied in Fig. 6.5. The proposed MMSE-based phase noise suppression scheme and the MMSE detection scheme are employed in this simulation. It is observed that the

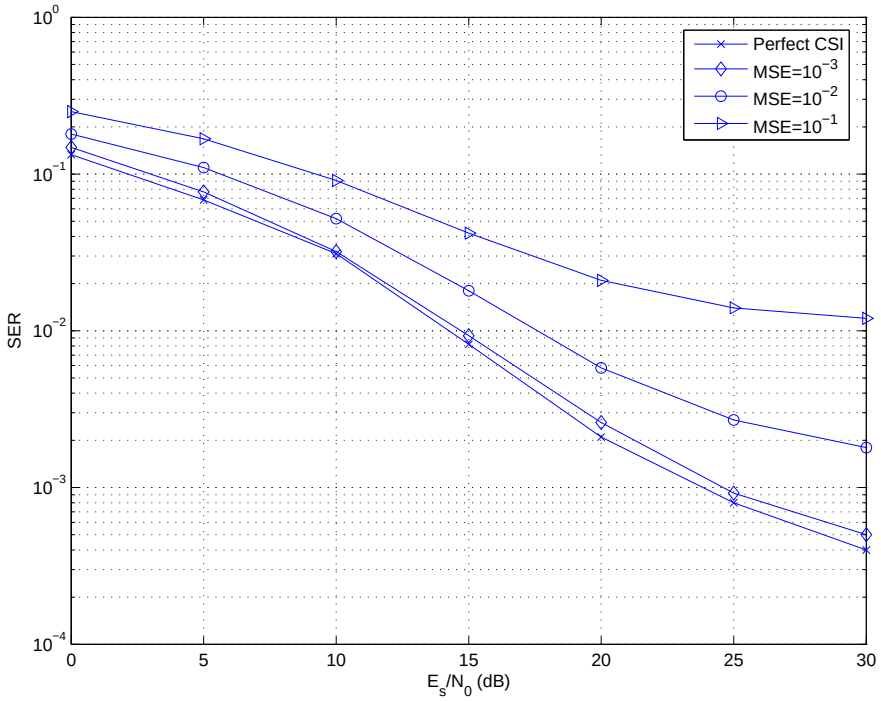

FIGURE 6.6. SER versus E_s/N_0 for MIMO-OFDM with different MSE ($\beta T_s = 10^{-6}$, $N_s = 64$, $v_s = 100$Km/h).

performance degradation is negligible only when the MSE value of channel estimation errors is small (e.g., 10^{-3}).

6.6. Conclusions

We have analyzed the impact of phase noise and channel time selectivity on the performance of MIMO-OFDM systems. Specifically, we have quantified ICI caused by phase noise and channel time variations. A phase noise suppression scheme based on the MMSE criterion is proposed, which is shown to effectively reduce the effect of phase noise. Performances of four detection schemes are compared, and it seems that none of them can effectively eliminate the error floor of MIMO-OFDM systems

in the presence of phase noise and doubly-selective fading. It is also observed that an increase in the 3-dB phase noise linewidth, the data symbol period, or the number of OFDM subcarriers lowers the achievable CIR. Moreover, it is found that an increase in channel estimation error could deteriorate the system performance dramatically.

7. CONCLUSIONS

OFDM, which is effective in avoiding ISI that multipath delay might cause, is very vulnerable to time-selective fading introduced by Doppler shift and phase noise, a random process caused by the fluctuation of the transmitter and receiver oscillators. Multi-antenna OFDM including MIMO-OFDM and ST-OFDM are capable of achieving spatial diversity and/or increasing spectral efficiency. However, similar to single-antenna OFDM, multi-antenna OFDM system is also sensitive to channel time variations and phase noise.

We have analyzed the impact of channel time selectivity on the performance of quasi-orthogonal ST-OFDM systems. Specifically, we have quantified ICI and evaluated ITAI caused by channel time variations. Performances of five detection schemes are compared, and it seems that none of them can effectively eliminate the error floor of ST-OFDM in a time-selective environment.

Frequency-domain correlative coding has been applied to mitigate the effect of time-selective fading to the performance of MIMO-OFDM systems. We derive the analytical expression of CIR as a function of the maximum Doppler shift and power-delay profile of the channel, the number of subcarriers, and the OFDM symbol duration. The CIR expression can be used to quantify the amount of ICI caused by channel time variations. Numerical results indicate that a simple correlative coding scheme can effectively increase CIR of a 128-subcarrier MIMO-OFDM system by as much as 3.0dB, and the improvement further increases as the number of subcarriers becomes larger.

In order to suppress the error floor of ST-OFDM systems over fast fading channels, we have proposed a scheme that combines frequency-domain correlative coding with a modified DF receiver. Performances of three detection schemes are compared, and it is found that the proposed scheme can effectively eliminate the error floor of the

quasi-orthogonal ST-OFDM system even in fast fading environments. It is observed that an increase in Doppler shift, symbol duration, or number of OFDM subcarriers lowers the achievable CIR.

Furthermore, we have analyzed the effects of phase noise to MIMO-OFDM systems over doubly-selective Rayleigh fading channels. Similar to single-antenna OFDM, MIMO-OFDM suffers from significant performance degradation due to phase noise and time-selective fading. We derive the expressions of CIR and SINR. After characterizing CPE caused by phase noise and ICI caused by phase noise as well as time-selective fading, we then propose an MMSE-based scheme to mitigate the effect of both phase noise and time-selective fading. We also evaluate and compare the performances of various detection schemes combined with the proposed CPE mitigation scheme. Through numerical results, we examine the relative performances and the potential error floors of these detection schemes.

In summary, we have not only analyzed the performance of multi-antenna OFDM systems in the presence of phase noise and channel time selectivity, but also proposed the corresponding solutions to the impairments of phase noise and Doppler shift on multi-antenna OFDM systems. The proposed methods successfully achieve outstanding performance with relatively low complexity, and are thus suitable for practical applications.

BIBLIOGRAPHY

[1] G. J. Foschini, "Layered space-time architecture for wireless communication in a fading environment when using multiple antennas," *Bell Labs Technical Journal*, vol. 1, pp. 41–59, Aug. 1996.

[2] D. Shiu, G. J. Foschini, M. J. Gans, and J. M. Kahn, "Fading correlation and its effect on the capacity of multielement antenna systems," *IEEE Trans. Commun.*, vol. 48, pp. 502–513, Mar. 2000.

[3] S. M. Alamouti, "A simple transmit diversity technique for wireless communications," *IEEE J. Select. Areas Commun.*, vol. 16, pp. 1451–1458, Oct. 1998.

[4] V. Tarokh, N. Seshadri, and A. R. Calderbank, "Space-time codes for high data rate wireless communication: Performance criterion and code construction," *IEEE Trans. Inform. Theory*, vol. 44, pp. 744–765, Mar. 1998.

[5] V. Tarokh, H. Jafarkhani, and A. R. Calderbank, "Space-time block codes from orthogonal designs," *IEEE Trans. Inform. Theory*, vol. 45, pp. 1456–1467, July 1999.

[6] H. Jafarkhani, "A quasi-orthogonal space-time block code," *IEEE Trans. Commun.*, vol. 49, pp. 1–4, Jan. 2001.

[7] O. Tirkkonen, A. Boariu, and A. Hottinen, "Minimal non-orthogonality rate 1 space-time block code for 3+ tx antennas," in *Proc. IEEE ISSSTA*, Sept. 2000, pp. 429–432.

[8] W. Su and X. Xia, "Quasi-orthogonal space-time block codes with full diversity," in *Proc. GLOBECOM*, Nov. 2002, pp. 1098–1102.

[9] N. Sharma and C. Papadias, "Improved quasi-orthogonal codes through constellation rotation," *IEEE Trans. Commun.*, vol. 51, pp. 332–335, Mar. 2003.

[10] T. A. Tran and A. .B. Sesay, "A generalized simplified ML decoder of orthogonal space-time block code for wireless communications over time-selective fading channels," in *Proc. IEEE Vehicular Technology Conf.*, 2002, pp. 1911–1915.

[11] F. C. Zheng and A. G. Burr, "Receiver design for orthogonal space-time block coding for four transmit antennas over time-selective fading channels," in *Proc. GLOBECOM*, Nov. 2003, pp. 128–132.

[12] F. C. Zheng and A. G. Burr, "Signal detection for non-orthogonal space-time block coding over time-selective fading channels," *IEEE Commun. Lett.*, vol. 8, pp. 491–493, Aug. 2004.

[13] D. Falconer, S. L. Ariyavisitakul, A. Benyamin-Seeyar, and B. Eidson, "Frequency domain equalization for single-carrer broadband wireless systems," *IEEE Commun. Mag.*, vol. 40, pp. 58–66, Apr. 2002.

[14] G. J. Stüber, J. R. Barry, S. W. Mclaughlin, Y. Li, M. A. Ingram, and T. G. Pratt, "Broadband MIMO-OFDM wireless communications," *Proceedings of the IEEE*, vol. 92, pp. 271–294, Feb. 2004.

[15] M. Russell and G. J. Stüber, "Interchannel interference analysis of OFDM in a mobile environment," in *Proc. IEEE Vehicular Technology Conf.*, 1995, pp. 820–824.

[16] J. Li and M. Kavehrad, "Effects of time selective multipath fading on OFDM systems for broadband mobile applications," *IEEE Commun. Lett.*, vol. 3, pp. 332–334, Dec. 1999.

[17] T. Pollet, M. Bladel, and M. Moeneclaey, "BER sensitivity of OFDM systems to carrier frequency offset and Wiener phase noise," *IEEE Trans. Commun.*, vol. 43, pp. 191–193, Feb. 1995.

[18] L. Tomba, "On the effect of Wiener phase noise in OFDM systems," *IEEE Trans. Commun.*, vol. 46, pp. 580–583, May 1998.

[19] A. G. Armada, "Understanding the effects of phase noise in orthogonal frequency division multiplexing (OFDM)," *IEEE Trans. Broadcast*, vol. 47, pp. 153–159, June 2001.

[20] S. Wu and Y. Bar-Ness, "A phase noise suppression algorithm for OFDM based WLANs," *IEEE Commun. Lett.*, vol. 6, pp. 535–537, Dec. 2002.

[21] G. Liu and W. Zhu, "Compensation of phase noise in OFDM systems using an ICI reduction scheme," *IEEE Trans. Broadcast*, vol. 50, pp. 399–407, Dec. 2004.

[22] S. Wu and Y. Bar-Ness, "OFDM systems in the presence of phase noise: consequences and solutions," *IEEE Trans. Commun.*, vol. 52, pp. 1988–1996, Nov. 2004.

[23] M. Uysal, N. AL-Dhahir, and C. N. Georghiades, "A space-time block-coded OFDM scheme for unknown frequency-selective fading channels," *IEEE Commun. Lett.*, vol. 5, pp. 393–395, Oct. 2001.

[24] Z. Liu, Y. Xin, and G. B. Giannakis, "Space-time-frequency coded OFDM over frequency-selective fading channels," *IEEE Trans. Signal Processing*, vol. 50, pp. 2465–2476, Oct. 2002.

[25] A. Stamoulis, S. N. Diggavi, and N. AL-Dhahir, "Intercarrier interference in MIMO OFDM," *IEEE Trans. Signal Processing*, vol. 50, pp. 2451–2464, Oct. 2002.

[26] T. C. W. Schnek, X.-J. Tao, P. F. M. Smulders, and E. R. Fledderus, "Influence and suppression of phase noise in multi-antenna OFDM," in *Proc. of IEEE VTC'04-Fall*, Sept. 2004 pp. 1443–1447.

[27] K. Nikitopoulos and A. Polydoros, "Decision-directed compensation of phase noise and residual frequency offset in a space-time OFDM receiver," *IEEE Commun. Lett.*, vol. 8, pp. 573–575, Sept. 2004.

[28] Y. Zhang and H. Liu, "Impact of time-selective fading on the performance of quasi-orthogonal space-time coded OFDM systems," *IEEE Trans. Commun.*, vol. 54, pp. 251–260, Feb. 2006.

[29] Y. Zhang and H. Liu, "Frequency-domain correlative coding for MIMO-OFDM systems over fast fading channels," *IEEE Commun. Lett.*, vol. 10, pp. 347–349, May 2006.

[30] Y. Zhang and H. Liu, "Decision-feedback receiver for quasi-orthogonal space-time coded OFDM using correlative coding over fast fading channels," to appear in *IEEE Trans. Wireless Commun.*

[31] Y. Zhang and H. Liu, "MIMO-OFDM systems in the presence of phase noise and doubly-selective fading," to appear in *IEEE Trans. Veh. Technol.*

[32] Y. Zhang and H. Liu, "Decision-feedback receiver for quasi-orthogonal space-time coded OFDM with correlative coding over fast fading channels," in *Proc. of IEEE VTC'05-Fall*, Sept. 2005, pp. 2102–2106.

[33] H. Bölcskei and A. J. Paulraj, "Performance of space-time codes in the presence of spatial fading correlations," in *Proc. Asilomar Conf.*, Sept. 2000, pp. 687–693.

[34] J. P. Kermoal, L. Schumacher, K. I. Pedersen, P. E. Mogensen, and F. Frederiksen, "A stochastic MIMO radio channel model with experimental validation," *IEEE J. Select. Areas Commun.*, vol. 20, pp. 1211–1226, Aug. 2002.

[35] J. G. Proakis, *Digital Communications*. New York, NY: McGraw-Hill, 4th ed., 2001.

[36] T. Pollet, M. Bladel, and M. Moeneclaey, "BER sensitivity of OFDM systems to carrier frequency offset and Wiener phase noise," *IEEE Trans. Commun.*, vol. 43, pp. 191–193, Feb. 1995.

[37] A. G. Armada, "Understanding the effects of phase noise in orthogonal frequency division multiplexing (OFDM)," *IEEE Trans. Broadcast*, vol. 47, pp. 153–159, June 2001.

[38] S. Verdú, *Multiuser Detection*. Cambridge, U.K.: Cambridge Univ. Press, 1998.

[39] A. Duel-Hallen, "Decorrelating decision-feedback multiuser detector for synchronous code-division multiple-access channel," *IEEE Trans. Commun.*, vol. 41, pp. 285–290, Feb. 1993.

[40] J. Cioffi, G. Dudevoir, M. Eyuboglu, and G. D. Forney, Jr., "MMSE decision feedback equalization and coding–Parts I and II," *IEEE Trans. Commun.*, vol. 43, pp. 2582–2604, Oct. 1995.

[41] O. Edfors, M. Sandell, J. -J. v. d. Beek, S. K. Wilson, and P. O. Börjesson, "OFDM channel estimation by singular value decomposition," *IEEE Trans. Commun.*, vol. 46, pp. 931–939, July 1998.

[42] S. Coleri, M. Ergen, and A. Bahai, "Channel estimation techniques based on pilot arrangement in OFDM systems," *IEEE Trans. Broadcast.*, vol. 48, pp. 223–229, Sept. 2002.

[43] O. Simeone, Y. Bar-Ness, and U. Spagnolini, "Pilot-based channel estimation for OFDM systems by tracking the delay-subspace," *IEEE Trans. Wireless Commun.*, vol. 3, pp. 315–325, Jan. 2004.

[44] H. Moose, "A technique for orthogonal frequency division multiplexing frequency offset correction," *IEEE Trans. Commun.*, vol. 42, pp. 2908–2914, Oct. 1994.

[45] A. Klein, G. K. Kaleh, and P. W. Baier, "Zero forcing and minimum mean-square-error equalization for multiuser detection in code-division multiple-access channels," *IEEE Trans. Veh. Technol.*, vol. 45, pp. 276–287, May 1996.

[46] A. Duel-Hallen, "Equalizers for multiple input/multiple output channels and PAM systems with cyclostationary input sequences," *IEEE J. Select. Areas Commun.*, vol. 10, pp. 630–639, Apr. 1992.

[47] Y. Zhao and S. G. Häggman, "Intercarrier interference compression in OFDM communication systems by using correlative coding," *IEEE Commun. Lett.*, vol. 2, pp. 214–216, Aug. 1998.

[48] B. Hassibi, "A fast square-root implementation for BLAST," in *34th Asilomar Conference on Signal, Systems, and Computers*, (Pacific Grove, California), pp. 1255–1259, Oct. 2000.

[49] J. Armstrong, "Analysis of new and existing methods of reducing intercarrier interference due to carrier frequency offset in OFDM," *IEEE Trans. Commun.*, vol. 47, pp. 365–369, Mar. 1999.

[50] Y. Zhao and S. G. Häggman, "Intercarrier interference self-cancellation scheme for OFDM mobile communication systems," *IEEE Trans. Commun.*, vol. 49, pp. 1185–1191, July 2001.

[51] H. Zhang and Y. Li, "Optimum frequency-domain partial response encoding in OFDM system," *IEEE Trans. Commun.*, vol. 51, pp. 1064–1068, July 2003.

[52] G. D. Forney, Jr., "Maximum-likelihood sequence estimation of digital sequences in the presence of intersymbol interference," *IEEE Trans. Inform. Theory*, vol. IT-18, pp. 363–378, May 1972.

[53] J. Hou, M. H. Lee, and J. Y. Park, "Matrices analysis of quasi-orthogonal space-time block codes ," *IEEE Commun. Lett.*, vol. 7, pp. 385–387, Aug. 2003.

[54] J. Kim, R. W. Heath, Jr., and E. J. Powers "Receiver designs for Alamouti coded OFDM systems in fast fading channels," *IEEE Trans. Wireless Commun.*, vol. 4, pp. 550–559, Mar. 2005.

[55] G. D. Golden, C. J. Foschini, R. A. Valenzuela, and P. W. Wolniansky, "Detection algorithm and initial laboratory results using V-BLAST space-time communication architecture," *Electron. Lett.*, vol. 35, pp. 14–16, Jan. 1999.

[56] W. Zha and S. D. Blostein, "Modified decorrelating decision-feedback detection of BLAST space-time system," in *Proc. ICC*, vol. 1, 2002, pp. 335–339.

[57] X. Cai and G. B. Giannakis, "Bounding performance and suppressing intercarrier interference in wireless mobile OFDM," *IEEE Trans. Commun.*, vol. 51, pp. 2047–2056, Dec. 2003.

APPENDICES

APPENDIX A. Proof that Υ is a circulant matrix

Since $\boldsymbol{\Upsilon}$ in Eq. (3.27) is the same for any antenna index p, we can replace vector $\boldsymbol{h}_l(n)$ of the channel matrix $\boldsymbol{H}$ in Eq. (3.5) with a scalar $h_{p,l}(n)$ (note that OFDM symbol index is omitted for notation simplicity), forming a new $N_s \times N_s$ matrix

$$\boldsymbol{\mathcal{H}} = \begin{bmatrix} h_{p,0}(0) & \cdots & 0 & h_{p,L-1}(0) & \cdots & h_{p,1}(0) \\ \vdots & & & \vdots & & \vdots \\ h_{p,L-1}(L-1) & \cdots & h_{p,1}(L-1) & h_{p,0}(L-1) & \cdots & 0 \\ \vdots & & & \vdots & & \vdots \\ 0 & \cdots & h_{p,L-1}(N_s-1) & \cdots & h_{p,1}(N_s-1) & h_{p,0}(N_s-1) \end{bmatrix}. \tag{A.1}$$

Let us also define

$$\begin{aligned} \boldsymbol{\mathcal{G}} &= \{g_{ij}^{(p)},\ i,j = 0,\cdots,N_s-1\} = \boldsymbol{U}\boldsymbol{\mathcal{H}}\boldsymbol{U}^H \\ \boldsymbol{\Upsilon} &= \{\gamma_{ij}^{(p)}\} = \{var(g_{ij}^{(p)})\}. \end{aligned} \tag{A.2}$$

We note that $\boldsymbol{U} = \{u_{ij}\} = [\boldsymbol{u}_0, \cdots, \boldsymbol{u}_{N_s-1}]$, where $u_{ij} = \frac{1}{\sqrt{N_s}} e^{-(2\pi\sqrt{-1}/N_s)ij}$. Since $\boldsymbol{\Upsilon}$ is independent of p, we omit antenna index p in the following discussion. If we denote $\boldsymbol{\mathcal{H}}$ as the sum of L matrices as $\boldsymbol{\mathcal{H}} = \sum_{l=0}^{L-1} \boldsymbol{\mathcal{H}}_{[l]}$, where $\boldsymbol{\mathcal{H}}_{[l]}$ is a matrix formed by cyclic left-shifting the diagonal matrix $diag\{h_l(0), \cdots, h_l(N_s-1)\}$ by l columns, we have

$$\boldsymbol{\mathcal{G}} = \boldsymbol{U}\boldsymbol{\mathcal{H}}\boldsymbol{U}^H = \sum_{l=0}^{L-1} \boldsymbol{\mathcal{G}}_l = \sum_{l=0}^{L-1} \boldsymbol{U}\boldsymbol{\mathcal{H}}_{[l]}\boldsymbol{U}^H \tag{A.3}$$

where $\boldsymbol{\mathcal{G}}_l = \{g_{l,ij}\}$. Because

$$\begin{aligned} E\left[h_l(n)\right] &= 0,\ l = 0,\cdots,L-1,\ n = 0,\cdots,N_s-1 \\ E\left[h_l(r)\cdot h_{l'}^*(s)\right] &= J_0(2\pi|r-s|f_dT_s)\delta_{l-l'}e^{-\frac{\tau_l}{\tau_{rms}}},\ r,s = 0,\cdots,N_s-1 \end{aligned} \tag{A.4}$$

it is easy to recognize that $\boldsymbol{\Upsilon} = \sum_{l=0}^{L-1} \boldsymbol{\Upsilon}_l$, where $\boldsymbol{\Upsilon}_l = \{\gamma_{l,ij}\} = \{var(g_{l,ij})\}$. Since the sum of circulant matrices of the same dimension is also a circulant matrix, we only need to prove that each $\boldsymbol{\Upsilon}_l$ is a circulant matrix.

For any integer n, let $[n]$ denote n modulo N_s, i.e., $[n]$ is the remainder from dividing n by N_s. Then $g_{l,ij}$ is obtained as

$$\begin{aligned} g_{l,ij} &= \boldsymbol{u}_i^T \boldsymbol{\mathcal{H}}_{[l]} \boldsymbol{u}_j^* \\ &= \sum_{n=0}^{N_s-1} u_{in} u_{j,[n-l]}^* h_l(n) \\ &= \boldsymbol{\eta}_{ij}^T \boldsymbol{h}_l \end{aligned} \tag{A.5}$$

where $\boldsymbol{\eta}_{ij} = [\eta_{ij0}, \cdots, \eta_{ij,(N_s-1)}]^T$, $\eta_{ijn} = u_{in} u_{j,[n-l]}^*$, and $\boldsymbol{h}_l = [h_l(0), \cdots, h_l(N_s - 1)]^T$. Thus

$$\begin{aligned} \gamma_{l,ij} &= var(g_{l,ij}) = var(\boldsymbol{\eta}_{ij}^T \boldsymbol{h}_l) \\ &= \boldsymbol{\eta}_{ij}^T cov(\boldsymbol{h}_l) \boldsymbol{\eta}_{ij}^* \\ &= \sum_{r=0}^{N_s-1} \sum_{s=0}^{N_s-1} \eta_{ijr} \chi(r,s) \eta_{ijs}^* \\ &= \sum_{r=0}^{N_s-1} \sum_{s=0}^{N_s-1} \chi(r,s) u_{ir} u_{j,[r-l]}^* u_{is}^* u_{j,[s-l]} \\ &= \frac{1}{N_s^2} \sum_{r=0}^{N_s-1} \sum_{s=0}^{N_s-1} \chi(r,s) e^{-(2\pi\sqrt{-1}/N_s) t_{ijrs}} \end{aligned} \tag{A.6}$$

where $\chi(r,s) = cov(h_l(r) \cdot h_l^*(s))$, and $t_{ijrs} = ir - j[r-l] - is + j[s-l]$. It suffices to show, for any fixed r and s, that $[t_{ijrs}] = [ir - j[r-l] - is + j[s-l]] = [j-i][s-r]$.

Also note that an $N_s \times N_s$ matrix $\boldsymbol{B} = \{b_{ij}\},\ 0 \le i, j \le N_s - 1$, is circulant if and only if $b_{ij} = \kappa_{[j-i]}$, i.e., if and only if b_{ij} depends only on $[j-i]$ and $e^{-(2\pi\sqrt{-1}/N_s)k} = e^{-(2\pi\sqrt{-1}/N_s)[k]}$ because $e^{2\pi\sqrt{-1}} = 1$. Thus from Eq. (A.6), we can conclude that $\boldsymbol{\Upsilon}_l$ is a circulant matrix if $h_l(n),\ n = 0, \cdots, N_s - 1$, are finite.

Moreover, from Eq. (A.6), we have

$$\begin{aligned}\gamma_{ij} &= \sum_{l=0}^{L-1} \gamma_{l,ij} \\ &= \frac{1}{N_s^2} \sum_{l=0}^{L-1} \sum_{r=0}^{N_s-1} \sum_{s=0}^{N_s-1} J_0(2\pi|r-s|f_d T_s) e^{-(2\pi\sqrt{-1}/N_s)t_{ijrs}} e^{-\frac{\tau_l}{\tau_{rms}}} \\ &= \frac{1}{N_s^2} \sum_{l=0}^{L-1} \left[N_s + 2 \sum_{m=1}^{N_s-1} (N_s - m) J_0(2\pi m f_d T_s) \cos\left(\frac{2\pi}{N_s}[j-i]m\right) \right] e^{-\frac{\tau_l}{\tau_{rms}}}. \quad \text{(A.7)}\end{aligned}$$

Let us define $\varpi_l^{(1)} = E[g_{l,ij} \cdot g_{l,i(j+1)}^*]$ and $\varpi_l^{(-1)} = E[g_{l,i(j+1)} \cdot g_{l,ij}^*]$. Similar to Eq. (A.6), we have

$$\begin{aligned}\varpi_l^{(1)} &= \sum_{r=0}^{N_s-1} \sum_{s=0}^{N_s-1} \eta_{ijr} \chi(r,s) \eta_{i(j+1)s}^* \\ &= \sum_{r=0}^{N_s-1} \sum_{s=0}^{N_s-1} \chi(r,s) u_{ir} u_{j,[r-l]}^* u_{is}^* u_{j+1,[s-l]} \\ &= \frac{1}{N_s^2} \sum_{r=0}^{N_s-1} \sum_{s=0}^{N_s-1} J_0(2\pi|r-s|f_d T_s) e^{-(2\pi\sqrt{-1}/N_s)t_{ijrs}^{(1)}} e^{-\frac{\tau_l}{\tau_{rms}}} \quad \text{(A.8)}\end{aligned}$$

where $t_{ijrs}^{(1)} = ir - j[r-l] - is + (j+1)[s-l]$. Similar to (A.8), we have

$$\varpi_l^{(-1)} = \frac{1}{N_s^2} \sum_{r=0}^{N_s-1} \sum_{s=0}^{N_s-1} J_0(2\pi|r-s|f_d T_s) e^{-(2\pi\sqrt{-1}/N_s)t_{ijrs}^{(-1)}} e^{-\frac{\tau_l}{\tau_{rms}}} \quad \text{(A.9)}$$

where $t_{ijrs}^{(-1)} = ir - (j+1)[r-l] - is + j[s-l]$. Finally, we have

$$\begin{aligned}\Omega_j =& E[g_{ij} \cdot g_{i(j+1)}^*] + E[g_{i(j+1)} \cdot g_{ij}^*] \\ =& \sum_{l=0}^{L-1} \varpi_l^{(1)} + \varpi_l^{(-1)} \\ =& \frac{1}{N_s^2} \sum_{l=0}^{L-1} \sum_{r=0}^{N_s-1} \sum_{s=0}^{N_s-1} J_0(2\pi|r-s|f_d T_s) e^{-\frac{\tau_l}{\tau_{rms}}} (e^{-(2\pi\sqrt{-1}/N_s)t_{ijrs}^{(1)}} \\ &+ e^{-(2\pi\sqrt{-1}/N_s)t_{ijrs}^{(-1)}}). \quad \text{(A.10)}\end{aligned}$$

APPENDIX B. Closed-form expression of $\{\boldsymbol{\Upsilon}\}_{ij}$ in the presence of phase noise

Since $\boldsymbol{\Upsilon}$ with dimension $N_s \times N_s$ in Eq. (6.8) is the same for any antenna index (i, j), we can replace matrix $\boldsymbol{H}_l(n)$ of the channel matrix $\boldsymbol{H}$ in Eq. (6.4) with a scalar $h_l(n)$ (note that OFDM symbol index is omitted for notational simplicity) and replace the zero matrix $\mathbf{0}$ with a scalar 0, forming a new $N_s \times N_s$ matrix $\boldsymbol{\mathcal{H}}$. If we denote $\boldsymbol{\mathcal{H}}$ as the sum of L matrices as $\boldsymbol{\mathcal{H}} = \sum_{l=0}^{L-1} \boldsymbol{\mathcal{H}}_{(l)}$, where $\boldsymbol{\mathcal{H}}_{(l)}$ is a matrix formed by cyclically left-shifting the diagonal matrix $diag\{h_l(0)e^{j\phi(0)}, \cdots, h_l(N_s-1)e^{j\phi(N_s-1)}\}$ by l columns, we have

$$\boldsymbol{\mathcal{G}} = \boldsymbol{U}\boldsymbol{\mathcal{H}}\boldsymbol{U}^H = \sum_{l=0}^{L-1} \boldsymbol{\mathcal{G}}_l = \sum_{l=0}^{L-1} \boldsymbol{U}\boldsymbol{\mathcal{H}}_{(l)}\boldsymbol{U}^H \tag{B.1}$$

where $\boldsymbol{U} = [\boldsymbol{u}_0, \cdots, \boldsymbol{u}_{N_s-1}]$ is the unitary DFT matrix. With the conditions that

$$\begin{aligned} E\left[h_l(n)e^{j\phi(n)}\right] &= 0,\ l = 0, \cdots, L-1,\ n = 0, \cdots, N_s-1 \\ E\left[h_l(r)e^{j\phi(r)} \cdot h_{l'}^*(s)e^{-j\phi(s)}\right] &= E\left[h_l(r) \cdot h_{l'}^*(s)\right] E\left[e^{j\phi(r)} \cdot e^{-j\phi(s)}\right] \\ &= J_0(2\pi|r-s|f_dT_s)\delta_{l-l'}e^{-\frac{\tau_l}{\tau_{rms}}-|r-s|\pi\beta T_s} \\ &\qquad r, s = 0, \cdots, N_s-1 \end{aligned} \tag{B.2}$$

it is recognized that $\boldsymbol{\Upsilon} = \sum_{l=0}^{L-1} \boldsymbol{\Upsilon}_l$, where $\boldsymbol{\Upsilon}_l$ is an $N_s \times N_s$ matrix and $\{\boldsymbol{\Upsilon}_l\}_{ij} = var(\{\boldsymbol{\mathcal{G}}_l\}_{ij})$. Since the sum of circulant matrices of the same dimension is also a circulant matrix, we only need to prove that each $\boldsymbol{\Upsilon}_l$ is a circulant matrix.

For any integer n, let $[n]$ denote n modulo N_s, i.e., $[n]$ is the remainder from dividing n by N_s. The $\{\boldsymbol{\mathcal{G}}_l\}_{ij}$ is obtained as

$$\{\boldsymbol{\mathcal{G}}_l\}_{ij} = \boldsymbol{u}_i^T\boldsymbol{\mathcal{H}}_{(l)}\boldsymbol{u}_j^* = \boldsymbol{\eta}_{ij}^T\boldsymbol{h}_l \tag{B.3}$$

where $\boldsymbol{\eta}_{ij} = [\eta_{ij0}, \cdots, \eta_{ij,(N_s-1)}]^T$, $\boldsymbol{u}_i = [u_{i0}, \cdots, u_{i,(N_s-1)}]^T$, $\eta_{ijn} = u_{in}u_{j,[n-l]}^*$, and $\boldsymbol{h}_l = [h_l(0)e^{j\phi(0)}, \cdots, h_l(N_s-1)e^{j\phi(N_s-1)}]^T$. Thus

$$\{\boldsymbol{\Upsilon}_l\}_{ij} = var(\boldsymbol{\eta}_{ij}^T \boldsymbol{h}_l) = \sum_{r=0}^{N_s-1}\sum_{s=0}^{N_s-1} \eta_{ijr}\chi(r,s)\eta_{ijs}^*$$
$$= \frac{1}{N_s^2}\sum_{r=0}^{N_s-1}\sum_{s=0}^{N_s-1} \chi(r,s)e^{-(2\pi\sqrt{-1}/N_s)t_{ijrs}} \quad \text{(B.4)}$$

where $\chi(r,s) = cov(h_l(r)e^{j\phi(r)} \cdot h_l^*(s)e^{-j\phi(s)})$ and $t_{ijrs} = ir - j[r-l] - is + j[s-l]$. It suffices to show, for any fixed r and s, that $[t_{ijrs}] = [ir - j[r-l] - is + j[s-l]] = [j-i][s-r]$. Also note that an $N_s \times N_s$ matrix $\boldsymbol{B}$ is circulant if and only if $\{\boldsymbol{B}\}_{ij} = \kappa_{[j-i]}$, i.e., if and only if $\{\boldsymbol{B}\}_{ij}$ depends only on $[j-i]$ and $e^{-(2\pi\sqrt{-1}/N_s)k} = e^{-(2\pi\sqrt{-1}/N_s)[k]}$ because $e^{2\pi\sqrt{-1}} = 1$. Thus, from Eq. (B.4), we can conclude that $\boldsymbol{\Upsilon}_l$ is a circulant matrix if $h_l(n),\ n = 0, \cdots, N_s - 1$, are finite.

Moreover, from Eq. (B.4), we have

$$\{\boldsymbol{\Upsilon}\}_{ij} = \sum_{l=0}^{L-1}\{\boldsymbol{\Upsilon}_l\}_{ij}$$
$$= \frac{1}{N_s^2}\sum_{l=0}^{L-1}\sum_{r=0}^{N_s-1}\sum_{s=0}^{N_s-1} J_0(2\pi|r-s|f_dT_s)e^{-(2\pi\sqrt{-1}/N_s)t_{ijrs}}e^{-\frac{\tau_l}{\tau_{rms}}-|r-s|\pi\beta T_s}$$
$$= \frac{1}{N_s^2}\sum_{l=0}^{L-1}\left\{N_s + 2\sum_{m=1}^{N_s-1}(N_s-m)J_0(2\pi m f_d T_s)\cos\left(\frac{2\pi}{N_s}[j-i]m\right)e^{-\pi\beta T_s m}\right\}e^{-\frac{\tau_l}{\tau_{rms}}}.$$
(B.5)

APPENDIX C. Variance of equivalent noise in the presence of phase noise

From the assumptions made in Eq. (6.5), it is clear that $\rho_{l,ij}(n)$ are independent Gaussian random variables with

$$E\left[\rho_{l,ij}(n)\rho^*_{l',i'j'}(n')\right] = e^{-\frac{\tau_l}{\tau_{rms}}}\left(1 - J_0^2(2\pi n f_d T_s)\right)\delta_{l-l'}\delta_{i-i'}\delta_{j-j'}\delta_{n-n'}.$$

With some simple manipulations, we have

$$\begin{aligned} E\left[\left(\boldsymbol{P}_{kk}\boldsymbol{x}_k\right)\left(\boldsymbol{P}_{kk}\boldsymbol{x}_k\right)^H\right] &= E\left[\boldsymbol{P}_{kk}\boldsymbol{P}_{kk}^H\right] \\ &= \left\{\frac{N_t}{N_s^2}\sum_{l=0}^{L-1} e^{-\frac{\tau_l}{\tau_{rms}}}\sum_{n=1}^{N_s-1}\left(1 - J_0^2(2\pi n f_d T_s)\right)\right\}\boldsymbol{I}_{N_r}. \end{aligned} \tag{C.1}$$

Also it is straightforward that $E\left[\{\boldsymbol{G}_{kk'}\}_{ij}\{\boldsymbol{G}_{kk'}\}^*_{i'j'}\right] = 0$, $i \neq i'$ or $j \neq j'$ due to $E\left[\{\boldsymbol{H}_l(n)\}_{ij}\{\boldsymbol{H}_l(n)\}^*_{i'j'}\right] = e^{-\frac{\tau_l}{\tau_{rms}}}\delta_{i-i'}\delta_{j-j'}$ and $\{\boldsymbol{G}_{kk'}\}_{ij} = \sum_{l=0}^{L-1}\sum_{n=0}^{N_s-1} u_{kn}u^*_{k',[n-l]}\{\boldsymbol{H}_l(n)\}_{ij}e^{j\phi(n)}$. Thus, we obtain

$$\begin{aligned} E\left[\left(\sum_{\substack{k'=0\\k'\neq k}}^{N_s-1}\boldsymbol{G}_{kk'}\boldsymbol{x}_{k'}\right)\left(\sum_{\substack{k'=0\\k'\neq k}}^{N_s-1}\boldsymbol{G}_{kk'}\boldsymbol{x}_{k'}\right)^H\right] &= \sum_{\substack{k'=0\\k'\neq k}}^{N_s-1} E\left[\boldsymbol{G}_{kk'}\boldsymbol{G}_{kk'}^H\right] \\ &= \left(N_t\sum_{k'=1}^{N_s-1}\gamma_{k'}\right)\boldsymbol{I}_{N_r}. \end{aligned} \tag{C.2}$$

Since $E\left[\boldsymbol{n}_k\boldsymbol{n}_k^H\right] = \sigma^2\boldsymbol{I}_{N_r}$, we have

$$\begin{aligned} E\left[\boldsymbol{e}_k\boldsymbol{e}_k^H\right] &= E\left[\left(\boldsymbol{P}_{kk}\boldsymbol{x}_k + \sum_{\substack{k'=0\\k'\neq k}}^{N_s-1}\boldsymbol{G}_{kk'}\boldsymbol{x}_{k'} + \boldsymbol{n}_k\right)\left(\boldsymbol{P}_{kk}\boldsymbol{x}_k + \sum_{\substack{k'=0\\k'\neq k}}^{N_s-1}\boldsymbol{G}_{kk'}\boldsymbol{x}_{k'} + \boldsymbol{n}_k\right)^H\right] \\ &= E\left[\boldsymbol{P}_{kk}\boldsymbol{P}_{kk}^H\right] + \sum_{\substack{k'=0\\k'\neq k}}^{N_s-1} E\left[\boldsymbol{G}_{kk'}\boldsymbol{G}_{kk'}^H\right] + E\left[\boldsymbol{n}_k\boldsymbol{n}_k^H\right] \\ &= \left\{\frac{N_t}{N_s^2}\sum_{l=0}^{L-1} e^{-\frac{\tau_l}{\tau_{rms}}}\sum_{n=1}^{N_s-1}\left(1 - J_0^2(2\pi n f_d T_s)\right) + N_t\sum_{k'=1}^{N_s-1}\gamma_{k'} + \sigma^2\right\}\boldsymbol{I}_{N_r}. \end{aligned} \tag{C.3}$$